POLITECNICO MILANO 1863

SCUOLA DI INGEGNERIA INDUSTRIALE E DELL'INFORMAZIONE

Danmarks Tekniske Universitet

DTU

Synchronized 4+4 Strokes Double Compression-Expansion Engine: 1-D Simulation and Sensitivity Analysis

Master of Science Thesis in
Mechanical Engineering - Automotive & Motorsport

Author: **Davide Morerio**

Student ID: 10713702
Advisor: Prof.Tommaso Lucchini
Co-advisors: Prof. Bengt Håkan Johansson
Academic Year: 2025-2026

Abstract - Italiano

Questa tesi di Laurea Magistrale esplora il potenziale termodinamico del Double Compression-Expansion Engine (DCEE), un'architettura di motore a combustione interna di tipo split-cycle progettata per superare i limiti intrinseci dei tradizionali motori a quattro tempi. Distribuendo i processi di compressione ed espansione su più cilindri, in particolare mediante stadi a bassa pressione (LP) e alta pressione (HP), il DCEE mira a ridurre le perdite per trasferimento termico e a raggiungere elevati rapporti di pressione complessivi con rapporti di compressione geometrici moderati nei singoli cilindri.

Il focus principale di questo lavoro è sulla configurazione sincronizzata 4+4 tempi, in cui i serbatoi tampone vengono eliminati per consentire uno scambio di gas istantaneo tra gli stadi, riducendo così le dissipazioni legate allo stoccaggio e migliorando l'integrità termodinamica del ciclo. Attraverso simulazioni numeriche monodimensionali condotte su GT-Power, è stato sviluppato un modello dettagliato per analizzare le caratteristiche del ciclo motore, i meccanismi di scambio dei gas e l'efficienza complessiva.

L'indagine include un'analisi parametrica sistematica di sensibilità volta a identificare le condizioni operative ottimali. I principali risultati possono essere riassunti come segue:

- **Incremento dell'efficienza:** La configurazione ottimizzata ha raggiunto un'efficienza termica al freno (BTE) massima del 48,66%, trainata principalmente da un'efficienza termica indicata del 53,92%.
- **Ottimizzazione della combustione:** L'ottimo globale è stato individuato per una durata della combustione pari a 30 CAD e un anticipo di accensione di 10 CAD.
- **Sensibilità all'overlap delle valvole:** Lo studio ha dimostrato che, sebbene un overlap moderato sia essenziale per un efficace lavaggio (scavenging), la sua eliminazione comporta una riduzione del 23,8% dell'efficienza termica, mentre un overlap eccessivo (30°) introduce perdite significative dovute al cortocircuito dei flussi.
- **Compromessi prestazionali:** La priorità data all'efficienza ha comportato una riduzione intenzionale della densità di potenza, con la potenza al freno che diminuisce da 104,27 kW a 90,7 kW.

Nonostante alcune limitazioni, quali l'assenza di un modello di knock e una geometria semplificata dei condotti, i risultati confermano che l'architettura DCEE sincronizzata 4+4 presenta un significativo potenziale per raggiungere efficienze termiche superiori rispetto ai motori a combustione interna tradizionali, configurandosi come una soluzione promettente per i sistemi di propulsione sostenibili del futuro.

Keywords: Double Compression-Expansion Engine (DCEE), Split-cycle engine, Synchronized 4+4 strokes, GT-Power simulation, Parametric sensitivity analysis.

Abstract - English

This Master of Science thesis explores the thermodynamic potential of the Double Compression-Expansion Engine (DCEE), a split-cycle internal combustion architecture designed to overcome the intrinsic limitations of conventional four, stroke engines. By distributing the processes of compression and expansion across multiple cylinders, specifically utilizing low-pressure (LP) and high-pressure (HP) stages,the DCEE aims to mitigate heat transfer losses and achieve high overall pressure ratios with moderate geometric compression ratios in individual cylinders.

The primary focus of this research is the synchronized 4+4 strokes configuration, where buffer tanks are eliminated to allow for instantaneous gas exchange between stages, thereby reducing storage-related dissipations and improving thermodynamic integrity. Using one-dimensional numerical simulations (GT-Power), a detailed model was developed to analyze the engine cycle characteristics, gas-exchange mechanisms, and overall efficiency.

The investigation includes a systematic parametric sensitivity analysis to identify optimal operating conditions. The main findings can be summarized as follows:

- **Efficiency enhancement:** The optimized configuration achieved a peak brake thermal efficiency (BTE) of 48.66%, driven primarily by an indicated thermal efficiency of 53.92%.
- **Combustion optimization:** The global optimum was identified at a combustion duration of 30 CAD and a spark advance of 10 CAD.
- **Valve overlap sensitivity:** The study demonstrated that while moderate overlap is essential for effective scavenging, removing it causes a 23.8% drop in thermal efficiency, whereas excessive overlap (30°) introduces significant short-circuiting losses.
- **Performance trade-offs:** Prioritizing efficiency resulted in a deliberate reduction in power density, with brake power decreasing from 104.27 kW to 90.7 kW.

Despite limitations such as the absence of a knock model and simplified duct geometry, the results confirm that the synchronized DCEE 4+4 architecture holds significant potential for achieving thermal efficiencies beyond those of traditional internal combustion engines, positioning it as a promising candidate for future sustainable propulsion systems.

Keywords: Double Compression-Expansion Engine (DCEE), Split-cycle engine, Synchronized 4+4 strokes, GT-Power simulation, Parametric sensitivity analysis.

Contents

Introduction

The internal combustion engine (ICE) has played a fundamental role in the development of modern society since its introduction in the late nineteenth century. The four-stroke cycle engine, first introduced by Nikolaus Otto, has enabled efficient transportation of people and goods and has contributed significantly to economic development and technological progress. Despite more than a century of continuous development and numerous technological improvements, the fundamental operating principle of the four-stroke engine has remained essentially unchanged.

In recent decades, increasing environmental concerns and stricter regulations on greenhouse gas emissions have placed the efficiency of energy conversion systems under intense scrutiny. The transportation sector is responsible for around 18 % of global carbon dioxide emissions, and improving the efficiency of propulsion systems remains a key pathway toward reducing fuel consumption and mitigating environmental impact. Although electrification is expanding rapidly, internal combustion engines are expected to remain relevant for several applications, including hybrid powertrains, heavy-duty transportation, and high energy-density applications.

For this reason, research continues to investigate new concepts capable of improving the thermodynamic efficiency of combustion engines beyond what can be achieved with conventional four-stroke architectures. One promising direction involves alternative thermodynamic cycles and engine architectures designed to reduce fundamental losses associated with heat transfer, incomplete expansion, and gas exchange processes.

Among these alternative concepts, split-cycle engines have attracted considerable attention, this architectural separation allows the individual processes to be optimized independently and enables new thermodynamic possibilities that are difficult to achieve in conventional engines. For example, separating compression and expansion into different cylinders can allow improved control of temperature, pressure, and heat transfer during the cycle.

One particular split-cycle concept is the Double Compression–Expansion Engine (DCEE). In this architecture the thermodynamic cycle is distributed among multiple cylinders performing different tasks, typically including low-pressure and high-pressure stages. By splitting the compression and expansion processes into multiple stages, the concept enables high overall pressure ratios while maintaining moderate geometric compression ratios in individual cylinders. This approach can reduce heat transfer losses, allow greater expansion of the exhaust gases, and improve overall thermodynamic efficiency.

Previous studies have demonstrated that such split-cycle concepts have the potential to achieve significantly higher brake thermal efficiencies compared to conventional engines. Simulation and experimental investigations of DCEE architectures have reported efficiencies exceeding 50%, indicating the potential for substantial reductions in fuel consumption if such systems can be successfully implemented.

Despite these promising results, several challenges remain. The separation of the cycle into multiple cylinders introduces additional gas exchange processes, which may lead to increased pumping losses. Furthermore, the engine architecture becomes more complex and may require careful optimization of cylinder geometry, valve timing, and system synchronization in order to achieve high efficiency.

The objective of this thesis is therefore to investigate the potential of a split-cycle internal combustion engine architecture to improve the efficiency of the conventional four-stroke engine. In particular, the work focuses on the analysis of a Double Compression–Expansion Engine configuration. The study aims to evaluate how such a concept could contribute to future developments of internal combustion engines by improving thermodynamic efficiency while maintaining feasible operating conditions.

To achieve this objective, numerical simulations are performed using a one-dimensional engine simulation environment (GT-Power by Gamma Technologies). The work focuses on the analysis of engine cycle characteristics, thermodynamic efficiency, and the influence of key design and operating parameters.

The results of this study provide insight into the potential benefits and limitations of the proposed engine architecture and contribute to the broader effort of exploring advanced combustion engine concepts capable of achieving higher efficiency in future propulsion systems.

Structure of the Thesis

The thesis is structured as follows.

Chapter 1 provides an overview of the state of the art of internal combustion engine concepts aimed at improving thermal efficiency. Particular attention is given to advanced cycle concepts, including double compression–expansion engines, and to the main thermodynamic and architectural principles underlying their potential benefits.

Chapter 2 introduces the synchronized DCEE 4+4 architecture investigated in this work. The operating principle of the concept is described, and the main assumptions underlying the synchronized configuration are discussed, with a specific focus on valve timing and the elimination of intermediate buffer volumes.

Chapter 3 presents the numerical modeling approach. The one-dimensional engine model is described in detail, including the representation of the low-pressure and high-pressure units, the adopted sub-models for combustion, heat transfer, and friction, and the main simulation assumptions.

Chapter 4 discusses the baseline performance of the synchronized DCEE architecture. The overall energy balance and efficiency breakdown are analyzed in order to quantify the achievable thermal efficiency and to highlight the main sources of losses.

Chapter 5 is devoted to the parametric analysis. The sensitivity of engine performance and efficiency to key operating and design parameters is investigated, allowing the robustness of the optimal operating point to be assessed and the main trade-offs of the architecture to be identified.

Finally, Chapter 6 summarizes the main findings of the study, discusses the implications of the results, highlights the limitations of the present work, and outlines possible directions for future research.

Research questions

This thesis investigates the potential of a synchronized double compression–expansion engine (DCEE) 4+4 architecture as an alternative internal combustion engine concept aimed at increasing thermal efficiency while maintaining feasible operation within conventional engine constraints. Beyond the general objective of maximizing brake thermal efficiency, the work is structured around a set of specific research questions intended to guide the numerical analysis and to clarify the contribution of the proposed architecture with respect to conventional four-stroke engines.

The first research question addresses the overall thermodynamic potential of the synchronized DCEE concept. In particular, this study investigates whether the DCEE 4+4 configuration can achieve a measurable increase in indicated and brake thermal efficiency under comparable operating conditions. This question is answered through a detailed analysis of the energy balance and efficiency breakdown, focusing on indicated efficiency, brake efficiency, and mean effective pressures.

The second research question focuses on the role of synchronization between the low-pressure and high-pressure units. The elimination of intermediate buffer volumes is a defining feature of the proposed architecture, and its impact on gas exchange efficiency, pumping losses, and overall cycle performance is systematically analyzed. Special attention is therefore dedicated to valve timing synchronization and its effect on pressure matching and loss minimization.

The third research question concerns the intrinsic limitations of the synchronized DCEE architecture. While high efficiency is a primary target, the analysis aims to identify the main trade-offs associated with the concept, particularly in terms of pumping work, heat transfer losses, and achievable power density. This allows the identification of structural constraints that may limit the applicability of the architecture in high-specific-power applications.

An additional research question addresses the robustness of the optimal operating point. The sensitivity of the maximum-efficiency condition to key operating and design parameters—such as air–fuel ratio, combustion phasing, combustion duration, and valve overlap—is investigated in order to assess whether the identified optimum represents a narrow local maximum or a practically achievable operating region.

Each of these research questions is addressed through dedicated numerical investigations based on a one-dimensional engine simulation framework. The mapping between research questions and thesis structure is as follows: the thermodynamic potential is mainly addressed in Chapters 4 and 5; the effects of synchronization are discussed in Chapters 2 and 4; the architectural limitations and trade-offs are analyzed in Chapters 5 and 6; and the robustness of the optimal point is investigated through parametric studies presented in Chapter 5.

Methodological framework

The research questions outlined above are addressed through a numerical investigation based on a one-dimensional engine simulation framework. The study adopts a steady-state, point-design approach, focused on the analysis of cycle-resolved thermodynamic quantities and energy balances, rather than on transient operation or control-oriented modeling.

A detailed one-dimensional model of a synchronized DCEE 4+4 architecture is developed using a commercial engine simulation environment. The model represents the low-pressure and high-pressure units explicitly and includes the full gas exchange process through synchronized valve actuation, without the use of intermediate buffer volumes. Standard sub-models are employed for combustion, heat transfer, and friction, ensuring consistency with established engine modeling practices.

The methodological approach combines reference operating points with extensive parametric analyses. After identifying a baseline configuration corresponding to maximum efficiency conditions, key operating and design parameters—such as air–fuel ratio, combustion phasing, combustion duration, and valve overlap—are systematically varied to quantify their influence on engine performance and losses. The analysis focuses on brake and indicated thermal efficiency, mean effective pressures, pumping work, and heat transfer losses as primary performance indicators.

This framework allows the research questions to be addressed in a controlled and internally consistent manner, enabling both the quantification of the achievable efficiency gains of the synchronized DCEE concept and the identification of its fundamental trade-offs and sensitivities.

1 | State of the art of ICEs

1.1. Introduction to Internal combustion engines

This first section will illustrate a brief introduction to internal combustion engines, in particular to SI 4-Stroke cycles.

1.1.1. Historical Background

The invention and evolution of the internal combustion engine (ICE) has been one of the most transformative technological developments of the past 150 years. Although numerous inventors had experimented with intermittent combustion machines during the first half of the nineteenth century, the decisive breakthrough came in 1876, when Nikolaus August Otto successfully built the first practical four-stroke engine.

This design, based on intake, compression, expansion, and exhaust strokes, enabled compact and durable machines that could power vehicles with long range and acceptable efficiency. The success of Otto's engine marked the transition from early prototypes, such as Étienne Lenoir's atmospheric engine of 1860, to commercially viable power units.

Parallel innovations soon followed. Rudolf Diesel's compression-ignition concept, patented in the 1890s, offered significantly higher thermal efficiency by relying on fuel auto-ignition at high compression ratios. Together, spark-ignition (SI) and compression-ignition (CI) engines established the two dominant combustion modes that still characterize the ICE family today. Their complementary fuel requirements, light distillates for SI and heavier fractions for CI, provided efficient utilization of crude oil, which further contributed to the worldwide diffusion of ICE technology.

Alternative architectures also emerged during the twentieth century. The Wankel rotary engine, introduced in the 1950s, promised high power density and smooth operation, but was limited by sealing issues and poor efficiency. Similarly, gas turbines and Stirling engines found niche applications, but could not challenge the balance of cost, durability, responsiveness, and fuel flexibility of the piston engine. This robustness explains why, despite the availability of electric motors (developed earlier in the nineteenth century by Faraday and Tesla) and batteries (Volta, 1792), the piston ICE has remained the dominant prime mover for transport.

From an energy-conversion perspective, the ICE owes its persistence to being "good enough"" in all relevant metrics: inexpensive, compact, lightweight, responsive, fuel-flexible, and durable . Its ability to operate on a wide variety of fuels, including carbon-neutral options, has become particularly relevant in the context of de-carbonization.

In recent decades, research has shifted toward addressing the inherent thermodynamic and mechanical limitations of conventional Otto and Diesel cycles. High peak pressures, knock, heat transfer losses, and pumping losses restrict the potential efficiency gains of classical cycles. This has led to the development of split-cycle concepts in which compression and expansion are distributed among different cylinders to optimize the thermodynamic process. The Double Compression Expansion Engine (DCEE) represents a significant step in this direction: by staging compression and expansion, it mitigates heat losses and allows extremely high effective compression ratios. Simulations, particularly with hydrogen as fuel, have demonstrated brake thermal efficiencies of up to 60.3% and brake thermal efficiency of 56% , surpassing even fuel cells at full load.

1.1.2. Four-stroke cycle and its processes

The four-stroke cycle, often referred to as the Otto cycle when spark ignition is used, is the fundamental operating principle of the vast majority of internal combustion engines. Its introduction by Nikolaus Otto in 1876 marked the beginning of modern engine technology. The defining feature of the four-stroke engine is that it requires two complete revolutions of the crankshaft (720° crank angle) to complete a thermodynamic cycle, comprising four distinct piston strokes: intake, compression, combustion/expansion, and exhaust. The process is described in the diagram below.

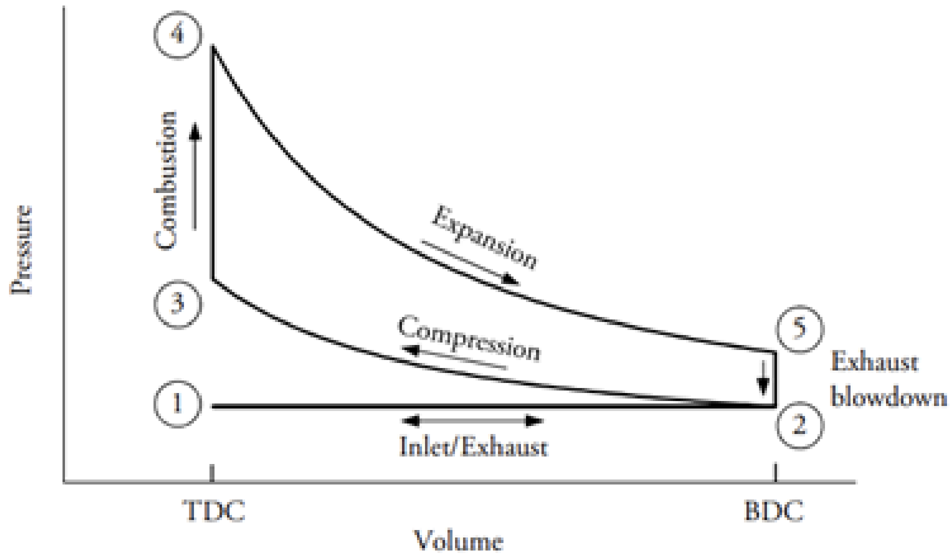

Figure 1.1: Pressure - Volume diagram of 4-stroke engine

Each stroke represents a transformation of the working fluid (air or air–fuel mixture), which can be described in terms of pressure–volume (p–V). Although the ideal cycle provides a simplified representation for efficiency analysis, real engines involve significant deviations due to the finite duration of combustion, heat transfer, friction, and fluid dynamic losses.

1. **Inlet stroke, 1 → 2** (TDC → BDC):

During the first stroke, the piston moves from top dead ad centre (TDC) to bottom dead centre (BDC) while the intake valve is open. A fresh charge of air (in CI engines) or an air–fuel mixture (in SI engines) is drawn into the cylinder. The pressure remains close to ambient, and the increasing volume allows mass flow into the chamber with relatively low pumping losses. The efficiency of this process strongly depends on volumetric efficiency and valve timing.

2. **Compression stroke, 2 → 3** (BDC → TDC):

Once the valves close, the trapped mass is compressed as the piston moves upward. This compression increases the pressure and temperature of the charge, preparing it for ignition. In SI engines, a spark ignites the mixture near the end of the compression stroke, whereas in CI engines, fuel is injected and auto-ignites due to the elevated air temperature. The compression ratio is a critical parameter, as higher ratios increase theoretical thermal efficiency but also raise risks such as knock in SI engines.

3. **Combustion/expansion, 3 → 4 → 5** (TDC → BDC):

Close to TDC, energy release occurs through combustion, dramatically increasing pressure and temperature in the cylinder. In the idealized Otto cycle, heat addition is modelled at constant volume, while in the Diesel cycle it occurs at constant pressure. In reality, combustion is neither instantaneous nor perfectly isochoric or isobaric. The resulting high-pressure gases push the piston downward, generating the positive work that powers the crankshaft. The enclosed area of the pressure–volume (p–V) diagram corresponds to the useful work output of the cycle.

4. **Exhaust stroke, 5 → 2** (BDC → TDC):

At the end of expansion, the exhaust valve opens, allowing blowdown, a rapid pressure release. The piston then rises back to TDC, expelling the burnt gases from the cylinder. This stroke requires work input, reducing net efficiency. Proper exhaust valve timing is crucial to minimize pumping losses and ensure effective scavenging for the next cycle.

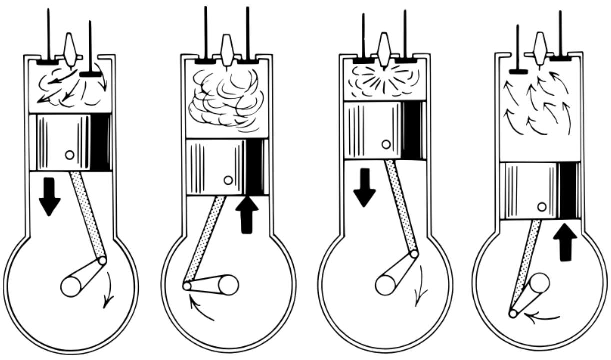

Figure 1.2: 4-Stroke engine

1.1.3. Real engine considerations

In practice, the four-stroke cycle deviates from the ideal representation. Valve events do not occur exactly at TDC or BDC: intake valves typically close late to improve cylinder filling, exhaust valves open early to relieve cylinder pressure before the piston rises, and a short period of valve overlap occurs when both intake and exhaust valves are open simultaneously. These timing strategies enhance breathing at high engine speeds but must be optimized to balance performance, efficiency, and emissions.

The four-stroke engine is therefore not only a mechanical sequence of piston motions but also a carefully tuned thermodynamic process. Its robustness, adaptability across fuels, and ability to scale from small motorcycles to large stationary units explain its dominance in modern transportation and industry.

The spark ignition (Otto) and compression ignition (Diesel) engines share the same fundamental structure of piston, valves, and crank mechanism, yet they operate on distinctly different thermodynamic cycles.

In the Otto cycle, representative of gasoline engines, a premixed charge of air and fuel is introduced into the cylinder and compressed to a ratio typically between 8:1 and 12:1, after which combustion is initiated by applying a high voltage to an external spark. Usually, the distance between positive and negative electrode is 0.8 mm and the diameter of the plasma channel is around 0.1 mm. [1] Ideally, this combustion is modeled as an iso-choric, or constant volume, heat addition, which leads to a sharp rise in pressure at top dead center before expansion delivers useful work. The limitation of this process is the risk of knock: as the compression ratio increases, the unburned mixture ahead of the flame front can auto-ignite, constraining the maximum efficiency that can be achieved, and ruining the engine components if the knock intensity is high enough.

In contrast, the Diesel cycle models the operation of compression ignition engines, where only air is compressed, generally to a much higher ratio of 14:1 to 22:1, raising its temperature well above the autoignition point of the fuel. When fuel is injected near the end of the compression stroke, it auto ignites without the need for a spark. The result is a slower pressure rise compared to the Otto process, but the higher compression ratio gives the Diesel engine a clear advantage in thermal efficiency. Thus, while the Otto cycle is more efficient at an equal compression ratio, real spark ignition engines are knock-limited, whereas Diesels exploit higher ratios to achieve superior fuel economy and durability.

The efficiency of internal combustion engines usually reaches 25%-35% BTE for SI engines and 35%-50% for CI engines, the theoretical limit for Otto and diesel cycle is set at 80% BTE.

1.2. Split cycle engines

This chapter will present an overview of the state of the art of Split-Cycle engines.

1.2.1. Introduction to Split-Cycle engines

The split-cycle internal combustion engine represents a refined evolution of the conventional four-stroke engine architecture, conceived to overcome intrinsic thermodynamic and mechanical limitations associated with performing all cycle phases within a single cylinder. In a traditional engine, the intake, compression, combustion, and exhaust processes occur sequentially in the same chamber, which constrains the independent optimization of each phase. This configuration results in high thermal gradients, increased heat transfer losses, limited expansion ratios, and ultimately doesn't allow to reach the maximum desirable efficiency.

The decoupling of functions allows each subsystem to be individually optimized: the compressor for volumetric efficiency and charge cooling, and the expander for combustion stability and effective expansion work extraction. Furthermore, the split-cycle configuration facilitates the implementation of recuperation systems, in which waste heat from the exhaust or the expander cylinder is recovered and reused to preheat the incoming charge, substantially improving overall thermal efficiency. As a result, split-cycle engines exhibit the potential to achieve brake thermal efficiencies exceeding 50%, approaching those of fuel-cell systems, while maintaining the robustness, scalability, and manufacturability of conventional internal combustion technology.

In split-cycle engines, the traditional four-stroke process can be divided in different ways depending on the desired thermodynamic and mechanical configuration. Broadly, two main splitting approaches exist: **vertical** and **horizontal**.

When the cycle is split **vertically**, the strokes of the conventional four-stroke engine are divided between two groups of cylinders. One group performs the cold phases, intake and compression, while the other performs the hot phase, expansion and exhaust. The high-pressure gas is transferred from the compression cylinder to the expansion cylinder, typically through a crossover passage or buffer chamber. This arrangement allows independent optimization of the compression and expansion processes, improved heat management, and the possibility of recuperating exhaust energy between the two stages.

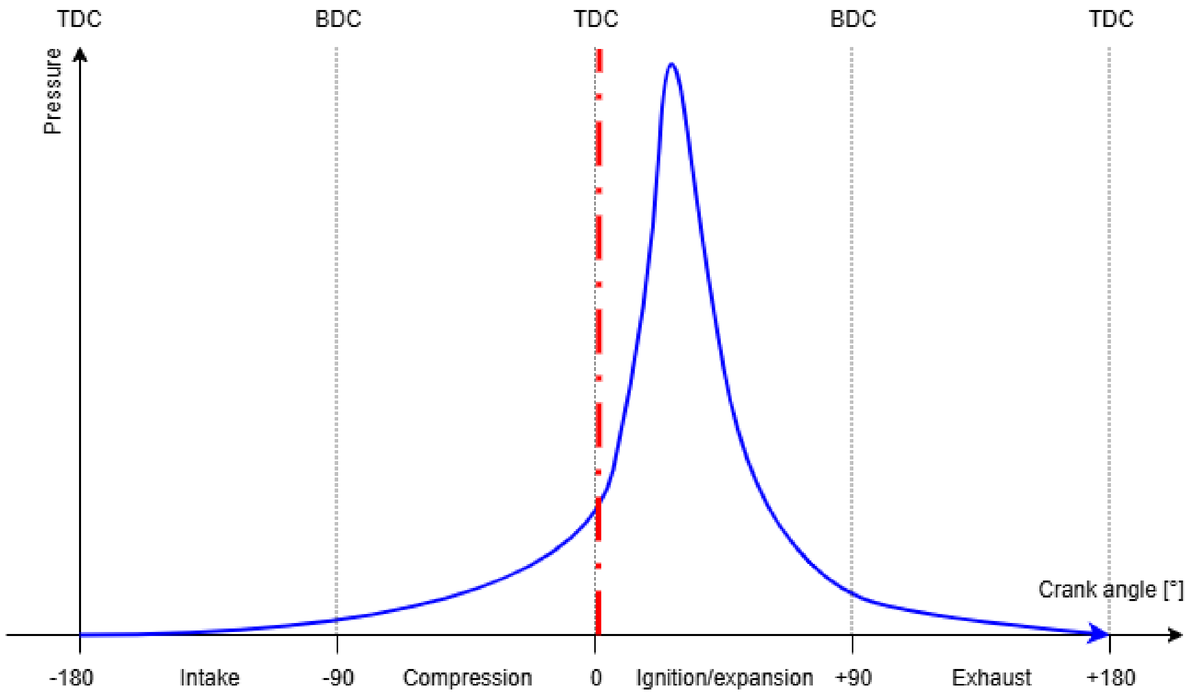

Figure 1.3: Vertical-Split architecture

By contrast, when the cycle is split **horizontally**, the division occurs within the thermodynamic loop itself: the compression and expansion processes are each subdivided into two distinct stages. This means that the working fluid undergoes a first (low-pressure) compression and a second (high-pressure) compression before combustion, and similarly, expansion is performed in two consecutive stages. The purpose of horizontal splitting is to reduce peak pressure and temperature by reducing the compression and expansion ratio for each stage, with the objective of improving overall cycle efficiency and enabling heat recovery between stages.

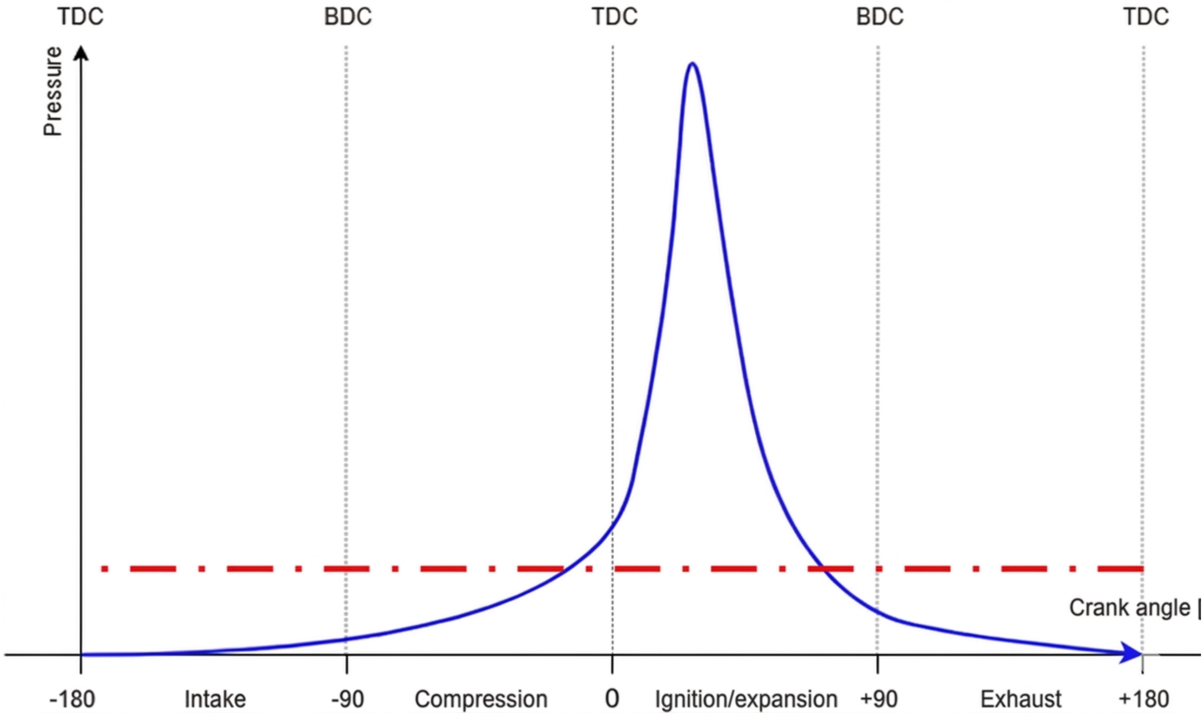

Figure 1.4: Horizontal-Split architecture

1.2.2. Vertical split architecture

In its most diffused configuration, one cylinder is dedicated to intake and compression, while another is responsible for combustion / expansion, and exhaust.

The two cylinders are interconnected through a **crossover passage** (or transfer duct), which transfers the compressed charge from the compression cylinder to the expansion cylinder. A crossover valve mechanism is required to control the mass flow between the two cylinders, typically opening around top dead centre (TDC) of the compression cylinder and slightly before the expansion stroke of the expander. This valve system represents one of the most challenging mechanical aspects of split-cycle designs, since it must operate at very high speed, under high pressure differentials, and with precise timing. [1]

The thermodynamic idea underpinning the split-cycle concept is to decouple compression and expansion ratios, thereby allowing each to be optimized independently. This separation opens up possibilities that are not feasible in conventional four-stroke designs, including:

- Applying different geometric compression and expansion ratios for compression and expansion;
- Incorporating external heat exchange or exhaust heat recovery in the crossover pas-

sage, effectively increasing cycle efficiency.

- Reducing peak gas temperatures in the compressor cylinder while maintaining high expansion work in the expander, which could theoretically improve thermal efficiency.

The process will work as follows: 1) **Intake:** ambient flows in the compression cylinder through inlet valves; 2) **Compression:** air or air-fuel mixture, depending on fuel strategy, undergoes compression; 3) **Cross-over:** a high-speed valve opens to transfer compressed charge; 4) **Combustion/expansion:** air is ignited either by CI or SI; 5) **Exhaust:** exhaust fumes are expelled from the cylinder via outlet valves. [1]

Although conceptually attractive, this process introduces new losses and challenges. The gas transfer between cylinders creates flow restrictions, and the finite duration of the crossover phase can delay combustion, sometimes resulting in late heat release and reduced efficiency. Furthermore, the division of functions leads to thermal management issues: the compressor runs relatively cool while the expander is exposed to high thermal loads, complicating cooling system design.

Moreover, since the compression and expansion ratio doesn't change, mechanical challenges that will be investigated in chapter 2.4 related to peak pressure and temperature will not be addressed.

This type of split-cycle engines has been implemented in **Dolphin** and **Scuderi**-type engines.

1.2.3. Vertical-split applications Dolphin engine (University of Brighton)

Abstract

The Recuperated Split Cycle Engine (RSCE) is an innovative thermodynamic concept that separates the compression and expansion/combustion processes into distinct cylinders, while recovering exhaust heat through a high-efficiency recuperator [4].

The HYDRATE project (Hydrogen Recuperated Advanced Thermal Engine), developed by Dolphin N2, extends this concept by integrating hydrogen combustion in a dual-fuel mode (hydrogen with a small diesel pilot) and by using advanced heat recovery and water injection techniques to achieve thermal efficiencies exceeding 50% (BTE) under simulation and test conditions [4].

Operating Principle

The RSCE thermodynamic process can be summarized as follows:

1. **Compression (Cold Cylinder):** ambient air is compressed up to around 60–70 bar. A fine water injection system (ThermoPower®) cools the charge during compression, achieving quasi-isothermal behaviour and reducing compressor work [4].
2. **Recuperation**: the compressed air flows through a recuperator, where it absorbs waste heat from the exhaust gases of the expander. The outlet temperature after recuperation typically reaches 600–700 °C, depending on load and flow balance [4].
3. **Combustion and Expansion** (Hot Cylinder): the preheated air enters the expander cylinder through high-speed transfer valves. Near top-dead-center, a pilot diesel injection initiates ignition, immediately followed by a high-pressure hydrogen injection. The hydrogen combustion provides the main energy release, driving expansion and mechanical work [4].
4. **Exhaust and Heat Recovery**: The exhaust gases, still at approximately 700 °C, transfer their heat back into the recuperator before exiting the system. This regenerative process maximizes the utilization of exhaust enthalpy and minimizes thermal losses [4].

Experimental Setup and Test Conditions

The experimental activities within the HYDRATE program were conducted on both single-cylinder and multi-cylinder configurations to validate the thermodynamic studies, the hydrogen combustion system, and the performance of the recuperated split-cycle architecture [4]. The single-cylinder expander test rig, internally designated as the Titan engine, was specifically designed to study hydrogen combustion behaviour under split-cycle operating conditions [4].

The cylinder had a displacement of approximately 1.6 litres, derived from a standard heavy-duty diesel unit, with a compression ratio of about 14:1. Tests were carried out at speeds between 1000 and 1500 rpm, corresponding to the intended operating range for heavy-duty applications [4].

Fuel was supplied through a dual-fuel injection system, consisting of a small pilot injection of ultra-low-sulphur diesel—typically between 0.5 and 2 % of the total energy input—to ensure stable ignition, followed by high-pressure hydrogen injection [4]. Hydrogen was delivered from 500 bar storage cylinders through a pressure-regulated manifold operating at approximately 350 bar, equipped with precision mass-flow controllers [4]. Compressed air was supplied externally, with a maximum delivery pressure of 70 bar, ensuring realistic charge conditions representative of the full engine cycle [4].

Hydrogen and Diesel have been delivered efficiently thanks to a dual-Fuel cylinder head, carefully developed using FEA and CFD simulations, exhaust system FEA and Intake Plenum FEA [4].

Instrumentation included high-resolution in-cylinder pressure transducers, crank-angle encoders, exhaust thermocouples, and flow meters for air and hydrogen [4]. A full gas-analysis system allowed continuous monitoring of exhaust composition, including NO formation. The measurements confirmed stable and complete hydrogen combustion with no indication of knocking or abnormal pressure rise [4]. Ignition timing remained well-controlled through the diesel pilot, and combustion phasing was repeatable across operating points [4].

At moderate loads of around 40 bar IMEP, indicated thermal efficiencies of up to 55 % were achieved, demonstrating the potential of the split-cycle hydrogen concept [4]. Minor valve leakage events were observed during transient phases, and hydrogen flow data required post-processing due to pulsation effects in the supply lines, but no critical failures or backfire incidents occurred during the campaign [4].

Following the single-cylinder work, a multi-cylinder prototype, the Upgrade 5 (U5.2DF) engine, was assembled to demonstrate system-level integration [4]. The configuration included two compressor cylinders and four expander cylinders operating on a common crankshaft, with optimized phase offsets to synchronize the thermodynamic sequence [4]. Intermediate air plenums and a compact recuperator were implemented between stages to smooth pressure pulsations and recover exhaust heat [4]. The engine was based on the mechanical structure of an IVECO Cursor 9 platform, modified to accommodate the split-cycle layout, additional cooling circuits, and dual-fuel injection hardware [4].

Initial firing and commissioning were successfully completed using diesel fuel, confirming proper mechanical operation and synchronization between the compressor and expander groups [4]. Hydrogen operation was postponed for safety and scheduling reasons, but numerical extrapolations based on the single-cylinder results predicted a brake thermal efficiency above 50 % once the hydrogen system is fully validated [4].

Advantages of HYDRATE concept

The HYDRATE engine embodies several distinctive advantages that collectively position it as a high-efficiency, low-emission alternative to conventional diesel powertrains [4]. Foremost among these is its remarkably high thermal efficiency, made possible by the combination of recuperative heat exchange and functional separation between compression and expansion [4]. By recovering energy from the exhaust stream and pre-heating

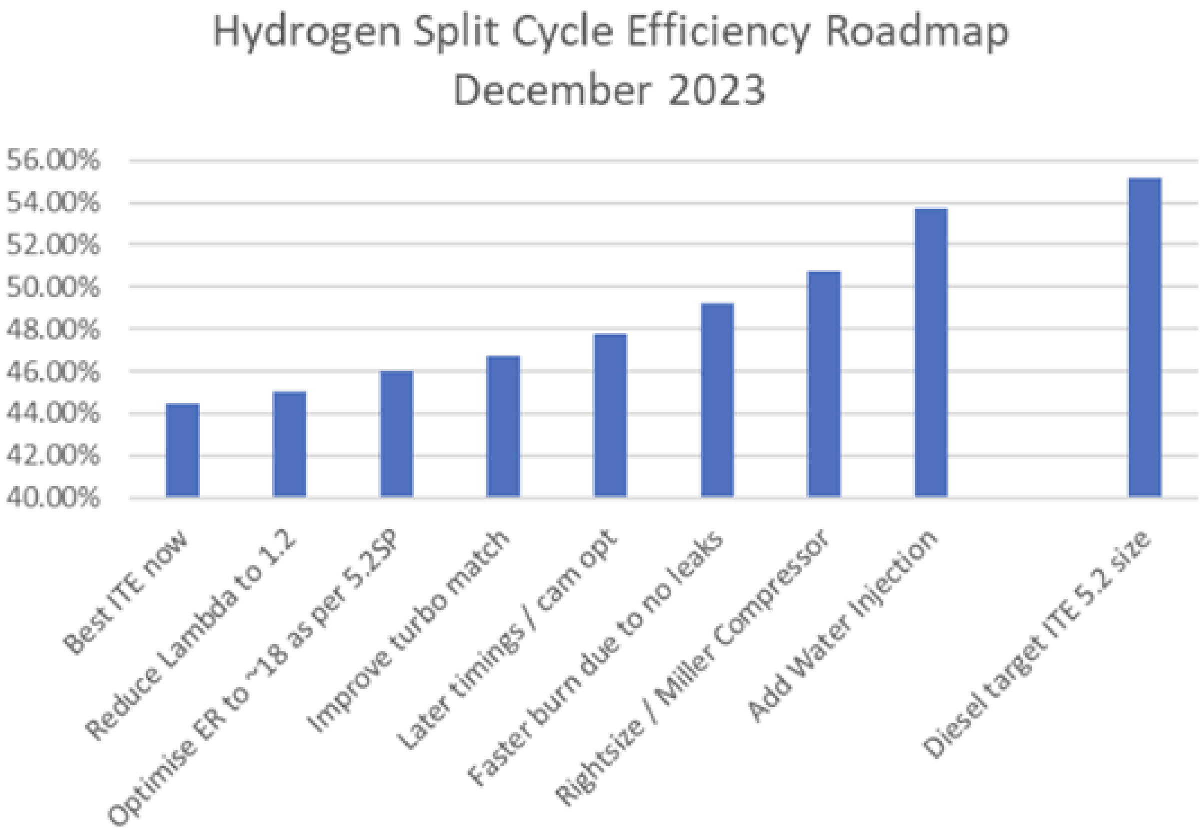

Figure 1.5: Efficiency road-map

the compressed charge air, the engine substantially reduces the exergy losses typical of conventional cycles [4]. Experimental and simulated results consistently indicate efficiency levels exceeding 50 % BTE [4]. Another major benefit lies in fuel flexibility. The dual-fuel arrangement permits seamless operation across a range of hydrogen-to-diesel ratios, enabling gradual transition toward fully renewable hydrogen operation while maintaining reliable ignition control [4].

In terms of environmental performance, the use of hydrogen as the primary fuel virtually eliminates carbon dioxide emissions, producing only water vapor at the exhaust [4]. In addition, the system architecture helps to lower peak in-cylinder temperatures. The combined effects of water injection during compression and staged combustion in the expander significantly limit NOx formation [4]. The recuperative cycle also offers intrinsic thermal-management advantages and allows integration into combined heat-and-power (CHP) systems or waste-heat recovery networks [4].

Limitations and challenges

While the HYDRATE engine presents outstanding thermodynamic potential, several technical and operational challenges remain before the concept can reach full industrial maturity [4]. The split-cycle configuration requires additional components and precise synchronization, increasing system complexity, weight, cost, and maintenance requirements [4].

A second critical aspect concerns hydrogen handling and safety [4]. High-pressure hydrogen operation introduces leakage and ignition risks, mitigated during the HYDRATE project through DSEAR-compliant safety protocols, leak detection, controlled venting, and burst discs [4]. Scaling the system to production environments will require further safety validation [4].

The durability of critical components also remains a challenge. Recuperators and plenums are exposed to cyclic thermal and pressure loading, with transient pressures reaching up to 255 bar [4]. FEA indicated acceptable short-term integrity but potential long-term fatigue limitations [4].

Economic and infrastructural considerations represent another barrier to widespread deployment [4]. Hydrogen cost estimates during the project were in the range of £16 per kilogram for small-scale supply chains [4]. Additional costs related to recuperators, tanks, and injectors must be balanced against efficiency gains [4]. Despite its benefits, some NOx formation remains, requiring EGR or SCR countermeasures [4]. Regulatory definitions of zero-emission propulsion may also affect future competitiveness [4].

Summary

The Dolphin Recuperated Split Cycle Engine (RSCE), developed within the HYDRATE project, represents one of the most advanced evolutions of the split-cycle concept [4]. Experimental and simulation results from the Upgrade 5 prototype confirmed brake thermal efficiencies above 50%, with potential up to 55% under optimized recuperated operation [4]. Exhaust enthalpy recovery exceeding 20%, reduced fuel consumption, moderate peak pressures, and low emissions demonstrate the system's strong potential as a near-term pathway toward net-zero propulsion [4].

1.2.4. Vertical-split applications - Scuderi engine

The Scuderi Split Cycle (SSC) engine represents an innovative reconfiguration of the internal combustion process, in which the conventional four strokes are divided between two mechanically coupled cylinders — a compressor and an expander — connected through a crossover passage [1]. This configuration enables independent optimization of compression and expansion and features post-top-dead-center (TDC) combustion to reduce peak temperature and pressure [1]. Developed by Carmelo Scuderi and later tested by the Southwest Research Institute (SwRI), the SSC achieved indicated thermal efficiencies up to 43–45%, and NOx reductions exceeding 50% compared to a baseline spark-ignited Otto engine [1].

The concept also demonstrated potential for pneumatic hybrid operation and low-speed high-torque performance [1]. However, challenges related to crossover losses (2–5% of IMEP), complex valve actuation, and thermal imbalance between cylinders limited its scalability [1].

The Scuderi engine thus remains a foundational milestone in split-cycle research, paving the way for subsequent recuperated and dual-stage architectures [1].

Operating principle and architecture

The Scuderi Split Cycle (SSC) engine divides the four-stroke cycle between two physically distinct cylinders connected via a crossover port [1]. The compressor cylinder performs the intake and compression strokes, while the expander cylinder executes the power and exhaust strokes.

At the end of compression, high-pressure air is transferred from the compressor to the expander through the crossover passage, controlled by crossover valves (XovrC and XovrE) [1]. This transfer occurs when the expander piston is slightly past its top dead center (TDC), typically with sonic gas velocity, promoting high turbulence and fast charge mixing

[1]. Fuel can be injected directly into the expander cylinder or into the crossover port, where it mixes with the incoming high-pressure air during transfer [1]. Combustion begins shortly after the crossover valves close and proceeds during the expansion stroke, which constitutes the most characteristic feature of the Scuderi cycle [1].

Because combustion occurs while the piston is already moving downward, peak in-cylinder temperatures and pressures are significantly reduced, resulting in lower NOx emissions and improved thermal efficiency [1]. Mechanically, the two pistons are connected to a single crankshaft with a phase angle offset of approximately 20° between the compressor and expander crankpins [1].

This phase shift ensures proper timing between compression, transfer, and expansion [1].

Both the intake and exhaust valves, as well as the crossover valves, are pneumatically actuated, providing fully variable valve actuation (VVA) capabilities [1].

This system allows flexible control over valve opening and closing timing (IVO, IVC, EVO, EVC), enabling the implementation of Miller or Atkinson-like cycles, where the expansion ratio exceeds the compression ratio [1].

A schematic operation of the Scuderi cycle can be summarized as follows:

- **Intake (Compressor Cylinder):** The intake valve opens, allowing air to fill the compressor cylinder at near-ambient pressure [1].
- **Compression (Compressor Cylinder):** The intake valve closes, and the air is compressed to high pressure and temperature [1].
- **Transfer Phase**: The crossover valves open, transferring compressed air from the compressor to the expander through the crossover port [1].
- **Combustion (Expander Cylinder):** Fuel is injected into the crossover flow or directly into the expander and ignited after TDC [1].
- **Expansion (Expander Cylinder):** The hot gases expand, producing work [1].
- **Exhaust (Expander Cylinder):** Burned gases are expelled through the exhaust valve, completing the cycle [1].

Advantages

The decoupling of strokes allows each cylinder to be thermodynamically optimized for its function [1]. Development and testing of the Scuderi engine were carried out by Southwest Research Institute (SwRI) under a multi-stage program between 2003 and 2009 [1]. Following early simulations and concept validation, SwRI constructed a single-pair research prototype composed of one compressor and one expander cylinder [1]. This prototype was designed to accommodate different operating configurations, including naturally aspirated and turbocharged spark-ignited (SI) operation [1].

The test engine incorporated pneumatically actuated intake, exhaust, and crossover valves providing variable valve actuation (VVA), spark ignition system for controlled combustion phasing, and advanced in-cylinder pressure measurement [1]. Initial testing was performed at 4000 rpm full load using optimized valve timing [1].

Another key strength of the Scuderi cycle is the reduction of peak in-cylinder temperature and pressure [1]. Whereas conventional Otto engines may reach 110 bar and 2500–2700 K, the Scuderi engine recorded peaks of only 70 bar and 2000–2100 K [1]. NOx formation was reduced by approximately 50–60% [1].

Moreover, the knock resistance of the SSC is notably superior [1]. Effective compression ratios up to 18:1 were demonstrated without detonation [1]. The sonic crossover jet enhances turbulence and mixing, enabling stable combustion even under lean conditions [1].

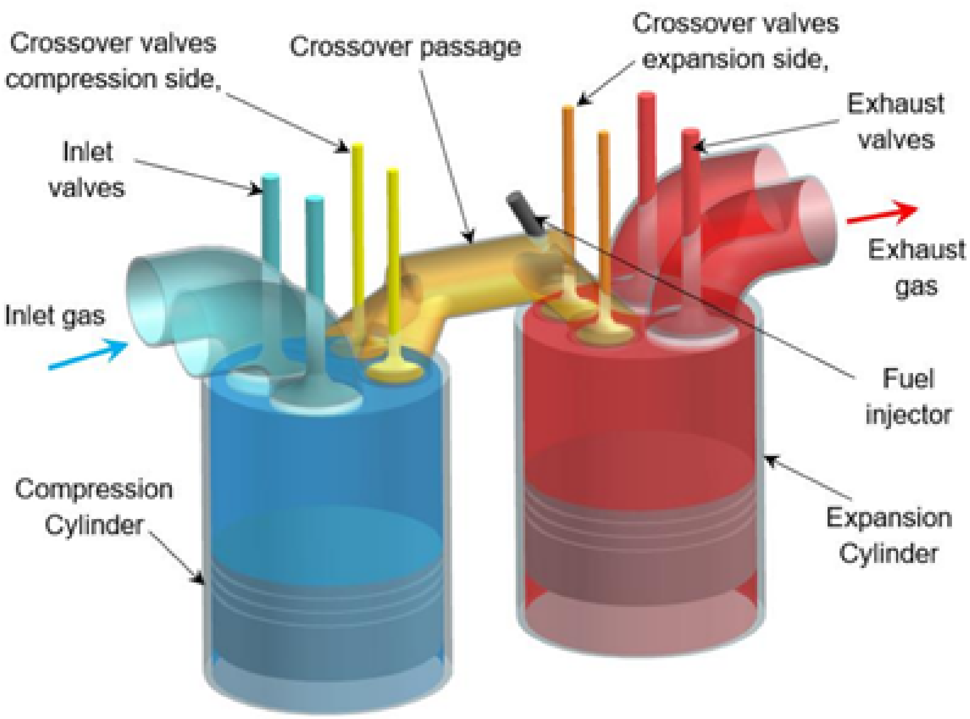

Figure 1.6: Scuderi engine

Limitations and challenges

Despite its technical merit, the Scuderi Split Cycle engine faces several intrinsic limitations [1]. Crossover flow losses of approximately 2–5% IMEP were measured at high speed [1]. Pressure drops across the crossover reached 0.4–0.5 bar per cycle at 4000 rpm [1].

Thermal imbalance between compressor and expander cylinders introduces additional challenges [1]. Wall temperature gradients approaching 400 K complicate thermal management and durability [1]. Pneumatic valve actuation further adds parasitic losses of 1–2% of mechanical power [1].

At high engine speeds, charge transfer limitations reduce volumetric efficiency by up to 10% [1]. At low load, combustion completeness is reduced to approximately 95–96% [1].

Summary

The Scuderi Split Cycle Engine stands as a landmark in split-cycle engine development [1]. Experimental data confirmed improved efficiency, reduced peak pressure, and significantly lower NOx emissions compared to conventional Otto engines [1]. Despite scalability limitations, the Scuderi concept laid the foundation for later recuperated split-cycle architectures such as the Dolphin RSCE and Double Compression–Expansion Engine (DCEE) [1].

1.2.5. Horizontal-split architecture

In a horizontally split configuration, both the compression and expansion processes are divided into two successive stages: a low-pressure (LP) and a high-pressure (HP) phase. In this arrangement, the working fluid is first partially compressed in the LP cylinder before being transferred to the HP cylinder, where the final compression occurs. After combustion, the high-pressure gases expand first in the HP expander and subsequently in the LP expander, completing the power extraction. The motivation for adopting a horizontally split cycle primarily stems from issues related to **peak pressure and temperature** management, which will be discussed in detail in Chapter 1.3.

The main objective of this configuration is to **distribute the total pressure ratio across two stages**, thereby reducing the peak pressures and temperatures reached within each individual cylinder. This staged process allows smoother thermodynamic transitions and improved control over heat transfer and mechanical loading. Moreover, it facilitates the integration of intercoolers or recuperative heat exchangers between stages, further enhancing thermal efficiency.

The only model that has been implemented as of the date of this thesis is the unsynchronized version of the double compression expansion engine (DCEE), Chapter 1.3 will be fully dedicated to the Unsynchronized DCEE since it represents the foundation of this master thesis work.

1.3. Unsynchronized Double Compression Expansion Engine (DCEE)

This sub-chapter will investigate the horizontal split architecture, in particular the DCEE.

1.3.1. Problem(s) statement

To fully understand the idea behind the horizontal-split architecture, and therefore behind DCEE it's necessary to discuss the limitations of the classical Otto and Diesel cycles, in order to address such problems. Otto cycle is characterized by four corner points with temperature and pressure, same as per Carnot cycle, a isentropic compression and expansion are present, heat addition and rejection at constant volume instead of constant temperature for Carnot. [3]
It's possible to demonstrate that efficiency in Otto cycle only depends on temperature before and after compression:

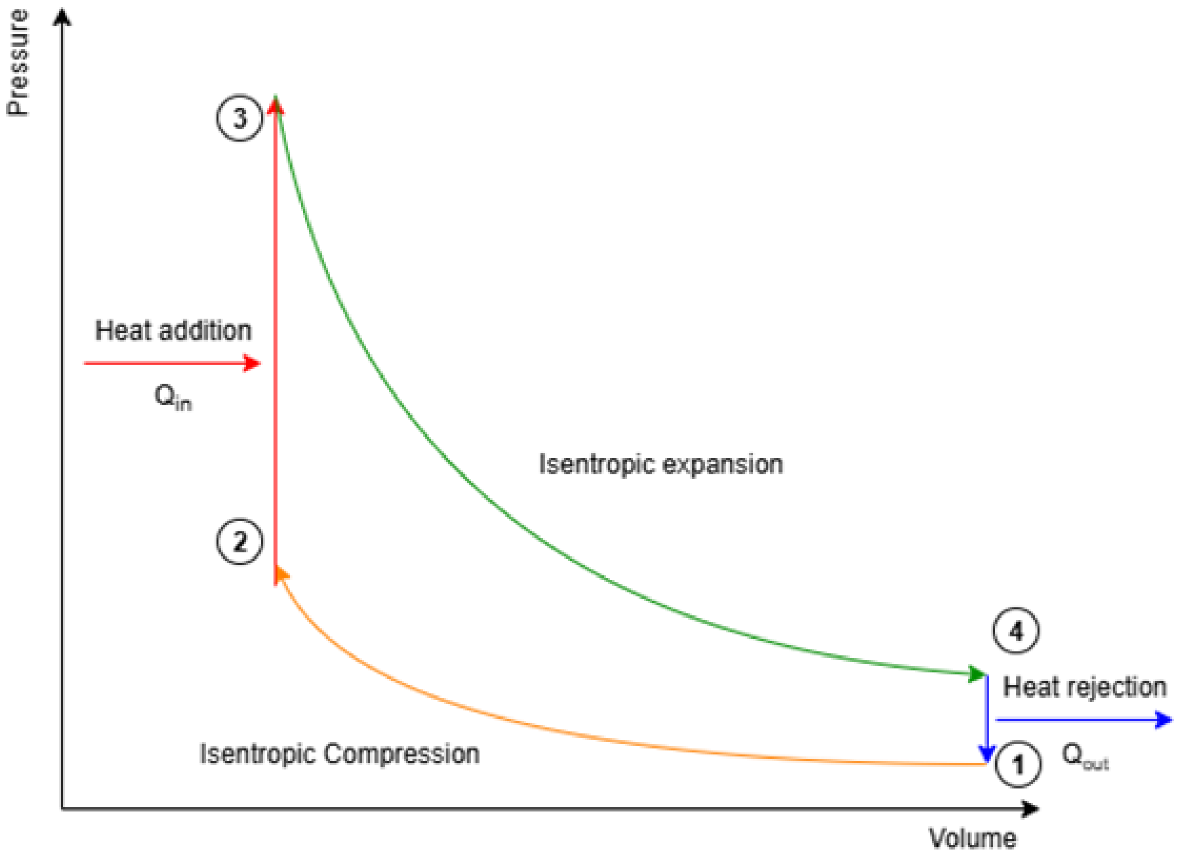

Figure 1.7: p-V diagram of Otto cycle

From first law of thermodynamics:

$$\delta U = Q - W \tag{1.1}$$

Since it's a cycle:

$$\delta U = 0 \tag{1.2}$$

$$Q_{in} - Q_{out} = Q = W \tag{1.3}$$

$$\eta_T = \frac{W}{Q_{out}} = \frac{Q_{in} - Q_{out}}{Q_{in}} = 1 - \frac{Q_{out}}{Q_{in}} \tag{1.4}$$

$$\eta_T = 1 - \frac{m \cdot c_v \cdot (T_4 - T_1)}{m \cdot c_v \cdot (T_3 - T_2)} = 1 - \frac{T_4 - T_1}{T_3 - T_2} \tag{1.5}$$

$$\frac{T_2}{T_1} = \left(\frac{V_1}{V_2}\right)^{\gamma-1} = r_c^{\gamma-1} = \left(\frac{V_4}{V_3}\right)^{\gamma-1} = \frac{T_3}{T_4} \tag{1.6}$$

$$\Rightarrow \frac{T_2}{T_1} = \frac{T_3}{T_4} \tag{1.7}$$

$$\eta_T = 1 - \frac{\left(\frac{T_4}{T_1} - 1\right) \cdot T_1}{\left(\frac{T_3}{T_2} - 1\right) \cdot T_2} = 1 - \frac{T_1}{T_2} = 1 - \frac{1}{R_C^{\gamma-1}} \tag{1.8}$$

The efficiency of the cycle, therefore, depends only on temperature before and after the compression stroke, same as per the Carnot cycle. The temperature after the Heat addition doesn't matter, thus amount of heat addition, C_v doesn't matter. [3]

The higher the load, more heat is added and T_3 becomes much higher than T_2. Then, for a given maximum temperature, the Otto cycle efficiency is much inferior to the Carnot cycle.

If we only add a very small amount of heat, T_3 becomes very close to T_2 and thus maximum temperature will be the very close to compression temperature. Then the Otto cycle will have almost the same efficiency as the Carnot cycle. For the ideal isochoric cycle:

$$\eta_T = 1 - 1/R_c^{\gamma-1} \tag{1.9}$$

In the classical Otto cycle two major limitations prevent the realization of its very high theoretical efficiency .

1. **High peak cylinder pressure**: the first concerns the extremely high peak cylinder pressures that result from large compression ratios. For instance, with a compression ratio of 60:1, the cycle would reach peak pressures on the order of 10^3 bar. [3]

2. **High heat losses**: the second limitation is related to severe heat transfer losses at high compression ratios.

   As the compression ratio increases, the combustion chamber exhibits a high surface-to-volume ratio at top dead centre, while combustion temperatures become very high.

   Together, these effects cause a significant amount of heat to be lost to the chamber walls. As a consequence, the practical efficiency gain quickly diminishes: when heat transfer losses are considered, a compression ratio of 60:1 provides no real benefit over values as low as 5:1. [3]

   Designing an engine structure capable of withstanding such loads is not only impractical but would also lead to excessive frictional losses, reducing the overall mechanical efficiency.

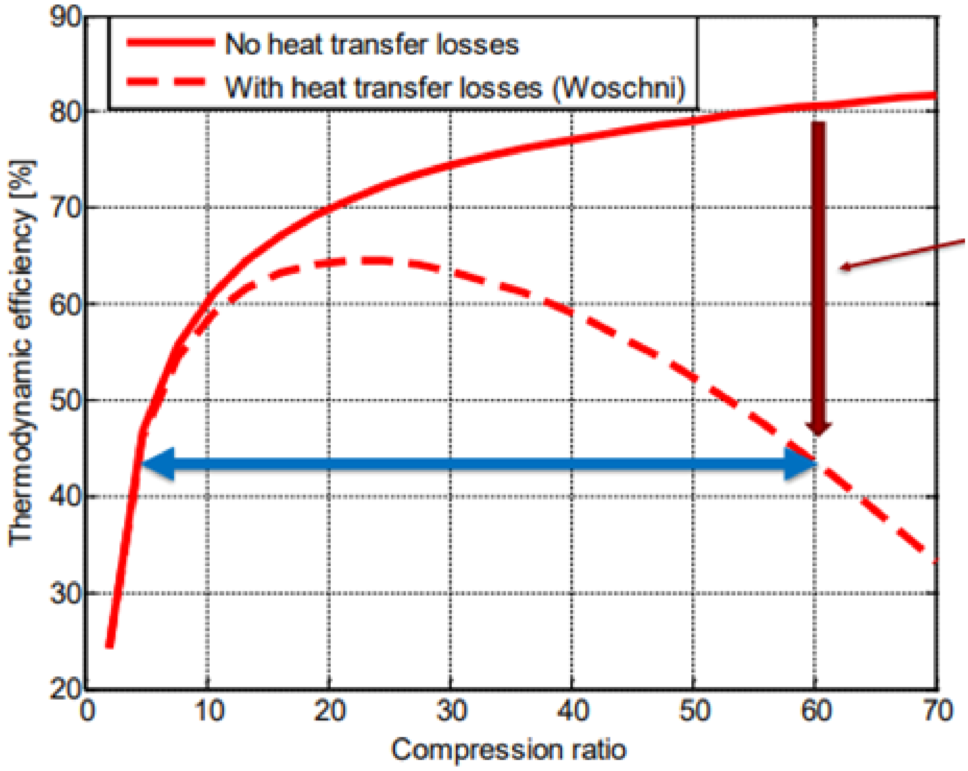

Figure 1.8: Thermodynamic efficiency as function of R_C[3]

To better understand the limitations of the Otto cycle, the following example is reported with hypothesized, but realistic data [3]

$$\gamma = 1.4, R_c = 60:1 \tag{1.10}$$

1.

$$P_1 = 1bar, T_1 = 320K \tag{1.11}$$

2. after compression:

$$P_2 = P_1 * R_c^{\gamma-1} = 309bar \tag{1.12}$$

$$T_2 = T_1 * R_c^{\gamma-1} = 1646K \tag{1.13}$$

3.

$$\gamma = 1.4,\ M = 29\ \Rightarrow\ C_v = 716\,\frac{kJ}{kg\,K},\ \lambda = 1 \tag{1.14}$$

$$T_3 = T_2 + dT = T_2 + \frac{1}{1+\frac{A}{F}} \cdot \frac{Q_{LHV}}{C_v} \tag{1.15}$$

$$= 1646 + \frac{1}{1+15.13} \cdot \frac{44 \times 10^6}{716} = 1646 + 3806 = \mathbf{5452\ K} \tag{1.16}$$

$$P_3 = P_2 \cdot \frac{T_3}{T_2} = 309 \cdot 3.31 = \mathbf{1022\ bar} \tag{1.17}$$

4. Expansion:

$$P_4 = P_3 \cdot R_c^{-\gamma} = 3.3 \text{ bar} \tag{1.18}$$

$$T_4 = T_3 \cdot R_c^{-(\gamma-1)} = 1060 \text{ K} \tag{1.19}$$

$$\eta_T = 1 - \frac{T_4 - T_1}{T_3 - T_2} = 0.806 \tag{1.20}$$

$$\text{IMEP} = 24.4 \text{ bar} \tag{1.21}$$

1. **Excessive peak pressure**

   One way to reduce such high cylinder pressures, 1022 Bar in this case, predicted at very high compression ratios is to replace constant-volume combustion with constant-pressure or mixed-mode combustion, as in Brayton or Diesel cycles.

   In these processes, heat is added while the piston is moving down, which allows the volume to increase during combustion.

   As a result, the pressure rise is null, this moderates the peak cylinder pressure to levels that can be tolerated by the engine structure, avoiding the need for excessively heavy and mechanically inefficient designs.

2. **Excessive heat transfer losses**

   At high compression ratios, the peak temperature of the cycle becomes extremely high, and the combustion chamber surface-to-volume ratio also increases, leading to severe heat transfer losses.

   This issue can be alleviated by reducing the peak temperature rise ($\mathrm{dT} = \mathrm{T_3} - \mathrm{T_2}$) rather than attempting to increase it.

   Strategies such as operating with lean mixtures (high lambda values) or adopting isobaric heat addition with higher specific heat (Cp instead of Cv) limit the maximum temperature reached in the cylinder. This concept, often referred to as low-temperature combustion, significantly decreases wall heat flux and allows the efficiency benefits of high compression ratios to be approached in practice. [3]

$$\gamma = 1.4, \quad R_c = 60 : 1$$

1. Starting point:

$$P_1 = 1 \text{ bar}, \qquad T_1 = 320 \text{ K}$$

2. Compression:

$$P_2 = P_1 \cdot R_c^{\gamma} = 309 \text{ bar}$$

$$T_2 = T_1 \cdot R_c^{\gamma-1} = 1646 \text{ K}$$

3. Combustion:

$$\gamma = 1.4, \ M = 29 \quad \Rightarrow \quad C_p = 1003 \, \frac{\text{kJ}}{\text{kg K}}, \qquad \lambda = 3$$

$$T_3 = T_2 + dT = T_2 + \frac{1}{1 + A/F} \cdot \frac{Q_{LHV}}{C_p} =$$

$$= 1646 + \frac{1}{1 + 3 \cdot 15.13} \cdot \frac{44 \times 10^6}{1003} = 1646 + 945 = \boxed{2591 \text{ K}}$$

$$P_3 = P_2 = \mathbf{309\ bar}$$

$$V_3 = V_2 \cdot \frac{T_3}{T_2} = V_2 \cdot 1.57$$

4. Expansion:

$$P_4 = P_3 \cdot R_e^{-\gamma} = 1 \text{ bar} \quad \text{gives } R_e = 60,$$

$$\text{and total expansion ratio of } 60 \cdot 1.57 = 94.2$$

$$T_4 = T_3 \cdot R_e^{-(\gamma-1)} = 504 \text{ K}$$

$$\eta_T = 1 - \frac{T_4 - T_1}{T_3 - T_2} = 0.806$$

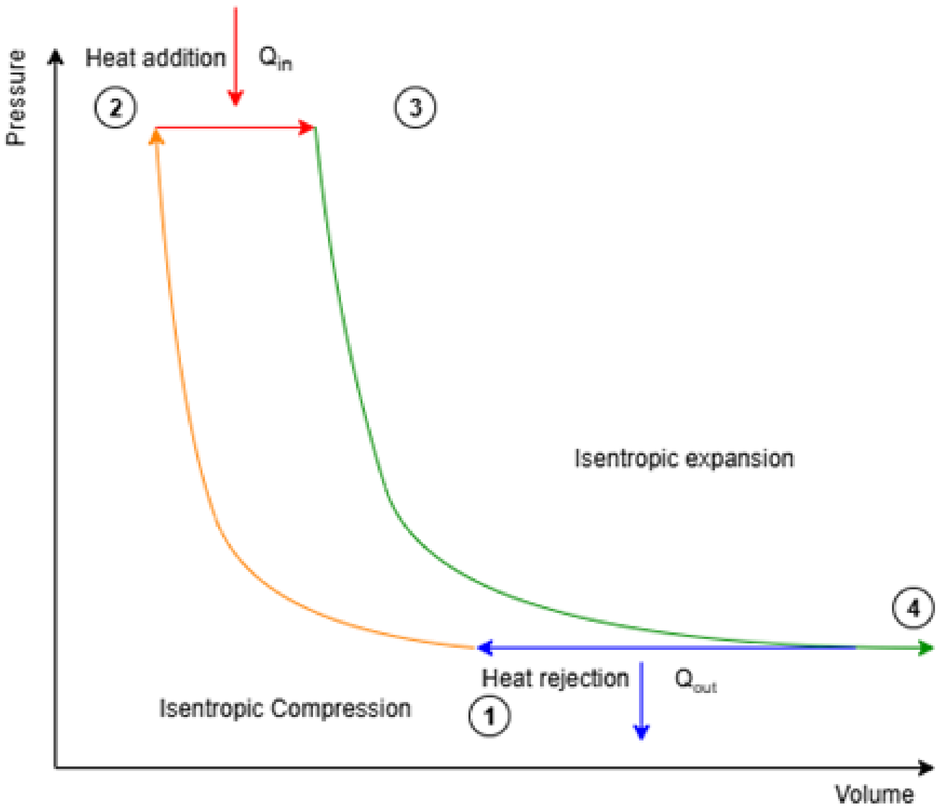

Figure 1.9: Brayton cycle

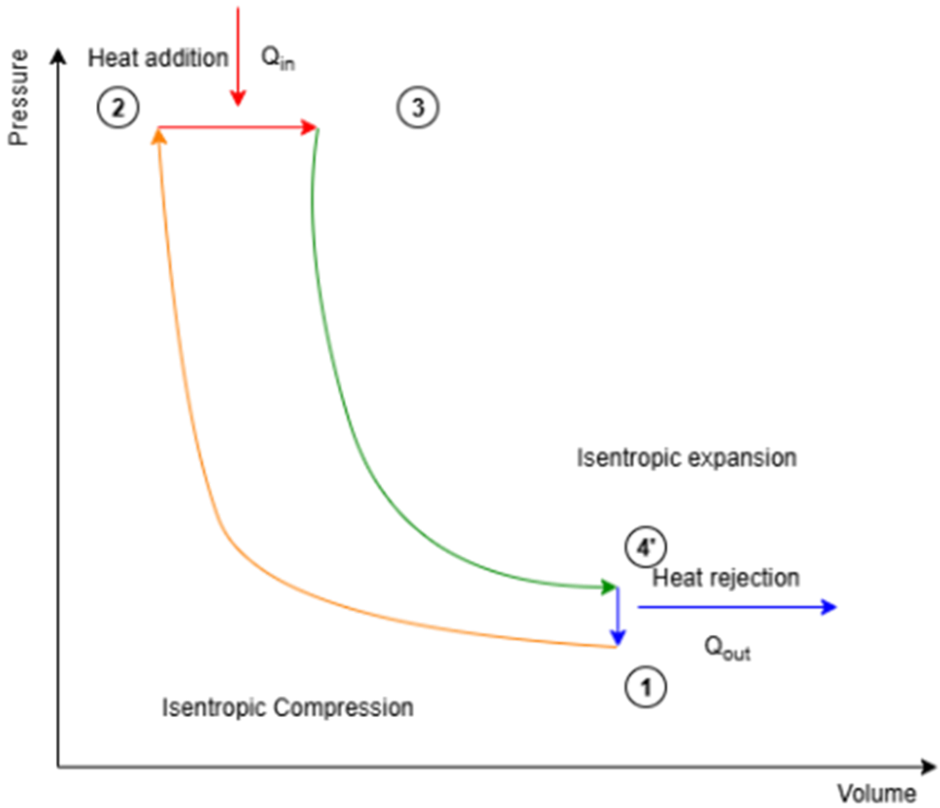

Figure 1.10: Diesel cycle

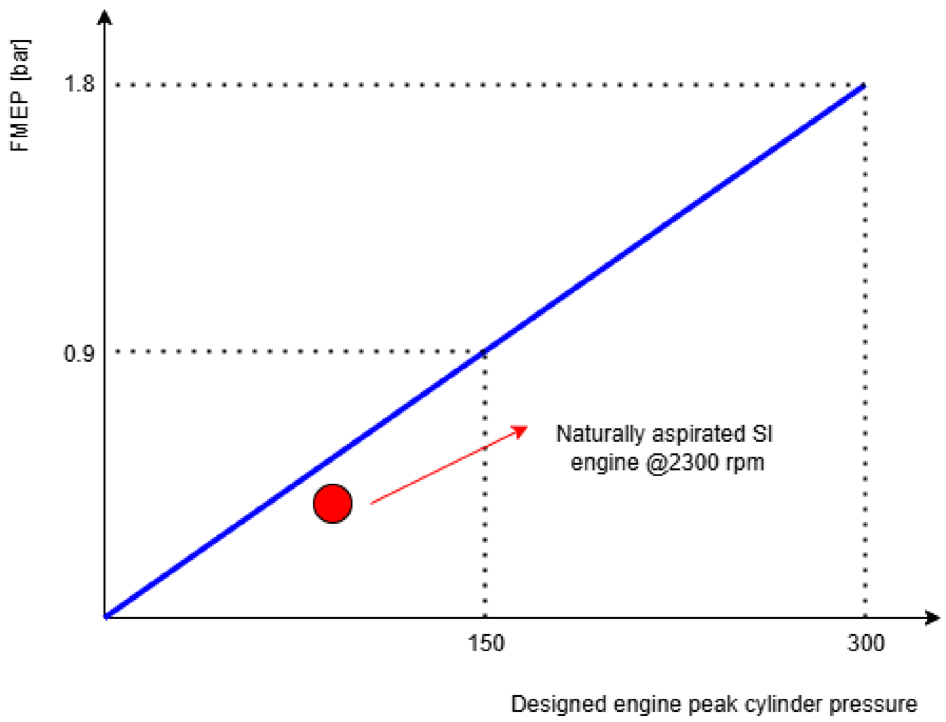

Figure 1.11: FMEP vs peak [3]

$$\text{IMEP} = \mathbf{6.06\ bar}, \quad 25\% \text{ lower than Otto cycle at } \lambda = 3$$

Very low IMEP values generate issues with friction, especially when the engine should be designed for high maximum pressure, engines that can handle high peak pressure have lower mechanical efficiency. FMEP stand for Friction Effective Mean Pressure, it's a loss term that represents the pressure equivalent of all mechanical and pumping losses inside the engine, it quantifies how much of the indicated pressure (therefore work) is lost before it becomes useful brake output. Formally is the difference between indicated mean effective pressure (IMEP, total work produced in the cylinder) and break mean effective pressure (BMEP, useful work measured at crankshaft).

$$FMEP = IMEP - BMEP \tag{1.22}$$

$$\eta_M = 1 - \frac{FMEP}{IMEP_{net}} \tag{1.23}$$

To overcome this drawback, one possible approach is to divide the overall compression and expansion processes into separate parts, so that each stage operates at a more favourable effective pressure ratio and avoids the excessive friction penalty associated with very low

IMEP.

1.3.2. Double Compression Expansion Engine - DCEE concept

In order to solve the issue related to excessive maximum pressure, compression and expansion processes can be divided into two equal stages, the overall compression ratio will be the product of the two. By considering the same 60:1 compression ratio:

$$\sqrt{60} = 7.75 => 7.75/1 * 7.75/1 = 60 : 1 \tag{1.24}$$

In order to solve the issue related to excessive heat losses, a cylinder with such compression ratio will have a good area/volume ratio at TDC, meaning much less heat losses.

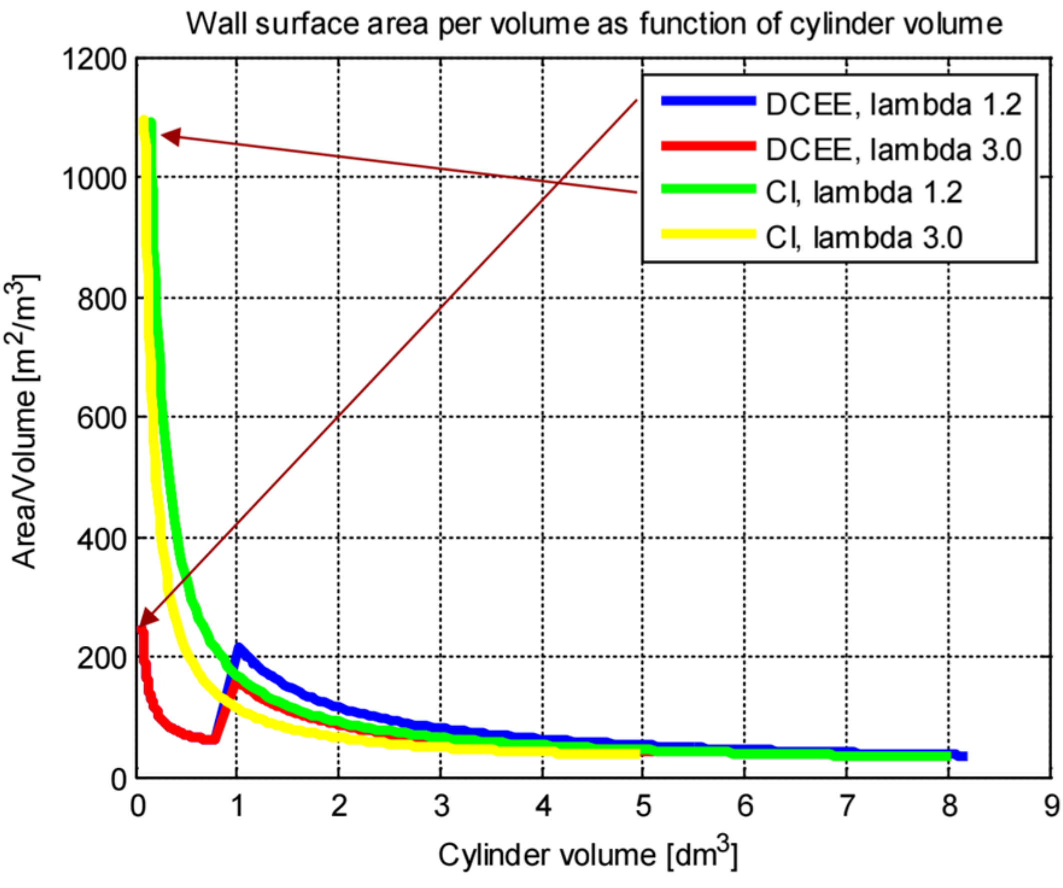

Figure 1.12: Wall surface area vs cylinder volume [3]

The fundamental idea behind the Double Compression Expansion Engine (DCEE) is to **address** precisely the **two intrinsic limitations of the classical Otto cycle**.

On one hand, the issue of **excessive peak pressures** is alleviated by modifying the

	Low Pressure cycle	High Pressure cycle
Peak Pressure	30 bar	300 bar
Load range BMEP	0-5 bar	35-80 bar
Friction FMEP	0.05-0.1 bar	1.2-2.2 bar

Table 1.1: DCEE Cycles characteristics [3]

combustion process so that heat addition is not purely isochoric, but instead incorporates constant-pressure characteristics, thereby moderating the maximum pressure rise. On the other hand, the problem of **excessive heat transfer losses** is mitigated by distributing the overall compression and expansion ratios across multiple cylinders.

This staged approach ensures that each unit operates with a more favorable surface-to-volume ratio and at moderated temperature levels, reducing wall heat flux. In essence, the DCEE concept builds upon the theoretical efficiency potential of the Otto cycle while restructuring the process to eliminate its two major practical barriers. The cycle is divided into two sub-cycles: In order two accommodate the two cycles at least 4 cylinders are required, since the engine is 4 stroke; two cylinders will manage the high pressure cycle 2 cylinders will manage the low pressure one.

In the framework of the Double Compression Expansion Engine (DCEE), two fundamental aspects must be addressed: the operating cycle configuration and the synchronization approach. The cycle configuration can follow two alternatives.

- **Operating configuration:** In the 2+4+2 strokes arrangement, the high-pressure cylinders operate according to the conventional four-stroke cycle (intake, compression, expansion, exhaust), while the low-pressure cylinders are dedicated to specific tasks, with one acting as a first-stage compressor and the other as a second-stage expander. In contrast, in the 4+4 strokes arrangement, all cylinders, both high- and low-pressure, perform the complete four-stroke sequence.

- **Synchronization**. In non-synchronized systems, two buffer tanks, one at low pressure and one at high pressure, are used to temporarily store the working fluid between the respective stages, thus decoupling the operation of the cylinders. In synchronized systems, instead, the absence of such tanks requires direct connection between cylinders, making accurate timing and coordination indispensable.

1.3.3. Unsynchronized DCEE 2+4+2 concept and operating principle

The first model that can be identified is the 2+4+2 strokes, unsynchronized. The simplest layout that has been theorized includes:

- 1 high - pressure cylinder: to allow HP compression and expansion of the working fluid;
- 2 low - pressure cylinders: one first-stage compressor, and one second-stage expander;
- 1 low- pressure buffer tank: to allow isobaric transfer of the working fluid from LP to HP cylinder;
- 1 high- pressure buffer tanks to allow isobaric transfer of the working fluid from combustor to LP expander.

Such model has already been implemented by Dr. Lam Nhut at Lund University, where he investigated both experimentally and via simulation the improvement in brake efficiency for unsynchronized DCEE.

LP Compressor

Valves layout:

- 1 inlet valve naturally aspirates air from environment;
- 1 outlet valve allows compressed air into LP buffer tank.

The low-pressure cylinder works on 2-strokes cycle completed over one full crankshaft revolution, following the following p - V diagram: **1** $\rightarrow$ **2**: Inlet of ambient air, cylinder moves from TDC to BDC; **2** $\rightarrow$ **3**: compression and transfer to LP pressure tank, valve opens close to TDC; **3** $\rightarrow$ **4**: transfer of working fluid to LP tank; **4** $\rightarrow$ **1**: re-expansion to equalize the in-cylinder pressure to ambient one.

HP combustor

valves layout:

- 1 inlet valve aspirates air from LP buffer tank;
- 1 outlet valve to HP buffer tank.

The high pressure cylinder works on 4-strokes cycle completed over two full crankshafts revolutions, following the following p-V diagram: **1** $\longrightarrow$ **2**: Inlet of compressed air from LP tank, cylinder moves from TDC to BDC; **2** $\longrightarrow$ **3**: second compression stage begins; **3** $\longrightarrow$ **4**: at the end of second compression stage fuel is injected and combustion is initiated; **4** $\longrightarrow$ **5**: second expansion stage, piston goes from TDC to BDC; **5** $\longrightarrow$ **6:** exhaust blow-down, combusted gas transfers to HP tank, partially allowing expansion; **6** $\longrightarrow$ **7:** exhaust gas is pushed to HP tank; **7** $\longrightarrow$ **1:** gas exchange where exhaust valve closes while inlet valve opens and a new cycle can be started again.

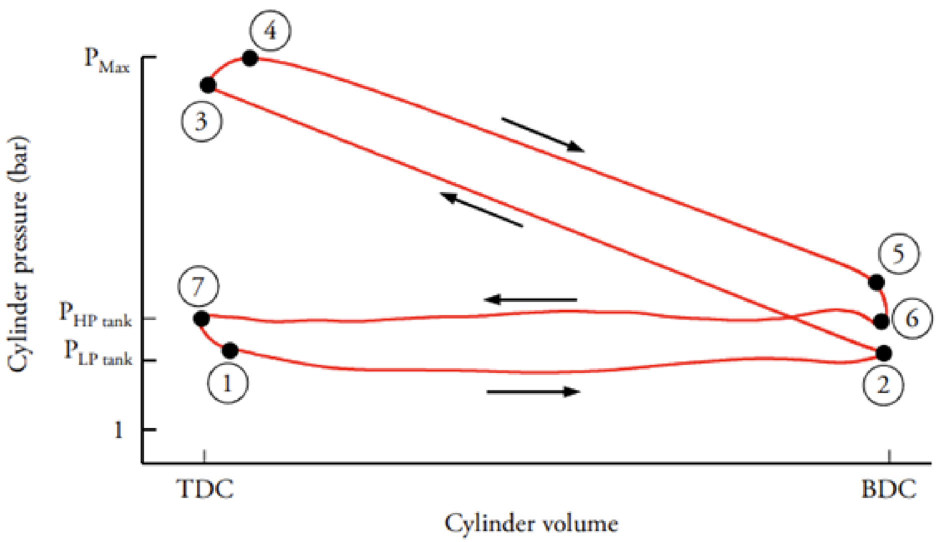

Figure 1.13: p-V diagram of HP cylinder

LP expander

- 1 inlet valve naturally aspirates air from HP buffer tank;
- 1 outlet valve allows air to ambient.

The low pressure expander works on 2-strokes cycle completed over one full crankshafts revolution, following the following p-V diagram:

1 $\longrightarrow$ **2**: Inlet of compressed exhaust fumes from HP tank, cylinder moves from TDC to BDC; **2** $\longrightarrow$ **3**: expansion, valve opens close to TDC; **3** $\longrightarrow$ **4**: gas is expelled into ambient through exhaust valve, close to TDC valve closes. **4** $\longrightarrow$ **1**: a short re-compression is performed to bring the in-cylinder pressure to the same level as the HP tank.

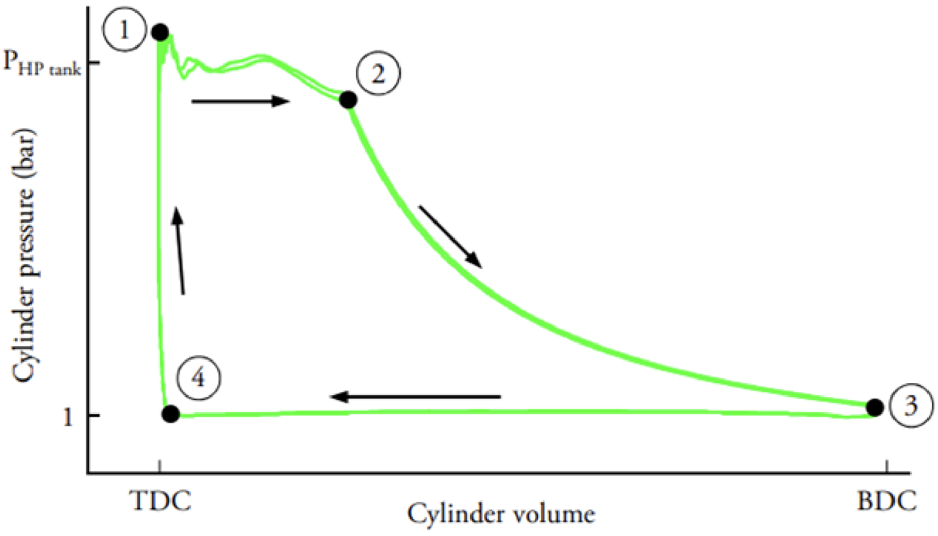

Figure 1.14: p-V diagram of LP expander

Results achieved

Experimental conditions and results The experimental campaign on the DCEE 2-4-2 single-cylinder test rig was designed to investigate how key boundary conditions affect combustion behavior and overall efficiency. [5] Tests were performed at a constant speed of 1200 rpm while systematically varying inlet conditions and fueling to quantify their influence on indicated efficiency and combustion characteristics. The experimental test rig, operated with 5 different nominal fueling rates and 3 inlet pressure levels, while keeping $\lambda > 1.2$ to ensure good combustion, test condition are summarized in the plot and results in the table below. As expected, peak cylinder pressure increases with inlet pressure and engine load, only OP10, where a slower combustion rate due to lower injection pressure reduces peak cylinder pressure. The peak of heat release for such point is lower compared to OP9, even though fueling rate is higher.

Majority of operating points achieved GIE between 46.3% and 47.6%, operating points that achieved GIE<46% have in common that λ is below 1.3. moreover, the highest fueling point (OP10), also suffers from later combustion phasing which reduces effective expansion ratios and GIE decreases to <44%.

The 2+4+2 concept, compared to the 4+4 that is going to be analysed in the following chapter, has the advantage of reducing flow losses due to larger available valve area in the cylinders' heads. [5]

The experimental study of the DCEE 2+4+2 concept demonstrated notable improvements over the 4+4 configuration (that will be analysed later) , primarily due to reduced

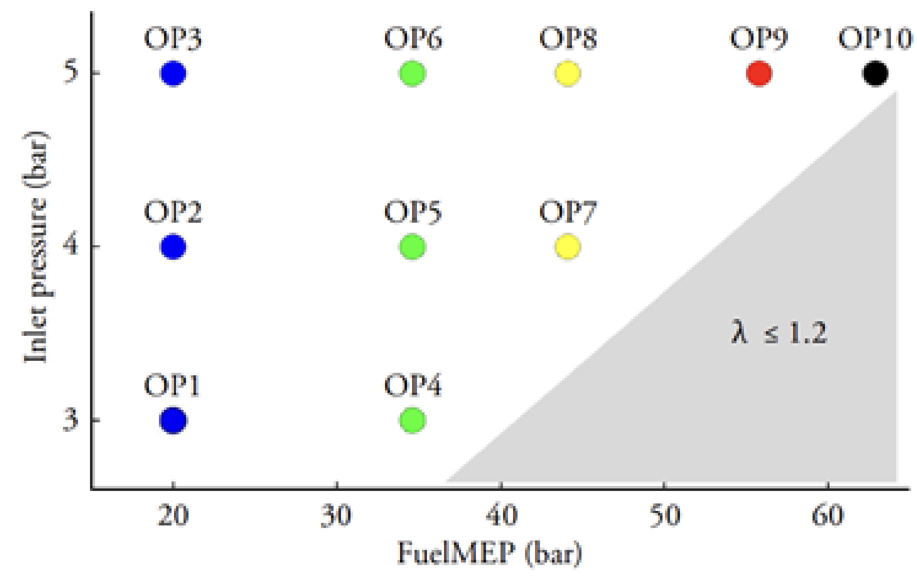

Figure 1.15: Experimental operating points 2+4+2 [5]

Operating point (OP)	1	2	3	4	5	6	7	8	9	10
P_{inlet} (bar)	3.0	4.0	5.0	3.0	4.0	5.0	4.0	5.0	5.0	5.0
Nom. *FuelMEP* (bar)		20			34		44		56	63
Fuel flow, $\dot{m}_f$ (g/s)	0.98	0.99	1.00	1.72	1.68	1.72	2.18	2.18	2.76	3.10
Inj. fuel mass, (mg/cycle)	98	99	100	172	168	172	218	218	276	310
CA_{50} (°CA aTDC$_{Fire}$)	4.7	5.1	6.7	9.3	8.7	9.3	11.5	9.7	10.7	13.3
$T_{exhaust}$ (°C)	393	346	292	605	525	417	638	503	580	663
Measured *FuelMEP* (bar)	19.9	20.1	20.3	34.8	34.1	34.9	44.1	44.2	55.8	62.9
λ (-)	2.31	2.92	3.85	1.27	1.56	2.20	1.28	1.67	1.36	1.24
η_C (%)	99.9	99.8	99.9	99.6	99.9	99.9	99.6	99.9	99.9	99.1
$IMEP_g$ (bar)	9.4	9.5	9.5	15.5	16.2	16.5	20.0	21.0	25.9	27.4
$IMEP_n$ (bar)	6.5	4.8	5.8	12.7	11.7	12.6	15.5	17.0	22.1	23.3
GIE (%)	47.0	47.5	46.7	44.6	47.5	47.2	45.3	47.6	46.3	43.6

Figure 1.16: Experimental results 2+4+2 [5]

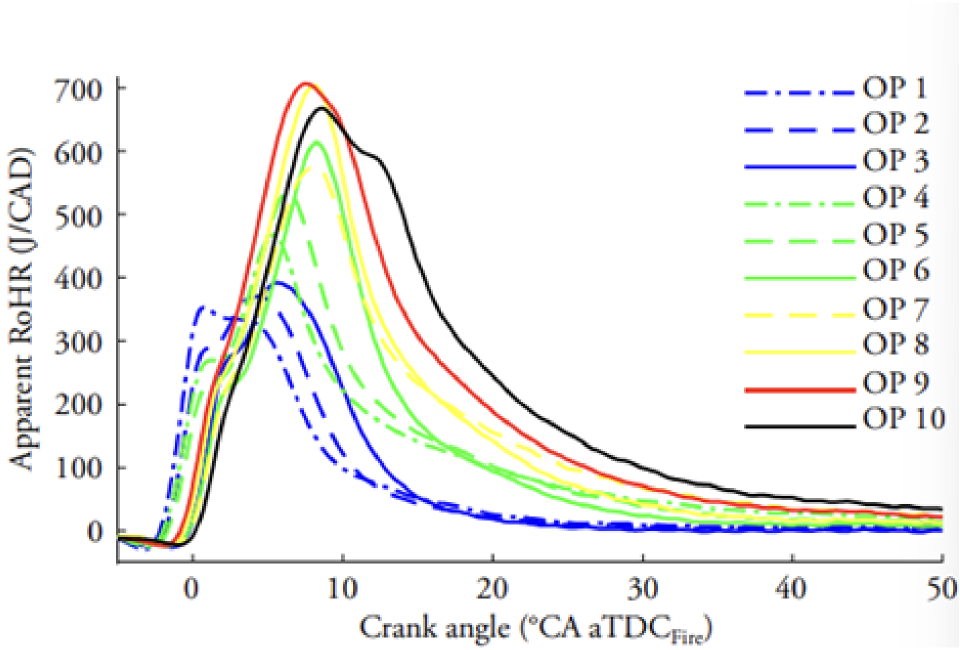

Figure 1.17: Apparent heat release rate [5]

flow losses from larger valve areas, the possibility of over-expansion, and flexible cylinder phasing. Ten operating points were tested at five fueling rates (20–63 bar FuelMEP) and three inlet pressures (3–5 bar). The gross indicated efficiency reached around 47 % for most points, although lower efficiencies (45.3 %) were observed when operating with lambda < 1.30, indicating poorer combustion efficiency. This drop could not be fully explained by combustion inefficiency alone; increased heat transfer and exhaust losses were also contributing factors.

Simulation results

To assess system brake efficiency, a GT-Power simulation model was calibrated using the experimental data. The simulations showed that excessive inlet pressure at low loads caused substantial efficiency losses. At 20 bar FuelMEP, brake efficiency decreased from 41.8 % at 3 bar inlet pressure to 29.4 % at 5 bar, mainly due to higher charge-air cooling losses and limited dilution benefits. The highest brake efficiency was achieved at 56 bar FuelMEP and 5 bar inlet pressure, reaching 51.0 %, and further increased to 52.8 % when the combustion cylinder exhaust ports were insulated, raising exhaust temperature by 30 °C. This operating condition was selected as the reference point for subsequent optimization studies. [5]

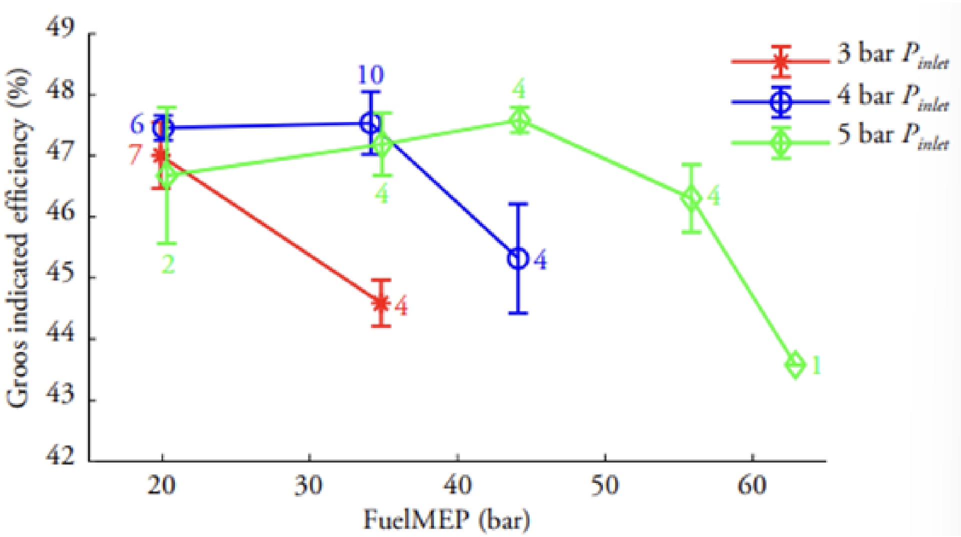

Figure 1.18: GIE for 10 operating points [5]

1.3.4. Unsynchronized DCEE 4+4 concept and operating principle

The second model that can be identified is the 4+4 strokes, unsynchronized. The simplest layout that has been theorized includes:

- 1 high -pressure cylinder: to allow HP compression and expansion of the working fluid;
- 1 low -pressure cylinder: to allow LP compression and expansion of the working fluid;
- 1 low-pressure buffer tank: to allow isobaric transfer of the working fluid from LP to Hp cylinder;
- 1 charge air-cooler: to decrease HP compressed gas temperature.

The LP cylinder has the same function of a turbocharger in 4-strokes engines (i.e. pre-compressing the working fluid before the combustor), with the difference that the turbo machine has been replaced with a piston machine.

LP cylinder

Valves layout :

- 1 inlet valve naturally aspirates air from environment;
- 1 inlet valve allows to transfer exhaust fumes from cross-over channel into the cylin-

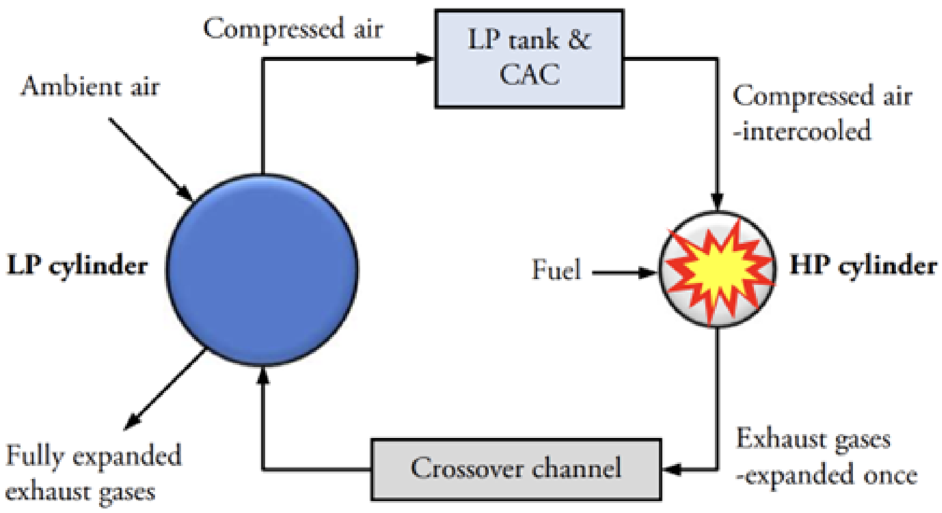

Figure 1.19: 4+4 unsynchronized DCEE concept [5]

der;

- 1 outlet valve allows compressed air into LP buffer tank;
- 1 outlet valve to allow expanded exhaust fumes to ambient.

The low pressure cylinder works on 4-strokes cycle completed over two full crankshafts revolutions, following the following p-V diagram: **1** $\rightarrow$ **2**: Inlet of ambient air, cylinder moves from TDC to BDC; **2** $\rightarrow$ **3**: compression and transfer to LP pressure tank, valve opens close to TDC-, **3** $\rightarrow$ **4**: transfer of working fluid to LP tank; **4** $\rightarrow$ **5**: Inlet of ambient air, cylinder moves from TDC to BDC, recomposition of residual air to match pressure at TDC; **5** $\rightarrow$ **6:** induction of combusted gas from HP cylinder and perform second expansion stroke. This happens simultaneously with HP cylinder's exhaust stroke (**5** $\rightarrow$ **6**); **6** $\rightarrow$ **1:** exhaust gas is expelled into ambient.

HP cylinder

Valves layout :

- 1 inlet valve naturally aspirates air from LP tank;
- 1 outlet valve to crossover channel;

The high pressure cylinder works on 4-strokes cycle completed over two full crankshafts revolutions, following the following p-V diagram: **1** $\rightarrow$ **2**: Inlet of compressed air from LP tank, cylinder moves from TDC to BDC; **2** $\rightarrow$ **3**: second compression stage close to TDC fuel is injected and combustion takes place; **3** $\rightarrow$ **4**: combustion; **4** $\rightarrow$ **5**: first expansion

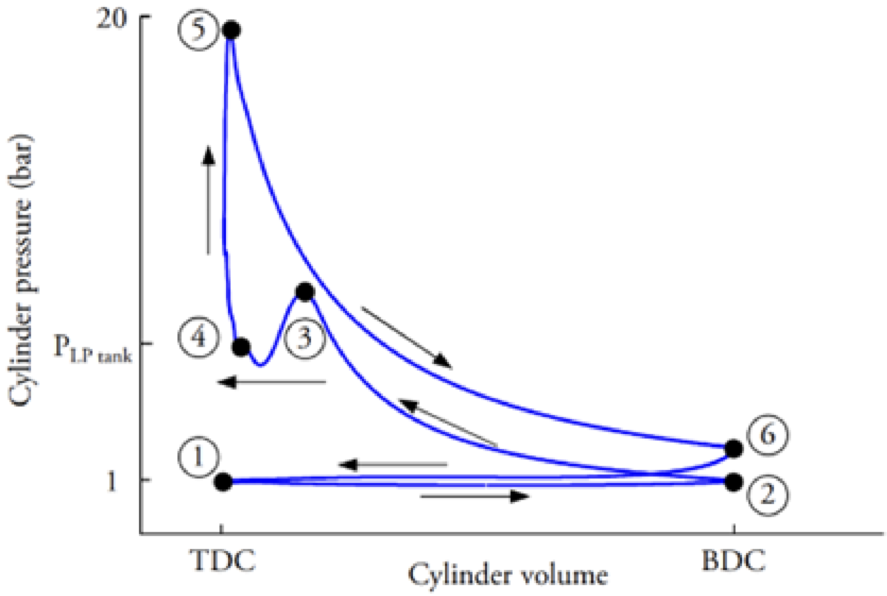

Figure 1.20: p-V diagram of LP cylinder

stage, piston goes from TDC to BDC; **5 → 6:**outlet stroke, combusted gas transfers to LP cylinder via the cross-over channel, since displacement of LP cylinder is larger than HP, this is a second expansion stage .

Results achieved

Simulation results The 4+4 strokes layout has been studied only using simulations and without experimental rigs, Assuming an intake pressure of 8 bar, a peak cylinder pressure of 300 bar, and low-temperature combustion, the brake efficiency reached 56.0% [5]. For comparison, a conventional compression-ignition combustion engine achieved a brake efficiency of 54.5%, although it was capable of operating at higher loads. The high-load DCEE configuration employs a charge air cooler, which reduces the charge temperature and consequently minimizes heat transfer losses while improving gas properties. As the concept does not rely on high dilution to achieve its performance, the overall load-handling capability is significantly enhanced [5]. Further analysis focused on the part-load efficiency of the DCEE concept, with two alternative load control strategies investigated. The first, the Lambda control strategy, adjusts only the fuel flow under low-load conditions, while the second, the Miller strategy, controls the air flow through late inlet valve closing. Each approach exhibited distinct advantages and drawbacks. The Lambda strategy demonstrated higher thermodynamic efficiency, attributed to the increased dilution associated with this method. However, this also led to higher cylinder pressures, resulting in increased mechanical friction losses. For the range of loads examined, the brake efficiency

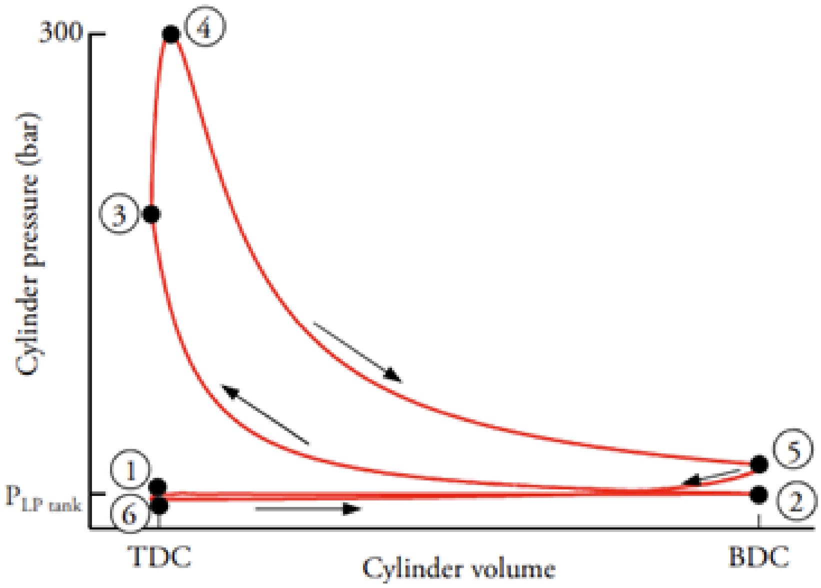

Figure 1.21: p-V diagram of HP cylinder

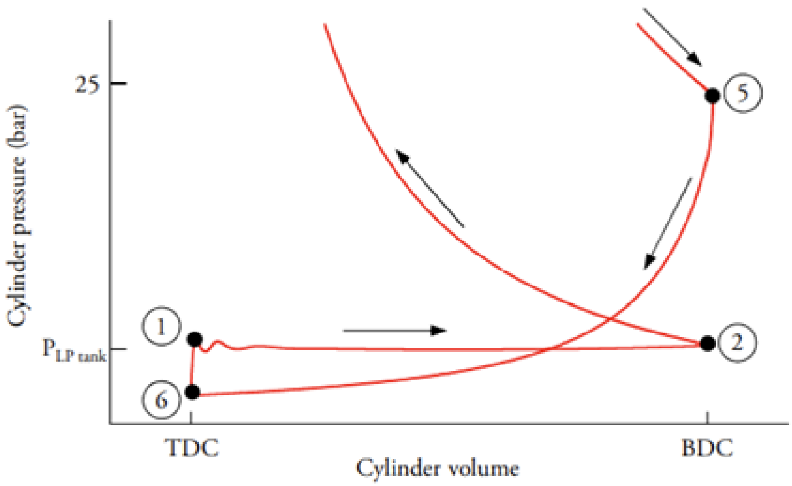

Figure 1.22: zoom of the diagram

was found to be highest when the Lambda control strategy was combined with charge air cooling. At low loads, the benefits of charge air cooling were limited due to the lower contribution of the expansion work, whereas at medium and high loads, the use of charge air cooling became increasingly advantageous, leading to improved overall system brake efficiency. It was also observed that the low-pressure (LP) cylinder represented a source of gas exchange losses, as it must handle four distinct gas flow paths. Consequently, the effective flow area available for the LP cylinder is only about half that of a conventional four-stroke engine, which inherently reduces the flow efficiency. A further drawback of the 4–4 configuration lies in the use of the same cylinders for both compression and expansion stages, which restricts the potential for over-expansion optimization. Moreover, synchronization of the high-pressure (HP) and low-pressure (LP) cylinders on the same working cycle eliminates the possibility of adjusting the phase relationship between them. This synchronization constraint limits the opportunity to use phase shifting as a means of balancing the engine in terms of noise, vibration, and harshness (NVH) characteristics. [5]

1.3.5. Considerations on unsynchronized DCEEs

In the non-synchronized configuration, the use of low- and high-pressure buffer tanks decouples the cylinders and removes the need for strict timing. While this eases the design of each sub-process, the introduction of external volumes leads to additional inefficiencies. [6]

Gas stored in the tanks is exposed to heat transfer with the walls, which increases thermal losses, and every filling and emptying process is accompanied by throttling and flow resistance that contribute to pressure losses. Moreover, the tanks add dead volume that does not contribute to work production but still affects the cycle dynamics, reducing the overall effectiveness of the concept. [6]

The synchronized version of the Double Compression Expansion Engine addresses these drawbacks by eliminating the intermediate tanks and directly coupling the low- and high-pressure cylinders. This results in a more compact layout with fewer parasitic losses but requires precise synchronization to secure proper charge transfer and avoid problems such as backflow or pressure mismatches. [6]

Without the stabilizing effect of the tanks, the system achieves a faster dynamic response, which is beneficial for applications with rapid load variations, but it also introduces challenges in terms of valve control and coordination. Investigating the synchronized concept is therefore essential to evaluate whether its efficiency benefits can outweigh the added complexity of control and phasing. [6]

In the next chapter the synchronized version of both cycles, 2+4+2 and 4+4, will be investigated to avoid such inefficiencies and heat losses.

1.3.6. Study on unshynchronized H2DCEEs

A recent and particularly relevant development in the field of advanced internal combustion concepts is the hydrogen double compression–expansion engine (H2DCEE). This configuration represents the extension of the double compression–expansion engine (DCEE) architecture to hydrogen fueling, with the aim of combining the thermodynamic benefits of the cycle with the potential of hydrogen as a zero-carbon energy carrier. In the study by Babayev et al. (2022), the H2DCEE was proposed and investigated using a combination of three-dimensional computational fluid dynamics (CFD) simulations, validated against experimental data, and one-dimensional GT-Power system modeling [6]. The central goal was to assess whether an internal combustion system based on hydrogen could reach efficiency levels comparable to fuel cells, which are often considered the benchmark for future transport powertrains. The authors started from the established DCEE framework, which separates the compression, combustion, and expansion processes into three dedicated cylinders. This arrangement allows for very high effective compression ratios, improved control over combustion phasing, and reduced heat transfer losses due to the possibility of highly insulating the expander unit. The study then coupled this architecture with high-pressure direct injection (HPDI) of hydrogen, operating in a non-premixed, compression-ignition mode. This strategy was chosen to avoid the efficiency limitations and knock propensity of spark-ignited hydrogen engines, while exploiting hydrogen's favourable reactivity and avoiding soot formation. Several system-level modifications were systematically explored to maximize brake thermal efficiency (BTE). These included insulating the expander, eliminating intercooling, dehumidifying the exhaust gas recirculation (EGR), and introducing a catalytic burner in the exhaust of the combustor. Each measure contributed incremental gains in efficiency, and their combined effect was shown to be significant. Furthermore, by employing a larger compressor capable of raising peak pressures to 300 bar, the authors demonstrated an additional efficiency increase, provided that sufficiently high injector–cylinder differential pressures were ensured. The optimization process also investigated the effect of equivalence ratio, finding that a lean mixture with lambda 1.4 offered the best compromise between combustion and mechanical efficiency. [6]

The results of this comprehensive parametric study were remarkable: the H2DCEE

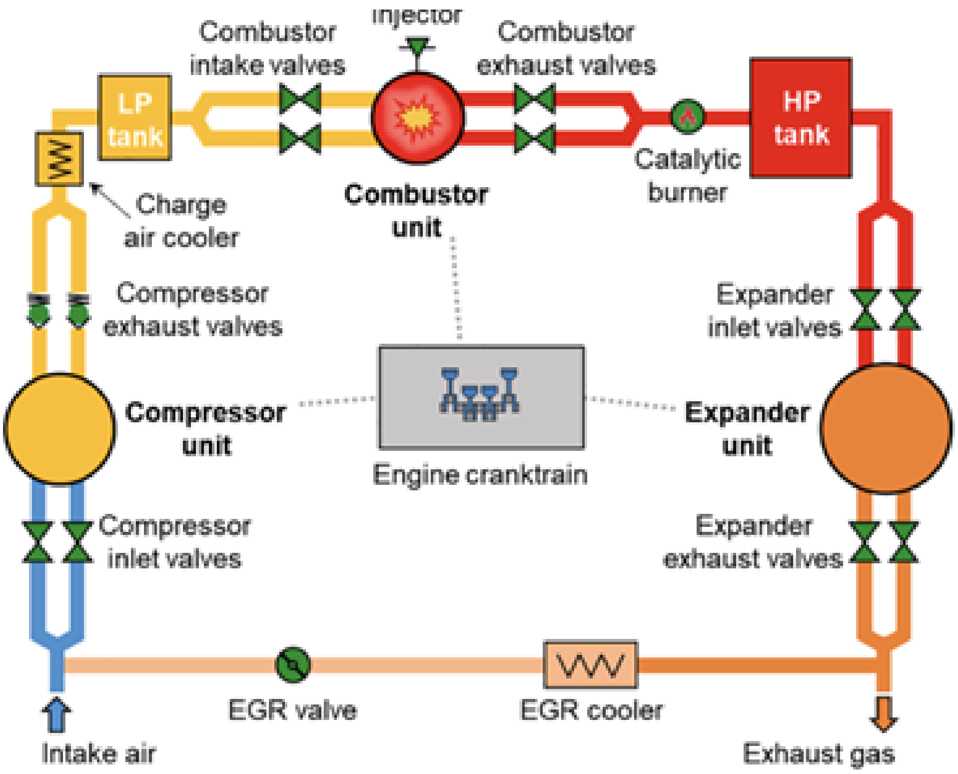

Figure 1.23: GT-Power layout for H2DCEE [6]

achieved a peak brake thermal efficiency of 60.3% at 45 bar brake mean effective pressure. This efficiency level is not only around five percentage points higher than the best-performing diesel-fueled DCEE configuration, but also approaches the typical efficiency of fuel cell systems. Importantly, the study also emphasized additional benefits unique to hydrogen combustion, such as the net molar expansion effect associated with hydrogen injection at top dead center, which directly increases the fraction of chemical energy converted into useful work, and the absence of a soot–NOx trade-off, which simplifies the path towards ultra-low emissions. [6]

Taken together, the H2DCEE study provides one of the most compelling demonstrations to date that internal combustion engines, when coupled with advanced cycle concepts and hydrogen fueling, can remain highly competitive in a decarbonized transport landscape. It shows that the combination of thermodynamic cycle innovation and hydrogen's unique combustion characteristics may enable engines to reach efficiencies previously considered attainable only by fuel cells. [6]

The development of the synchronized DCEE has the potential to push efficiency levels beyond those already achieved with the non-synchronized architecture. While conventional internal combustion engines rarely exceed brake thermal efficiencies of 40–45%, the hydrogen-fueled DCEE (H2DCEE) has already demonstrated the possibility of surpassing 60%. [6]

Introducing synchronization could further reduce dissipation losses associated with intermediate tanks and mass transfer, thereby improving the thermodynamic performance of the cycle. This means that the synchronized configuration might allow DCEEs to go beyond the already remarkable efficiency advantage it holds over traditional ICEs, strengthening its role as a highly competitive pathway for sustainable propulsion. [6]

2 | Synchronized DCEEs

Synchronization in the Double Compression Expansion Engine (DCEE) refers to the **direct coupling** of the compressor, combustor, and expander cylinders **without the use of intermediate buffer tanks.**
In the non-synchronized configuration, low- and high-pressure accumulators act as reservoirs that smoothen the flow and simplify operation, but at the expense of additional heat transfer losses and gas-dynamic inefficiencies. By contrast, a synchronized arrangement requires precise phasing of the cylinders but enables the working fluid to be transferred directly between stages, minimizing storage-related dissipations and improving the thermodynamic integrity of the cycle.

This architectural shift makes synchronization a promising step for unlocking higher efficiencies in DCEE systems.

2.1. Synchronized DCEE 2+4+2 concept and operating cycle

The first model that can be identified is the 2+4+2 strokes. The simplest layout that has been theorized includes:

- 2 high -pressure combustors: to allow HP compression and expansion of the working fluid;
- 1 low -pressure compressor: to allow LP compression of the working fluid;
- 1 low -pressure expander: to allow LP expansion of the working fluid;

The LP cylinder has the same function of a turbocharger in 4-strokes engines (i.e. pre-compressing the working fluid before the combustor), with the difference that the turbo machine has been replaced with a piston machine. In this case it's possible to see that no buffer tanks are present, therefore valve timing between HP and LP cylinders must be tuned carefully in order to allow timed and efficient gas exchange. Moreover, the connecting pipes must be carefully dimensioned to avoid them working as buffer thanks,

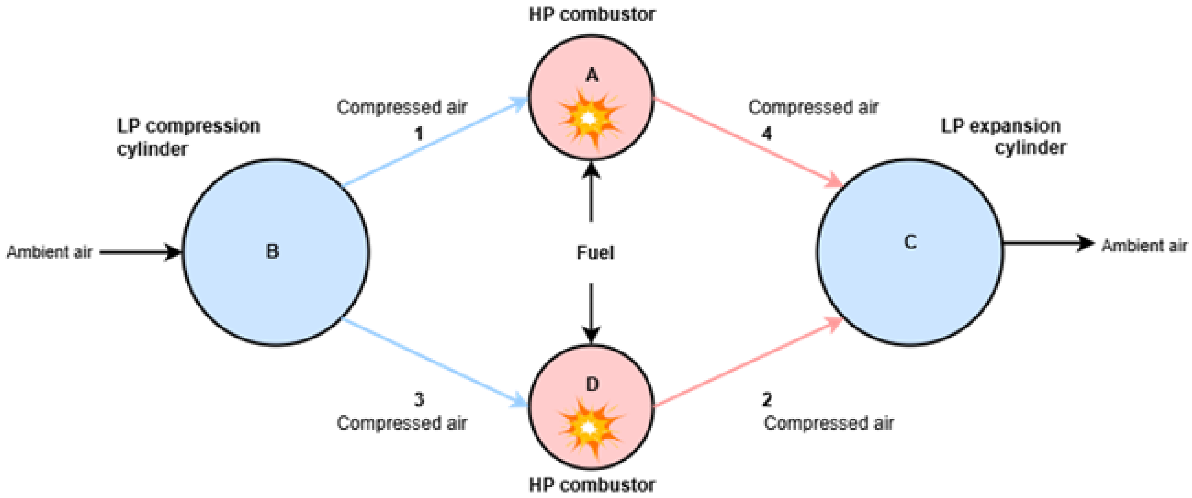

Figure 2.1: 2+4+2 Synchronized DCEE concept

increasing losses and decreasing efficiency.

LP compressor

Valves layout:

- At least 1 inlet valve, probably 2 to naturally aspirate air from environment;
- At least 2 outlet valves, to allow compressed air into each HP combustors;

The low-pressure compressor works on 2-strokes cycle completed over one full crankshafts revolution, following the following p -V diagram:

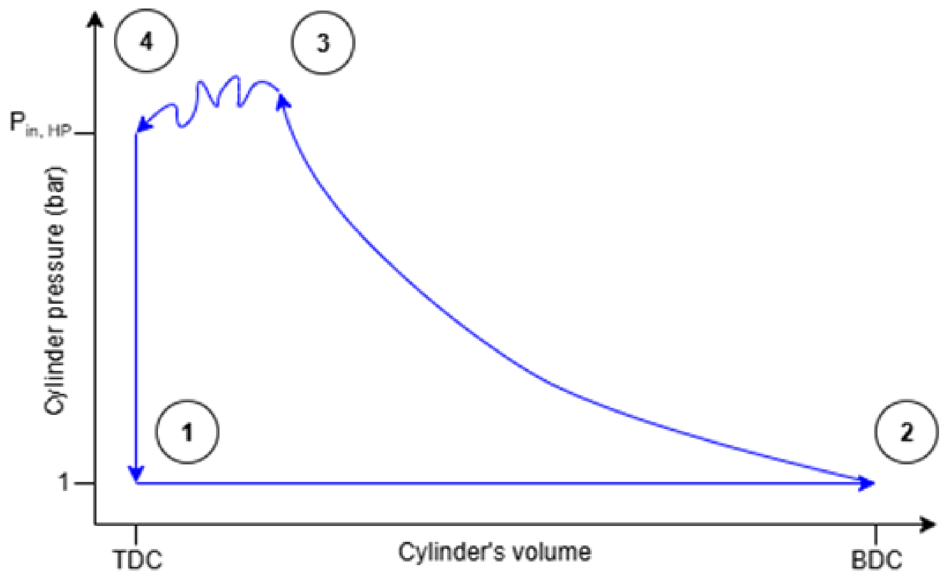

Figure 2.2: LP compressor working cycle

1 → 2: **Inlet** of ambient air, cylinder moves from TDC to BDC, pressure remains constant;

2 → 3: **compression,** valve opens close to TDC;

3 → 4: **transfer** of working fluid to HP cylinder;

4 → 1: **re-expansion** to equalize the in-cylinder pressure to ambient one;

LP expander

Valves layout:

- At least 2 inlet valves, to allow exhaust gas from each HP combustors into it;
- At least 1 outlet valve, probably 2 to allow expanded air into ambient;

The low-pressure expander works on 2-strokes cycle completed over two full crankshafts revolutions, following the following p-V diagram:

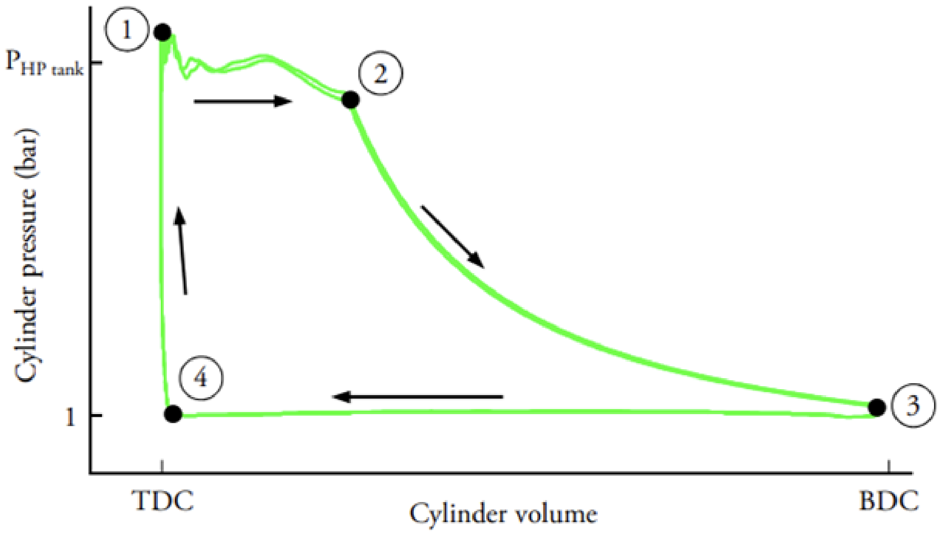

Figure 2.3: LP expander working cycle

1 → **2**: **gas transfer** from HP combustor to LP expander;

2 → **3**: **2nd stage expansion,** inlet valve opens and air ;

3 → **4**: **exhaust** transfer of exhaust fumes to ambient;

4 → **1**: **re-expansion** to equalize the in-cylinder pressure to HP outlet one;

HP combustor

Valves layout:

- At least 1 inlet valve, probably 2 to allow 1-stage compressed air in HP cylinder;
- At least 1 inlet valve, probably 2 to allow 1-stage expanded air to LP cylinder;
- The high-pressure combustor works on 4-strokes cycle completed over two full crankshafts revolutions, following the following p-V diagram:

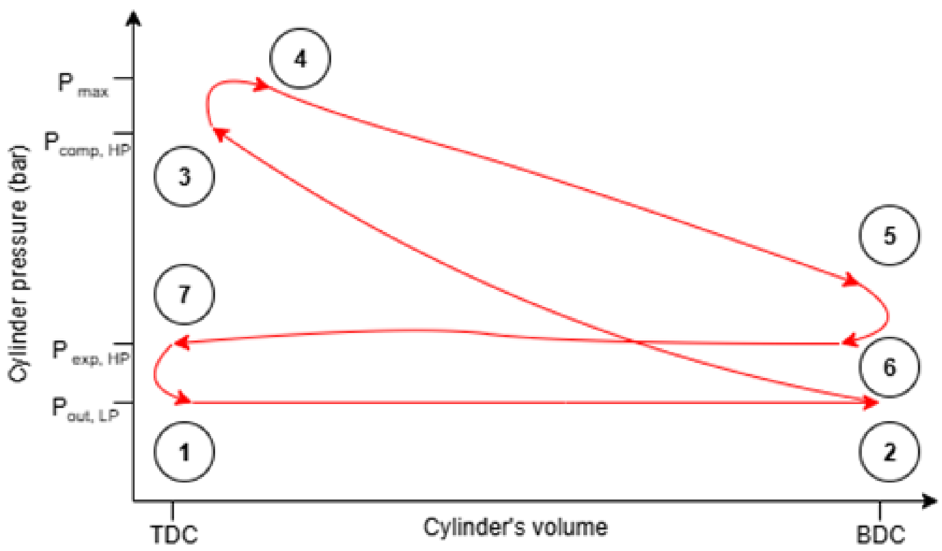

Figure 2.4: HP cylinder working cycle

1 → **2**: Inlet of compressed air from LP tank, cylinder moves from TDC to BDC; **2** → **3**: second compression stage;
3 → **4**: at the end of second compression stage fuel is injected and combustion is initiated;
4 → **5**: second expansion stage, piston goes from TDC to BDC;
5 → **6:** exhaust blow-down, combusted gas transfers to HP tank, partially allowing expansion;
6 → **7:** exhaust gas is pushed to HP tank;
7 → **1:** gas exchange where exhaust valve closes while inlet valve opens and a new cycle can be started again.

Synchronization

In the synchronized Double Compression–Expansion Engine (DCEE), the operation of the different cylinders becomes directly interdependent.
Since the buffer tanks are removed, the gas exchange between low-pressure and high-pressure stages takes place instantaneously.
This requires the strokes of **compressor, combustor, and expander cylinders** to be carefully phased so that each unit delivers or receives the working fluid at the correct timing. Any mismatch in synchronization would cause maldistribution, pressure fluctuations, or even backflow, severely compromising performance. Precise synchronization is therefore essential to guarantee a smooth transfer of mass and energy between stages, and it represents both a design challenge and a key enabler for unlocking the full efficiency potential of the concept. The synchronization of the strokes in the 2+4+2 engine can be

observed in the diagram below.

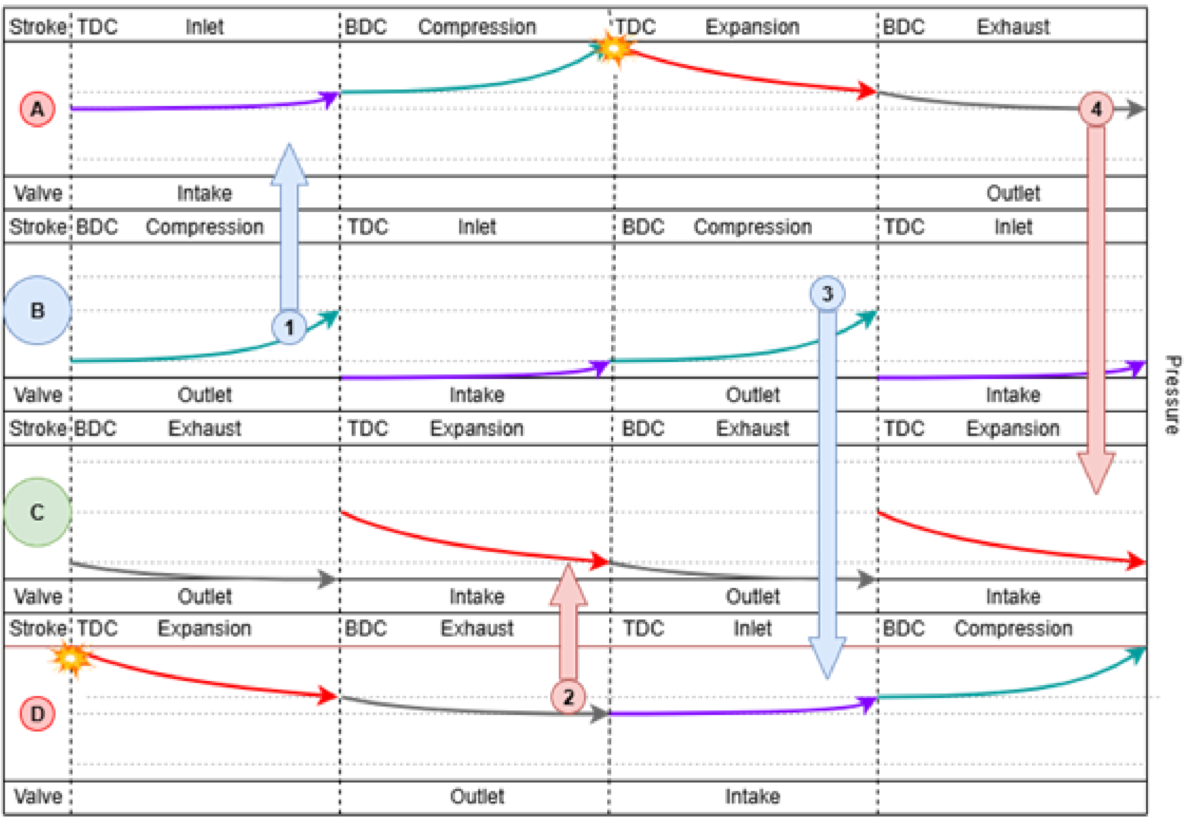

Figure 2.5: Strokes' distribution of 2+4+2 DCEE

From this first scratch of the synchronization of the strokes it's possible to appreciate that during the entire cycle the same stroke is not taking place at the same time in any of the cylinders, the red and blue arrow highlight the gas-exchange between cylinders, red arrows for HP to LP cylinders and blue arrow for LP to HP cylinders. It's possible also to appreciate how the power stroke in the HP cylinders is equally spaced along the cycle, there will be a **power stroke every 180°**.
Moreover, it's possible to appreciate how cylinder B will only work as compressor and C as expander, meaning that B will maintain a lower temperature than C, since combustion gases will only be conveyed in the latter. This layout can bring both positive and negative aspect that will be investigated in the next chapters. Such aspects may be relative to:

- Asymmetrical load on crankshaft;
- Combustion efficiency;
- Overall engine efficiency;
- Temperature in cylinders, therefore material choice.

2.2. Synchronized DCEE 4+4 concept and its operating cycle

The second model that can be identified is the 4+4 strokes. The simplest layout that has been theorized includes:

- 2 high -pressure combustors: to allow HP compression and expansion of the working fluid;
- 2 low -pressure cylinders: to allow LP 1^{st}-stage compression of air and 2^{nd}-stage expansion of exhaust fumes.

In this case, as in the previous one, it's possible to see that no buffer tanks are present, therefore valve timing between HP and LP cylinders must be tuned carefully in order to allow timed and efficient gas exchange. Moreover, the **connecting pipes must be carefully dimensioned** to avoid them working as buffer thanks, increasing losses and decreasing efficiency. Two main differences are present between the 2+4+2-strokes model and the 4+4-strokes model:

1. **Opposite directions of flows:** while in the 2+4+2 model the flow initiated by 1^{st} the power stroke follows the same direction of the one initiated by the 2^{nd} power stroke (From B to D), in the 4+4 model the flow initiated by the power stroke in B goes on the opposite direction compared to the one initiated by the power stroke in A.
2. **Role of LP cylinders:** the LP cylinders can't be identified as "Compressor" or "Expander" since they both execute 4-strokes cycles instead of 2-strokes ones.

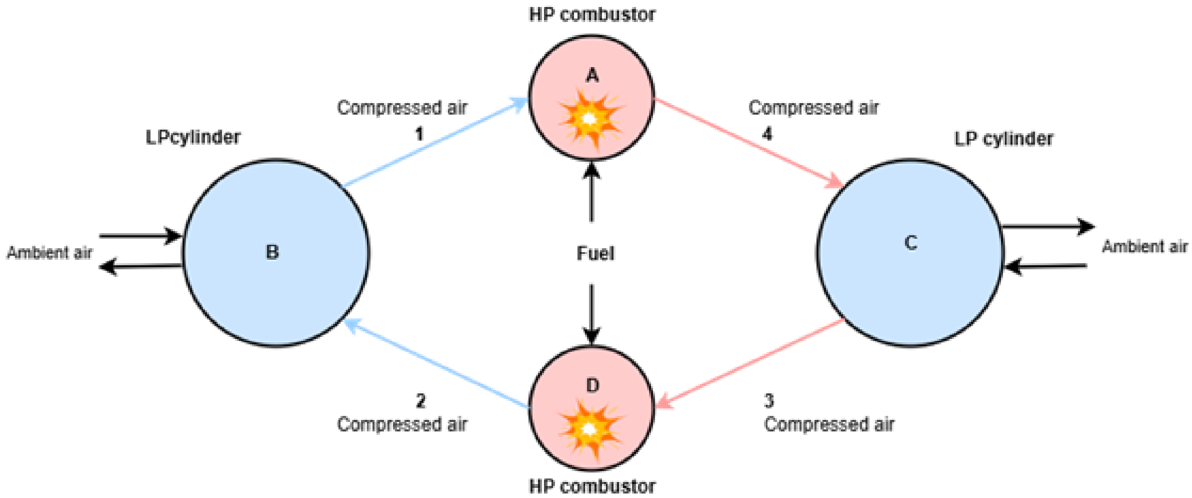

Figure 2.6: 4+4 DCEE Synchronized concept

LP cylinders

Valves layout:

- At least 1 inlet valve, to naturally aspirate air from environment;
- At least 1 exhaust valve, to allow exhaust gases into environment;
- At least 1 inlet valve, to allow transfer of exhaust gases from the HP combustor;
- At least 1 outlet valve, to allow transfer of compressed air into the HP combustor;

The low-pressure compressor works on 4-strokes cycle completed over one full crankshafts revolution, following the following p-V diagram:

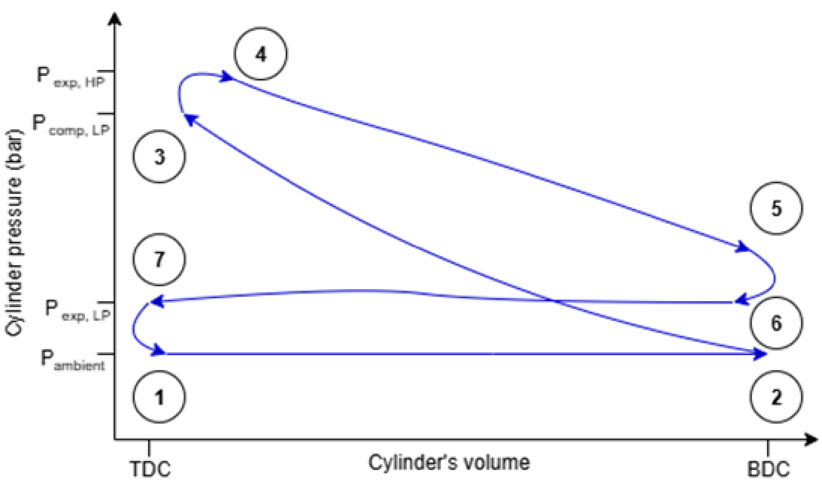

Figure 2.7: LP cylinder working cycle

1 → 2: **Inlet** of ambient air, cylinder moves from TDC to BDC, pressure remains constant;

2 → 3: **1st-stage compression,** valve opens close to TDC;

3 → 4: transfer of compressed air to HP cylinder and exhaust fumes from HP cylinder;

4 → 5: 2nd-stage expansion of exhaust fumes from HP cylinders;

5 → 6: exhaust blow-down;

6 → 7: exhaust of 2nd-stage expanded air;

7 → 1: re-equalization of pressure to pressure one.

HP cylinders

Valves layout:

- At least 1 inlet valve, probably 2 to allow intake of first-stage-compressed air from LP unit;
- At least 1 outlet valve, probably 2 to allow exhaust gases into the relative LP unit;

The low-pressure compressor works on 2-strokes cycle completed over one full crankshafts revolution, following the following p-V diagram:

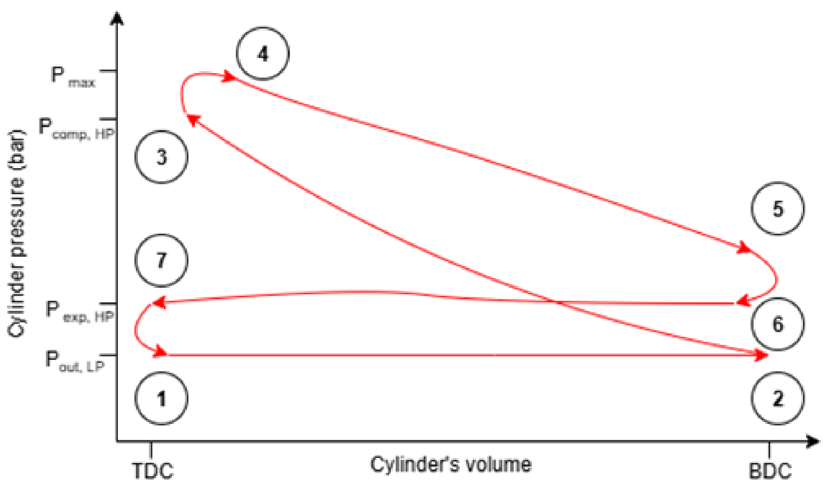

Figure 2.8: HP combustor working cycle

1 → 2: Inlet of compressed air from LP cylinder, cylinder moves from TDC to BDC;

2 → 3: second compression stage;

3 → 4: at the end of second compression stage fuel is injected and combustion is initiated;

4 → 5: first expansion stage, piston goes from TDC to BDC;

5 → 6: exhaust blow-down, combusted gas transfers to LP cylinder, partially allowing

expansion;
6 → 7: exhaust gas is pushed to LP cylinder;
7 → 1: gas exchange where exhaust valve closes while inlet valve opens and a new cycle can be started again.

Synchronization

In the 4+4 DCEE synchronization is very important in order to minimize thermodynamics losses allowing a smooth flow along the cycle.

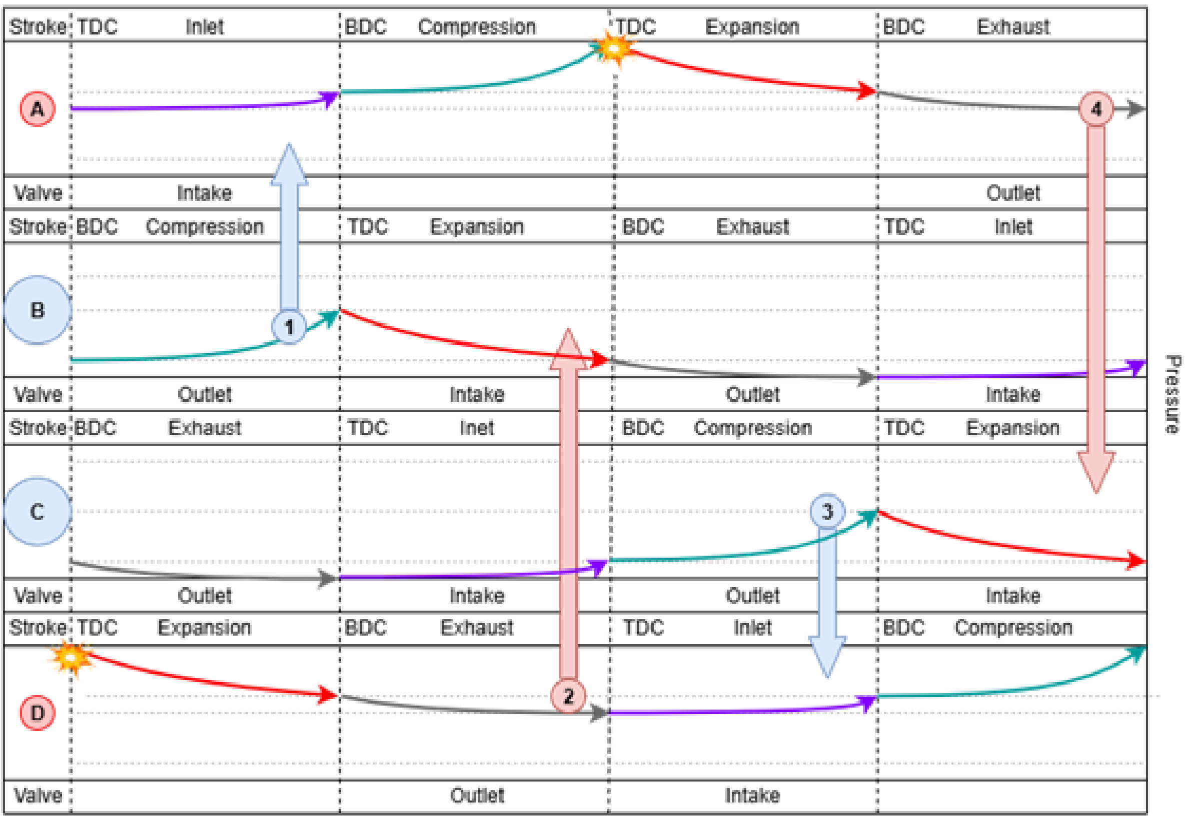

Figure 2.9: Strokes' distribution of 4+4 DCEE

From this first representation of the synchronization of the strokes it's possible to appreciate that during the entire cycle the same stroke is not taking place at the same time in any of the cylinders, the red and blue arrow highlight the gas-exchange between cylinders, red arrows for HP to LP cylinders and blue arrow for LP to HP cylinders. It's possible also to appreciate how the power stroke in the HP cylinders is equally spaced along the cycle, there will be a **power stroke every 180°**.
In this configuration LP units will complete a full 4 strokes cycle, working both as compressor and expander. This layout can bring both positive and negative aspect that will

be investigated in the next chapters. Such aspects may be relative to:

- symmetry of temperature and distribution along the engine block
- impossibility of optimizing the LP and HP units independently for compression / expansion work
- **Inlet** valves of the HP unit and **Compression** valve of the LP unit must be synchronized to allow smooth gas exchange between LP an HP units;
- **Exhaust** valves of the HP unit and **Expansion** valve must be synchronized to allow smooth gas exchange between HP and LP units.

3 | 4+4 Strokes model set up and metrics

3.1. Introduction

This chapter presents the setup of the numerical model developed in GT-Power, which is used to investigate the behavior of the engine considered in this thesis. The primary objective of the model is to reproduce the main thermodynamic, fluid-dynamic, and combustion processes of the engine with sufficient physical fidelity, providing a reliable foundation for the performance and efficiency analyses presented in the following chapters.

The chapter first introduces the overall architecture of the model and the modeling philosophy adopted. The selected configuration and the main underlying assumptions are described, as the definition of the global layout plays a key role in correctly capturing the gas-exchange processes, compression and expansion phases, and the interactions between the different engine subsystems.

The model is then described component by component. For each element—such as **cylinders, intake and exhaust systems, valves, connecting pipes, the adopted modeling approach, key parameters**, and the rationale behind the chosen solutions are discussed. Particular attention is given to ensuring consistency between the numerical representation and the expected physical behavior of the real system, while maintaining a balance between model accuracy and numerical robustness.

Finally, the main simplifying assumptions introduced in the model are addressed, together with their implications and limitations. This allows the reader to clearly understand the level of detail of the simulation model and to correctly interpret the results discussed in the subsequent chapters.

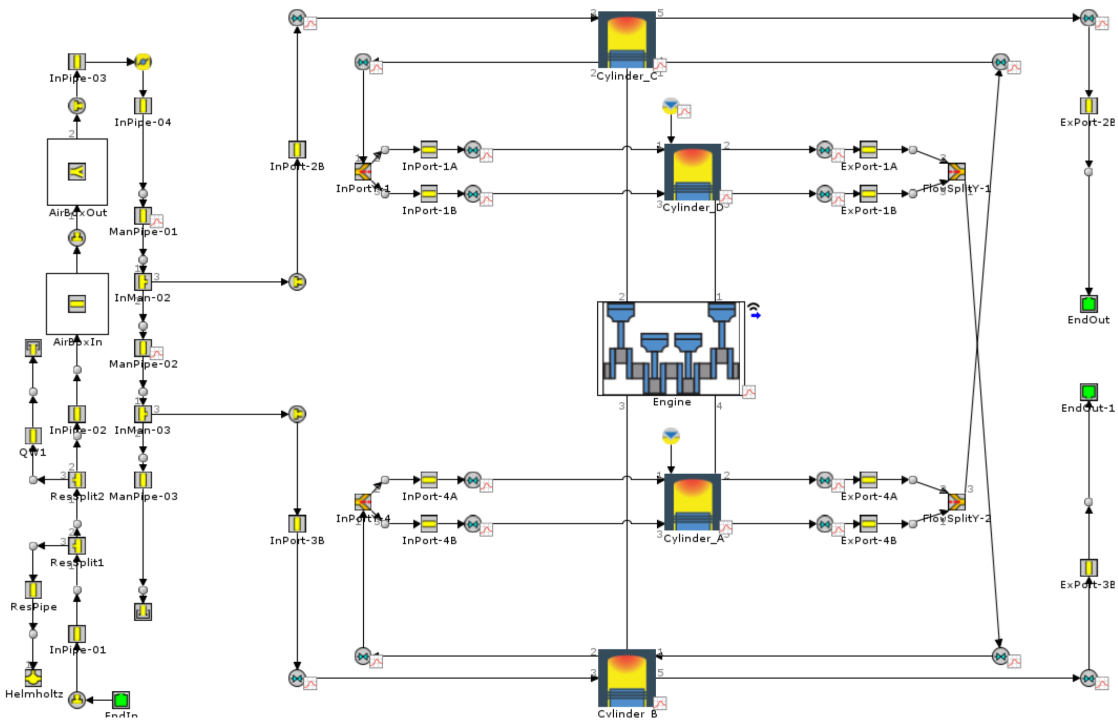

Figure 3.1: Layout of 4+4 strokes DCEE

3.2. Cylinders

The cylinder model plays a central role in the GT-Power simulation, as it governs the evolution of the in-cylinder thermodynamic state throughout the engine cycle. All the main physical phenomena that directly influence engine performance, such as compression and expansion, heat transfer to the walls, combustion, and fuel evaporation, are modeled at the cylinder level.

In this section, the modeling approach adopted for the cylinders is introduced. The definition of the in-cylinder initial conditions, thermal boundary conditions, and the selection of the sub-models used to describe heat transfer, combustion, and in-cylinder evaporation are presented. These modeling choices have a direct impact on the predicted pressure and temperature histories, and therefore on the accuracy of the overall engine simulation.

Each of these aspects will be investigated individually in the following subsections, where the adopted models and parameters are described in detail and their role within the overall simulation framework is discussed.

3.2.1. In-Cylinder initial state

The initial thermodynamic state of the in-cylinder working fluid is defined to provide a physically consistent starting point for the simulation. The working fluid inside two of the cylinders is modeled as a homogeneous mixture of **indolene and air**, with mass fractions of **0.08** and **0.92**, respectively. This composition is selected to represent a typical premixed charge while maintaining numerical robustness during the initial engine cycles, in the remaining cylinders initial state is modeled as **exhaust fumes**.

At the beginning of the simulation, the in-cylinder pressure is set equal to ambient conditions, whereas temperature is set to **900 K**. These initial values are not intended to represent a specific operating point of the engine, but rather to ensure **stable convergence** toward the periodic steady-state solution. After a limited number of cycles, the influence of the initial conditions becomes negligible, and the in-cylinder state is governed by the imposed boundary conditions and the selected sub-models.

3.2.2. Wall temperature

The thermal boundary conditions of the cylinder are defined by prescribing **constant wall** temperatures for the main solid components. A uniform and time-invariant temperature is assumed for the cylinder head, piston crown, and cylinder liner, representing averaged steady-state thermal conditions.

The temperature of the **cylinder head** is set to **575 K**, the temperature of the **piston crown** is set to **575 K**, and the temperature of the **cylinder liner** is set to **400 K**. This simplified approach allows the main effects of heat transfer between the in-cylinder gases and the surrounding walls to be captured, while avoiding the complexity of a fully coupled thermal model. The use of constant wall temperatures is considered appropriate for steady-state simulations and ensures numerical stability and repeatability of the results.

3.2.3. Heat transfer model

Heat transfer between the in-cylinder gases and the surrounding walls is modeled using the **WoschniGT** correlation-based heat transfer model implemented in GT-Power. The model evaluates the convective heat transfer coefficient as a function of the instantaneous in-cylinder pressure, temperature, gas properties, and a characteristic gas velocity representative of the bulk charge motion.

In its general form, the convective heat transfer coefficient h is expressed as:

$$h = C\, D^{-0.2}\, p^{0.8}\, T^{-0.53}\, w^{0.8}$$

where:

- h is the convective heat transfer coefficient $[\mathrm{W\,m^{-2}\,K^{-1}}]$,
- B is the cylinder bore [m],
- p is the instantaneous in-cylinder pressure [Pa],
- T is the instantaneous in-cylinder gas temperature [K],
- w is the characteristic gas velocity $[\mathrm{m\,s^{-1}}]$,
- C is an empirical constant (typically $C \approx 3.26$ in SI units).

The characteristic gas velocity w accounts for both piston-induced flow and combustion-induced turbulence and is commonly modeled as:

$$w = C_1\, \bar{u}_p + C_2\, \frac{V_d}{V} \left(\frac{p - p_m}{p_m} \right) \tag{3.1}$$

where:

- $\bar{u}_p$ is the mean piston speed,
- V_d is the displacement volume,
- V is the instantaneous cylinder volume,
- p_m is the motored cylinder pressure,
- C_1 and C_2 are calibration constants.

During the compression and expansion phases, the first term dominates the gas velocity, while during combustion the pressure difference term significantly increases the turbulence level, leading to higher heat transfer near top dead center (TDC).

An **overall convection multiplier** equal to **1.0** is applied, indicating that no global scaling of the default WoschniGT correlation is introduced. The contribution of the different heat transfer surfaces is adjusted through the specification of a **head-to-bore area ratio** equal to **1.3** and a **piston-to-bore area ratio** equal to **1.03**, which define the effective heat transfer areas of the cylinder head and piston relative to the bore area.

Radiative heat transfer is neglected by setting the **radiation multiplier** to **ignored**, under the assumption that convective heat transfer dominates the overall heat exchange under the investigated operating conditions. The reference gas temperature used to evaluate the convective heat flux is computed using the **hybrid** temperature evaluation method, which combines bulk and near-wall gas temperature effects to provide a stable and physically representative driving temperature difference.

Attribute	Object Value
Heat Transfer Model	WoschniGT
Overall Convection Multiplier	1
Individual Convection Multipliers	
Head/Bore Area Ratio	1.3
Piston/Bore Area Ratio	1.03
Radiation Multiplier	ign
Convection Temperature Evaluation	hybrid
Low Speed Heat Transfer Enhancement for Woschni* Models	✓

Figure 3.2: Woschni heat transfer model

Finally, the **low-speed heat transfer enhancement** option for Woschni-based models is enabled. This correction improves the prediction of heat transfer during low piston speed conditions, such as near top dead center and bottom dead center, where classical correlations tend to under-predict the heat transfer coefficient.

3.2.4. Combustion model

The combustion process is modeled using a **Wiebe function**-based heat release model, which prescribes the fraction of fuel burned as a function of crank angle. This approach allows the main effects of combustion phasing and duration on the in-cylinder pressure and temperature evolution to be captured while maintaining limited model complexity.

The cumulative burned fuel fraction $x_b(\theta)$ is defined according to the classical Wiebe formulation:

$$x_b(\theta) = 1 - \exp\left[-a\left(\frac{\theta - \theta_0}{\Delta\theta}\right)^{m+1}\right]$$

where θ is the crank angle, θ_0 is the combustion start angle, $\Delta\theta$ is the combustion duration, m is the Wiebe exponent, and a is a coefficient chosen to achieve the desired fraction of burned fuel at the end of combustion.

In this model, the combustion phasing is defined by the **anchor angle**, corresponding to the crank angle at which **50% of the fuel mass is burned** (θ_{50}). The combustion duration is defined as the crank angle interval between **10% and 90% burned fuel fraction**. Both the anchor angle (θ_{50}) and the burn duration ($\Delta\theta_{10\text{–}90}$) are treated as model inputs.

The **Wiebe exponent** is set to **2**, resulting in a symmetric heat release profile representative of a conventional premixed combustion process. The total fraction of fuel burned is set to **0.998**, ensuring nearly complete combustion while preserving numerical robustness.

The rate of combustion, required for the calculation of the heat release rate, is obtained by differentiating the Wiebe function with respect to the crank angle:

$$\frac{dx_b}{d\theta} = \frac{a(m+1)}{\Delta\theta}\left(\frac{\theta-\theta_0}{\Delta\theta}\right)^m \exp\left[-a\left(\frac{\theta-\theta_0}{\Delta\theta}\right)^{m+1}\right] \tag{3.2}$$

A **two-temperature zone** combustion model is adopted, distinguishing between burned and unburned gas regions within the cylinder. This allows a more accurate estimation of in-cylinder temperatures during combustion, which is particularly relevant for heat transfer and thermodynamic efficiency predictions.

The air burning enhancement factor is left at its default value, implying no additional correction to the combustion rate due to turbulence or mixing effects. The burned fuel fractions at the start and end of the combustion duration are fixed at their default values of **10%** and **90%**, respectively, consistently with the definition of the Wiebe burn duration.

3.2.5. In-Cylinder evaporation model

The in-cylinder fuel evaporation process is modeled using a **predictive spray evaporation model** specifically developed for direct injection applications in GT-Power. This model accounts for the main physical phenomena governing spray evolution and evaporation, including spray penetration, liquid jet breakup into droplets, entrainment of surrounding air and residual gases, and the resulting droplet evaporation rates.

The spray development is resolved based on a phenomenological description of momentum exchange between the injected liquid fuel and the in-cylinder gas, allowing the spray penetration and dispersion to be predicted as a function of injection conditions and in-cylinder thermodynamic state. The breakup of the liquid jet into droplets and the subsequent evaporation process are modeled to capture the coupling between heat transfer, mass transfer, and local gas composition.

A simplified, non-predictive evaporation model based on a prescribed time constant is available in GT-Power under the name `EngCylEvaporation`. However, this approach is not adopted in the present model, as it does not explicitly resolve the spray physics and provides reduced sensitivity to injection system parameters.

3.2.6. Geometry

The cylinder geometry is defined separately for the **HP** and **LP** cylinders. The two configurations share the same stroke and kinematic assumptions, while the **bore** and some derived geometric parameters differ. Table 3.1 summarizes the adopted values.

The **connecting rod length** is defined based on a typical rod-to-crank ratio. The crank radius is computed as r = stroke/2, and the connecting rod length is set as $l = 3.6\,r$. With a stroke of 90 mm, this gives $r = 45$ mm and $l = 162$ mm.

The **compression ratio** is set to **12** for the HP cylinder and **150** for the LP cylinder. The LP stage primarily performs compression and transfers the compressed charge to the HP stage, which further compresses it; therefore, a high compression ratio is prescribed for the LP cylinder to represent this operating role.

Table 3.1: Cylinder geometry and key kinematic parameters for the HP and LP cylinders.

Parameter	**HP cylinder**	**LP cylinder**
Bore [mm]	**75**	**150**
Stroke [mm]	**90**	**90**
Crank radius r = stroke/2 [mm]	**45**	**45**
Rod-to-crank ratio l/r [-]	**3.6**	**3.6**
Connecting rod length $l = 3.6\,r$ [mm]	**162**	**162**
Compression ratio [-]	**12**	**150**
TDC clearance height [mm]	**0.8**	**0.5**

3.3. Valves

3.3.1. Layout

The valve system plays a key role in defining the gas exchange and inter-stage coupling of the engine. A total of **16 valves** are included in the model, distributed between the **high-pressure (HP)** and **low-pressure (LP)** cylinders and serving different functional roles within the cycle.

The valves are first classified based on the cylinder group to which they belong.

The **HP cylinders** are equipped with conventional gas exchange valves. Each HP cylinder features two intakes valves and two exhaust valves, resulting in a total of **4 HP intake valves** and **4 HP exhaust valves**. These valves control the admission of compressed charge into the HP cylinders and the discharge of exhaust gases to LP cylinders.

The **LP cylinders** are equipped with four distinct valve types, reflecting their dual role in gas exchange and inter-stage pressure transfer. Specifically, each LP cylinder includes:

- one **LP intake valve**, connecting the LP cylinder to the ambient intake,
- one **LP exhaust valve**, discharging the LP cylinder to the ambient exhaust,
- one **compression valve**, which connects the LP cylinder to the HP cylinder during the first compression phase,
- one **expansion valve**, which connects the HP cylinder to the LP cylinder during the first expansion phase.

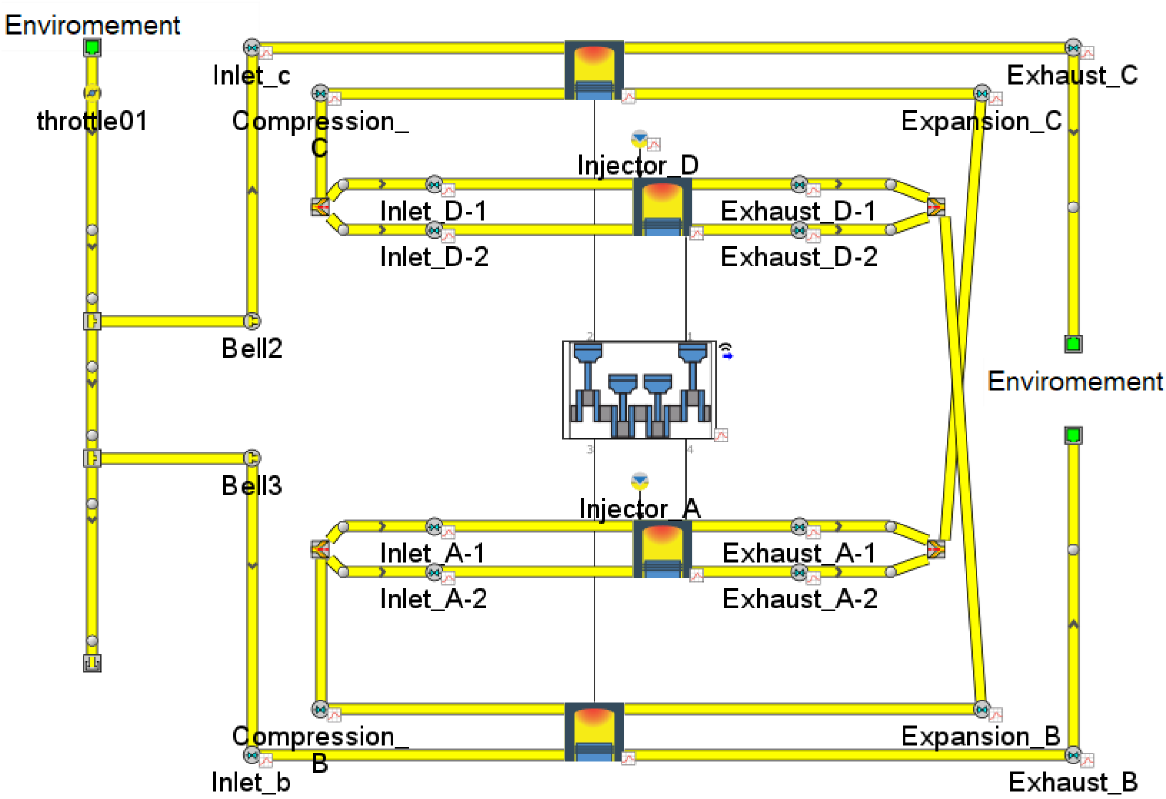

Figure 3.3: Valve names and positioning

As a result, the LP stage includes **2 LP intake valves**, **2 LP exhaust valves**, **2 compression valves**, and **2 expansion valves**. Together with the HP valves, this configuration leads to a total of **16 valves** implemented in the GT-Power model.

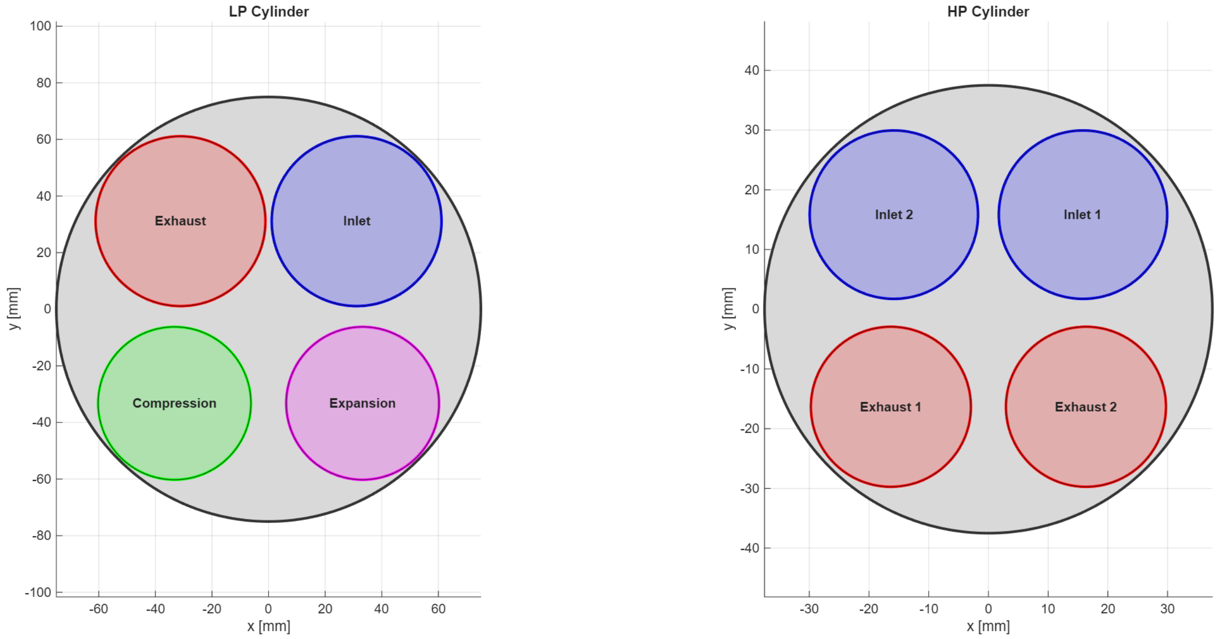

Figure 3.4: Valve sizing and positioning

As a first design choice, and in accordance with established academic literature, in particular the internal combustion engine textbook by Johansson [2], the valve layout and sizing were selected to ensure adequate flow capacity while maintaining realistic geometric constraints. Following these guidelines, the minimum distances between valves were set to approximately **3.5 mm** between intake valves, **6 mm** between exhaust valves, and **5.35 mm** between intake and exhaust valves.

Based on these constraints, an initial valve sizing and dynamic parameter definition was established. The adopted geometric and dynamic valve parameters used in the GT-Power model are summarized in Table 3.2.

Table 3.2: Geometric and dynamic parameters of the valves used in the GT-Power model.

Valve	**Max lift** [mm]	**Diameter** [mm]	**Spring preload** [mm]	**Stop stiffness** [N/m]	**Stop damping** [-]
In_LP	**10.2**	**63.0**	**9.0**	1×10^9	**0.98**
Ex_LP	**10.0**	**62.0**	**9.0**	1×10^9	**0.98**
Com	**10.2**	**54.0**	**9.0**	1×10^9	**0.98**
Exp	**10.2**	**54.0**	**9.0**	1×10^9	**0.98**
In_HP	**10.2**	**28.2**	**9.0**	1×10^9	**0.98**
Ex_HP	**10.0**	**26.8**	**9.0**	1×10^9	**0.98**

Valves connecting the cylinders to atmosphere have been designed with bigger diameters in order to minimize pumping losses. The same dynamic parameters are applied to all valve types. The **spring preload setting length** defines the initial compression of the valve spring, while the **stop stiffness** and **stop damping** parameters control the valve contact behavior at maximum lift. The upstream and downstream pressure areas are left at their default values, as provided by the `ValveCamDynConn` template.

The discharge coefficient is modeled as a function of normalized valve lift, with an initial linear increase followed by a plateau at higher lift values, representing the transition from lift-limited to area-limited flow. The same discharge coefficient curve is applied for both forward and reverse flow directions.

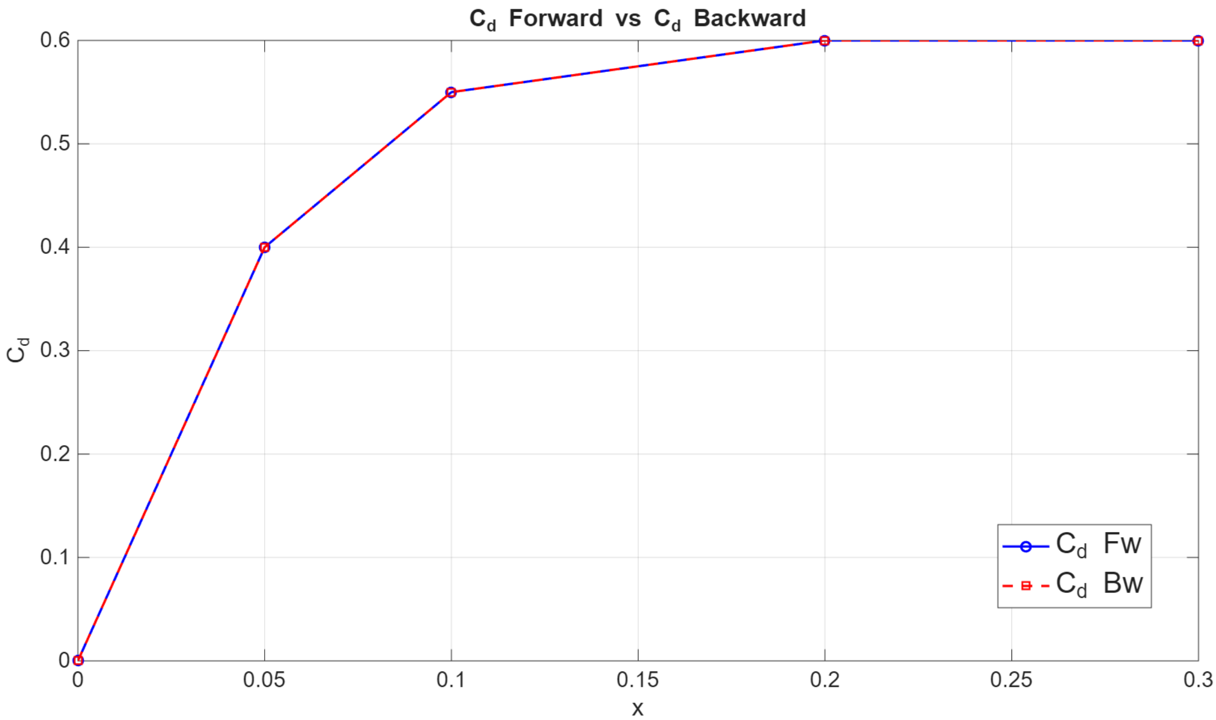

Figure 3.5: FW e BW Discharge coefficient

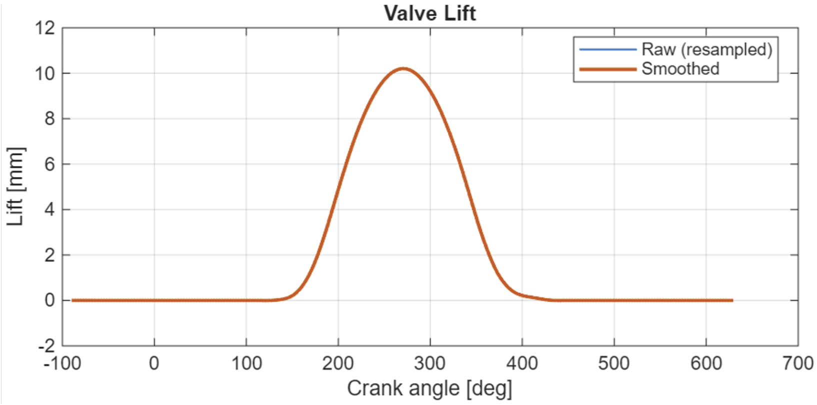

Figure 3.6: Valve's lift profile

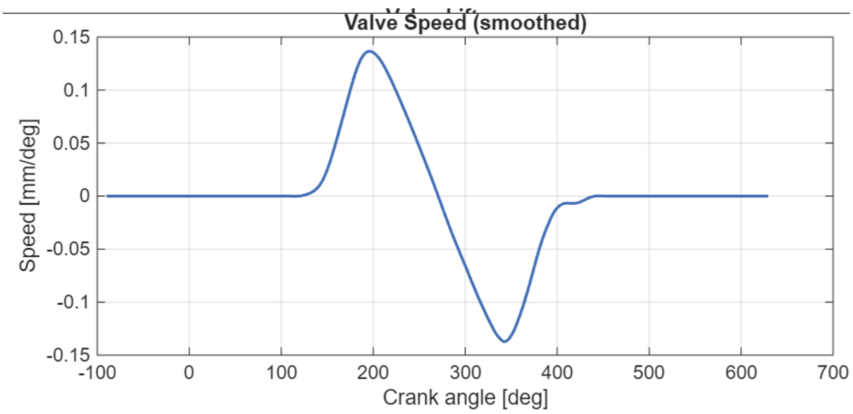

Figure 3.7: Valve's speed profile

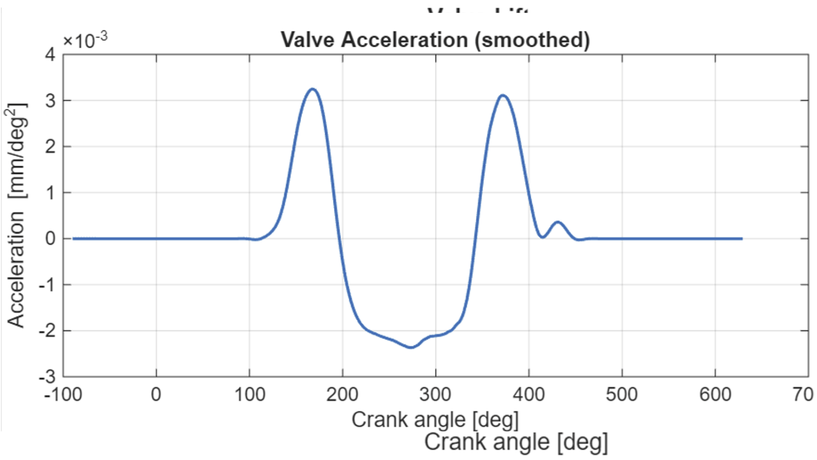

Figure 3.8: Valve's acceleration profile

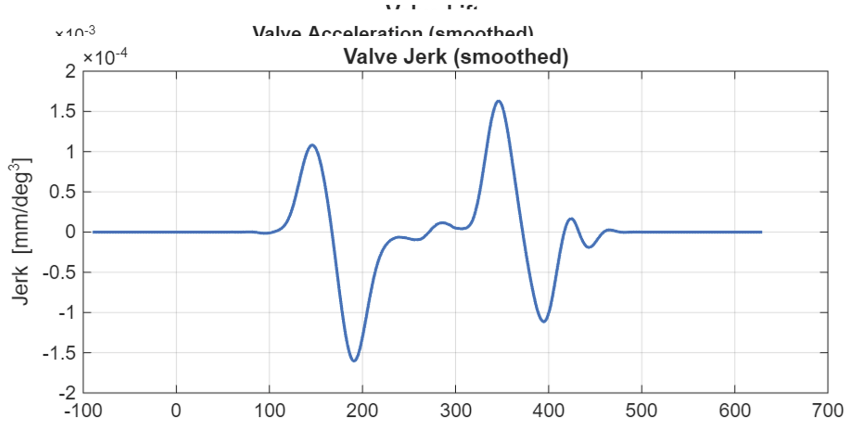

Figure 3.9: Valve's jerk profile

3.3.2. Timing and Inter-Cylinder synchronization

In a synchronized Double Compression Expansion Engine (DCEE), unlike unsychronized architectures, the absence of intermediate buffer tanks requires a precise **temporal coordination** of valve events, both with respect to the **crank angle** and among **different cylinders**, in order to preserve pressure continuity and avoid irreversible losses.

First, the valve timing of each cylinder must be accurately phased with the crank angle to correctly reproduce the functional stages of a **conventional four-stroke cycle**, namely intake, compression, expansion, and exhaust. Even though different cylinders in the DCEE architecture may be dedicated to specific functions, the global valve-event scheduling must **collectively fulfill the requirements of a complete four-stroke thermodynamic cycle** over 720 crank-angle degrees. Any deviation in this synchronization would result in improper gas exchange, increased pumping work, and degraded cycle efficiency.

Second, an **inter-cylinder synchronization** of valve events is mandatory to guarantee a direct and loss-minimized transfer of the working fluid between low-pressure (LP) and high-pressure (HP) cylinders. In particular, the following valve-event pairs must be synchronized:

- the **compression** valve of LP cylinder **C** with the **inlet valve**s of HP cylinder **D**;
- the **exhaust** valves of HP cylinder D with the **expansion** valve of LP cylinder B;
- the **compression** valve of LP cylinder **B** with the **inlet** valves of HP cylinder **A**;
- the **exhaust** valves of HP cylinder **A** with the **expansion** valve of LP cylinder **C**.

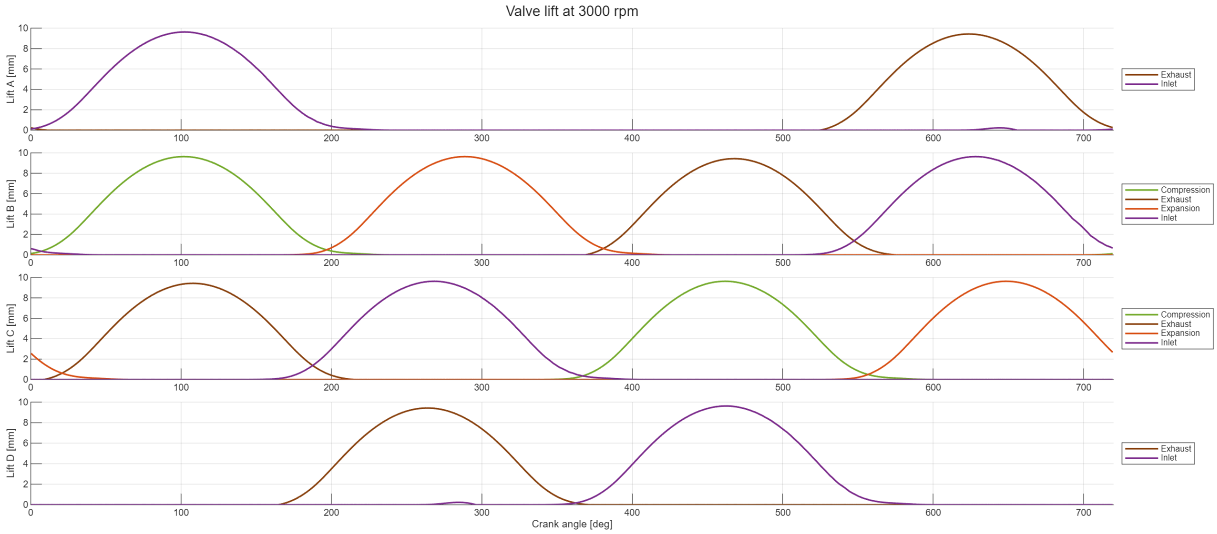

Figure 3.11: Valves lift profiles vs global CA

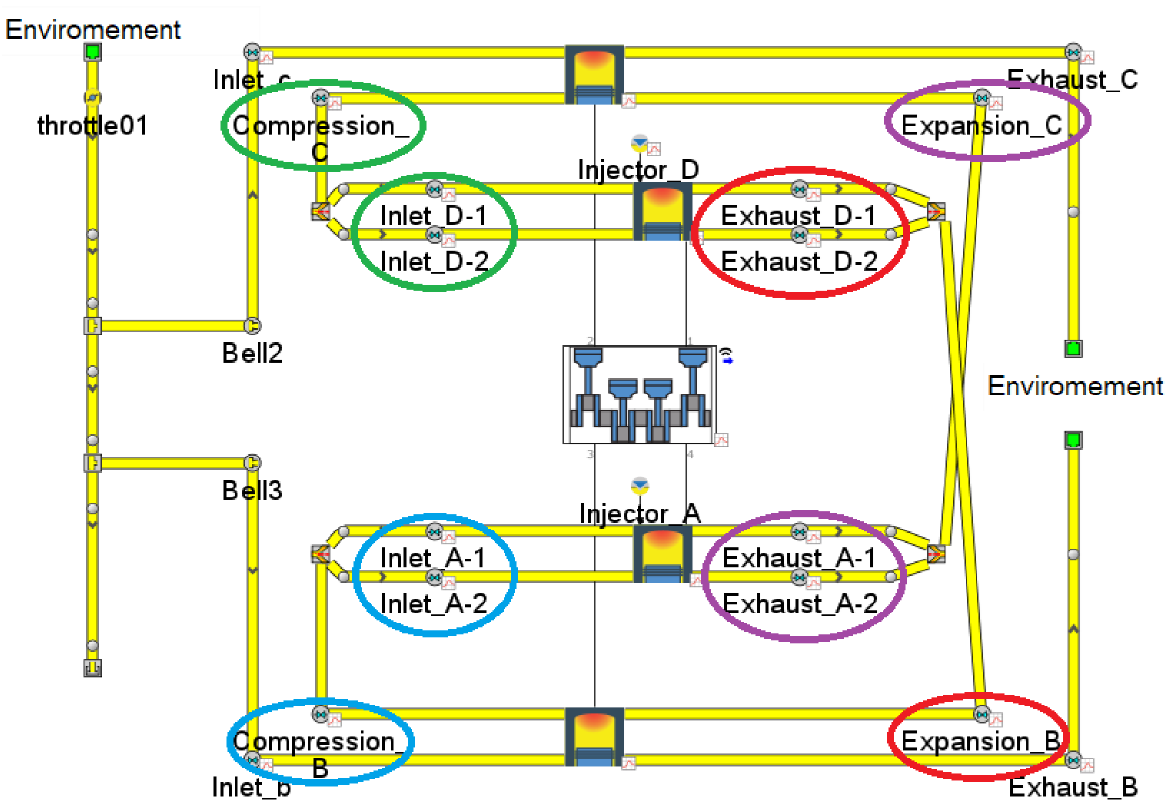

Figure 3.10: Valve timing

This synchronization ensures that pressure and mass-flow continuity are maintained during the inter-cylinder gas transfer, avoiding throttling effects, backflow phenomena, and unnecessary entropy generation.

3.4. Engine crankcase

The crankcase model defines the mechanical structure of the engine and the kinematic relationships between the **cylinders, crankshaft, and bearings**. It includes the description of mechanical friction losses, the cylinder ordering and crankshaft phasing, the firing order, and the treatment of crankshaft inertia. These elements collectively define the mechanical behavior of the engine and ensure consistency between the thermodynamic cycle and the underlying mechanical architecture.

3.4.1. Friction model

The mechanical friction losses associated with the crank–slider mechanism are modeled through a friction mean effective pressure (FMEP) formulation. The adopted friction model parameters used in the GT-Power crankcase definition are summarized in Table 3.3.

Table 3.3: Friction model parameters used for the engine crankcase.

Parameter	**Unit**	**Value**
Constant part of FMEP	bar	**0.2**
Peak cylinder pressure factor	–	**0.002**
Mean piston speed factor	bar/(m/s)	**0.04**
Mean piston speed squared factor	bar/(m/s)^2	**0.0**
Engine speed at friction transition	RPM	**0**

3.4.2. Cylinder arrangement

The cylinder arrangement and crankshaft phasing are defined to reflect the functional separation between high-pressure (HP) and low-pressure (LP) cylinders. The cylinder order along the crankshaft is defined as **HP–LP–LP–HP**. Cylinders belonging to the same pressure stage operate in phase, while the HP and LP groups are phased **180°** apart from each other.

For simplicity in the definition of the gas exchange and inter-cylinder piping connections, an **inline four-cylinder layout** is adopted. The normalized axial distance between adjacent connecting rods along the crankshaft is set to **0.5**. A **main bearing** is introduced on the crankshaft after each connecting rod journal, ensuring a realistic representation of crankshaft support and load distribution.

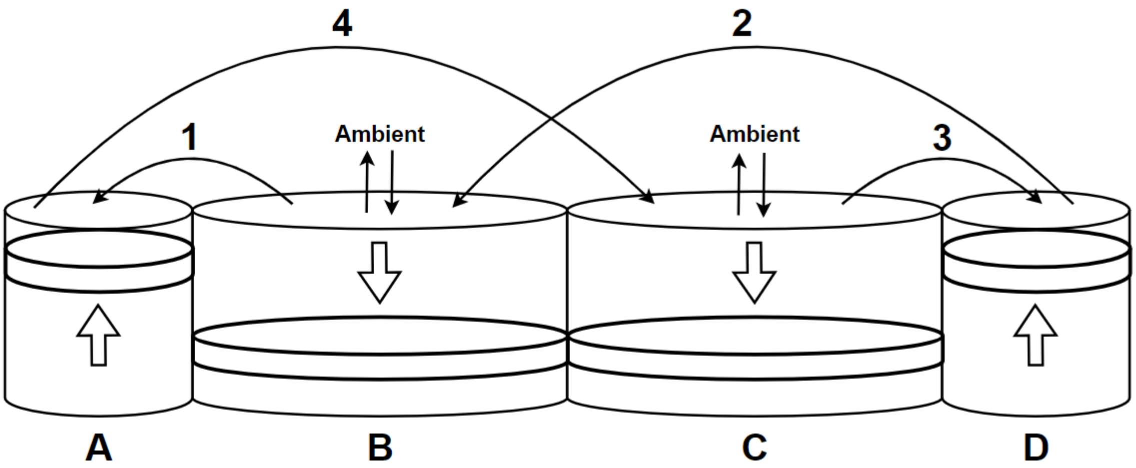

Figure 3.12: Cylinders' layout

3.4.3. Firing order

The firing order is the following: **D, B, A, and C**. Each firing event is separated by **180° of crank angle**, ensuring uniform spacing of combustion events over the engine cycle. This firing order is consistent with the selected crankshaft phasing and the relative timing between HP and LP cylinders.

3.4.4. Engine components' inertia

Since all simulations are performed under **steady-state operating conditions**, transient rotational effects are not considered. As a result, the **crankshaft inertia is neglected** in the model. This assumption is justified by the absence of speed transients and allows the numerical formulation to be simplified without affecting the accuracy of steady-state performance and efficiency predictions.

3.5. Fuel Injectors

Fuel delivery is handled by a **direct injection system** (GDI) consisting of two injectors, one for each high-pressure (HP) cylinder. The main characteristics and control assumptions of the injector system adopted in the GT-Power model are summarized in Table 3.4.

Table 3.4: Main characteristics and modeling assumptions of the injector system.

Parameter	Unit	Value / Description
Injection type	–	Direct injection
Number of injectors	–	2 (one per HP cylinder)
Injected fuel	–	Indolene
Fuel temperature	K	**300**
Maximum fuel mass flow rate	g/s	**12**
Injection duration at 4000 rpm	°CA	**∼120**
Injection location	–	HP cylinders

The injected fuel mass is regulated through a **closed-loop control strategy** based on the air mass flow entering the engine through the intake throttle (`Throttle 1`) and a target **fuel–air (FA)** ratio defined as a function of engine speed. The injector pulse width is adjusted to deliver the required fuel mass, ensuring consistency between the prescribed FA ratio and the instantaneous air flow. Injection starts about **70°** of **Crank angle** after inlet valve opening, a square-shaped profile as been chosen.

Table 3.5: Injector geometric parameters used to achieve the required fuel delivery.

Parameter	Unit	Value
Nozzle hole diameter	mm	**0.12**
Number of holes per nozzle	–	**8**
Nozzle discharge coefficient C_d	–	**0.7**

3.6. Piping and connections

The piping network defines the flow connections between the intake system, the LP and HP cylinders, and the exhaust boundary conditions. The **intake system** was directly imported from an existing GT-Power model of a naturally aspirated **4-cylinder GDI** engine, in order to start from a realistic and validated intake layout.
On the exhaust side, the flow downstream of the **LP exhaust** is discharged directly to the **ambient environment**, as no dedicated exhaust line or aftertreatment system is considered in the present synchronized layout study.

Since the focus of this work is the **synchronized** configuration, the piping between components is intentionally kept as compact as possible to minimize **dead volumes** and reduce undesired filling/emptying dynamics. For this reason, all interconnecting pipes listed in Table 3.6 are assigned a uniform length of **10 mm**. The table summarizes the four pipe groups used to connect intake to LP cylinders, LP to HP cylinders, HP to LP cylinders, and LP exhaust to ambient conditions.

Table 3.6: Piping connections and geometric parameters adopted for the synchronized layout.

Pipe group	**Connection**	**Qty**	**D [mm]**
Intake–LP	Intake system → LP cyl	**2**	**54.0**
LP–HP (compression)	LP comp. valve → HP int. valves (Y-split)	**4**	**29.5**
HP–LP (expansion)	HP exh → LP exp. valve (Y-merge)	**4**	**27.0**
LP exhaust–ambient	LP exhaust valve → environment	**2**	**60.0**

3.7. Environmental conditions

Environmental conditions are modeled following standard test conditions, a temperature of 298 K or 25 °C and pressure of 1 Bar has been imposed.

3.8. Mean Effective Pressure and Efficiency Metrics

To evaluate the conversion of the fuel chemical energy into useful engine output, it is convenient to express the different energy contributions in terms of mean effective pressure. In this way, all the quantities are normalized by the displaced volume and can be compared on a common basis.

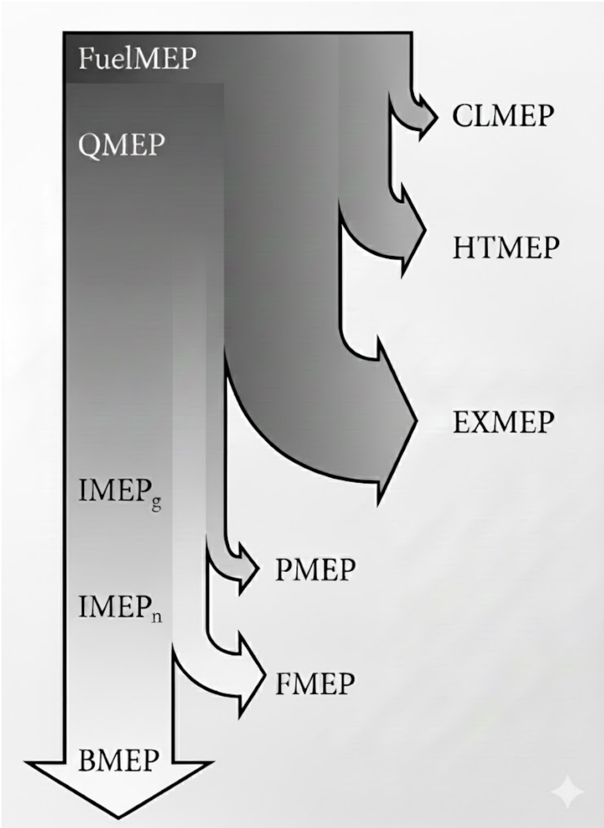

Figure 3.13: Energy flow from fuel on top to useful mechanical energy at the bottom, all expressed as mean effective pressures

Figure 4.1 illustrates the energy-flow path from the fuel input to the final brake work delivered at the shaft. Starting from the fuel energy, a sequence of losses can be identified, including combustion imperfections, heat transfer to the walls, exhaust energy losses, pumping work, and mechanical friction. The remaining part corresponds to the effective brake output of the engine.

Figure 3.14: Schematic energy distribution from fuel input to brake output, expressed in terms of mean effective pressure.

3.8.1. Definitions of mean effective pressure

The fuel energy supplied to the cycle, normalized by the displaced volume, is defined as the fuel mean effective pressure:

$$\mathrm{FuelMEP} = \frac{m_f\, Q_{\mathrm{LHV}}}{V_d} \tag{3.3}$$

where m_f is the injected fuel mass, Q_{LHV} is the lower heating value of the fuel, and V_d is the cylinder displaced volume.

The amount of released heat can be written in normalized form as the heat mean effective pressure:

$$\mathrm{QMEP} = \frac{Q}{V_d} \tag{3.4}$$

where Q represents the total heat released during the cycle.

The gross indicated mean effective pressure accounts for the positive work developed during the main closed portion of the cycle:

$$\mathrm{IMEP}_g = \frac{1}{V_d} \int_{-180}^{180} p\, dV \tag{3.5}$$

The net indicated mean effective pressure includes the complete loop and therefore also reflects the gas-exchange process:

$$\mathrm{IMEP}_n = \frac{1}{V_d} \oint p\, dV \tag{3.6}$$

The final useful work available at the crankshaft is expressed by the brake mean effective pressure:

$$\mathrm{BMEP} = \frac{W_b}{V_d} \tag{3.7}$$

where W_b is the brake work.

3.8.2. Loss terms

The difference between the fuel energy input and the heat effectively released in the cylinder is associated with combustion losses. This contribution is written as:

$$\mathrm{CLMEP} = \mathrm{FuelMEP} - \mathrm{QMEP} \tag{3.8}$$

The heat transferred from the working gases to the chamber walls can be expressed as:

$$\mathrm{HTMEP} = \frac{Q_{ht}}{V_d} \tag{3.9}$$

where Q_{ht} denotes the heat rejected through wall heat transfer.

The energy carried away with the exhaust gases is represented by the exhaust mean effective pressure:

$$\text{EXMEP} = \frac{Q_{exh}}{V_d} \tag{3.10}$$

where Q_{exh} is the exhaust energy loss.

The pumping loss is obtained from the difference between gross and net indicated work:

$$\text{PMEP} = \text{IMEP}_g - \text{IMEP}_n \tag{3.11}$$

Mechanical friction losses are instead evaluated as the difference between net indicated output and brake output:

$$\text{FMEP} = \text{IMEP}_n - \text{BMEP} \tag{3.12}$$

3.8.3. Efficiency decomposition

Based on the previous definitions, the overall energy-conversion chain can be separated into four main efficiency terms.

The **combustion efficiency** quantifies how much of the fuel chemical energy is converted into released heat:

$$\eta_C = \frac{\text{QMEP}}{\text{FuelMEP}} = 1 - \frac{\text{CLMEP}}{\text{FuelMEP}} \tag{3.13}$$

The **thermodynamic efficiency** measures how effectively the released heat is transformed into gross indicated work:

$$\eta_T = \frac{\text{IMEP}_g}{\text{QMEP}} = 1 - \frac{\text{HTMEP} + \text{EXMEP}}{\text{QMEP}} \tag{3.14}$$

The **gas-exchange efficiency** accounts for the losses associated with intake and exhaust pumping:

$$\eta_{GE} = \frac{\text{IMEP}_n}{\text{IMEP}_g} = 1 - \frac{\text{PMEP}}{\text{IMEP}_g} \tag{3.15}$$

The **mechanical efficiency** describes the fraction of net indicated work that remains available as brake work after friction losses:

$$\eta_M = \frac{\text{BMEP}}{\text{IMEP}_n} = 1 - \frac{\text{FMEP}}{\text{IMEP}_n} \tag{3.16}$$

Finally, the overall **brake efficiency** can be written as the product of the previous contributions:

$$\eta_B = \eta_C \, \eta_T \, \eta_{GE} \, \eta_M = \frac{\text{BMEP}}{\text{FuelMEP}} \tag{3.17}$$

This formulation is especially useful because it separates the different physical mechanisms responsible for efficiency degradation. As a result, it becomes easier to identify whether the dominant limitation of a given engine configuration originates from combustion quality, thermodynamic losses, gas-exchange penalties, or mechanical friction.

4 | Baseline results

4.1. Introduction

This chapter presents the **baseline results** obtained from the simulation of the proposed engine concept. The objective of this chapter is to analyse the fundamental thermodynamic behaviour and the main performance characteristics of the engine under the selected **baseline operating point**. The baseline case serves as a reference condition for the interpretation of the engine behaviour and for the comparison with the parametric studies presented in the following chapters.

The analysis is carried out through several complementary perspectives in order to provide a comprehensive understanding of the engine operation. First, the **in-cylinder thermodynamics** are investigated. Particular attention is given to the evolution of the **in-cylinder pressure**, the corresponding **pressure–volume (P–V) diagrams**, and the interaction between the different cylinders involved in the engine cycle. These analyses allow the main thermodynamic processes occurring during compression, combustion and expansion to be examined.

Subsequently, the overall **engine performance** is evaluated. The results are discussed in terms of key performance indicators such as **power output**, **specific power**, **torque**, and **thermal efficiency**. These quantities provide a global assessment of the engine capabilities and allow a comparison with conventional internal combustion engines.

Finally, the results are analysed using the **Mean Effective Pressure (MEP) framework**. This approach allows the different contributions to the engine work output and losses to be quantified. In particular, quantities such as **IMEP**, **BMEP**, **PMEP**, and **FMEP** are evaluated in order to identify the main sources of losses within the engine cycle.

The chapter is organized as follows. **Section 4.2** focuses on the analysis of the **in-cylinder thermodynamics**, thanks to in-cylinder pressure traces. **Section 4.3** discusses the resulting **pressure-volume diagrams**, while **Section 4.4** analyzes the different **heat**

release rate in order to quantify the contributions to the overall engine work output and associated losses. Section 4.5 is focused on in-cylinder temperature evolution, section 4.6 analyzes the resulting engine performance and finally section 4.7 has its focus on Mean effective pressures.

4.2. In-Cylinder Thermodynamics

The thermodynamic processes occurring inside the cylinders determine the work exchange of the engine cycle and therefore strongly influence the resulting performance. A detailed analysis of the in-cylinder conditions allows the interpretation of the global engine metrics presented later in terms of efficiency, power output and mean effective pressures.

In this section, the thermodynamic behaviour of the cylinders is analysed in order to provide a deeper understanding of the simulated engine cycle. The analysis focuses on the evolution of the **in-cylinder pressure as a function of crank angle** and on the **pressure–volume representation of the cycle**, which directly illustrates the work transfer during the compression and expansion processes.

Furthermore, the combustion process is examined through the analysis of the heat release characteristics. This provides additional insight into the combustion phasing and burn duration, which play a key role in determining the overall engine efficiency.

The results presented in this section form the basis for the performance analysis discussed in the following sections.

4.2.1. Pressure traces

The in-cylinder pressure evolution provides direct insight into the thermodynamic processes occurring during the engine cycle. By analysing the pressure traces as a function of crank angle, it is possible to identify the main phases of the cycle, including compression, combustion and expansion, as well as to evaluate the pressure levels reached in the different stages of the process.

The pressure trace of the LP cylinder is shown in Figure 4.1. Starting from approximately ambient pressure, the **pressure increases** during the compression phase until reaching a **peak value** of **8.8 bar** at around 180 CAD. This represents the first stage of compression of the working fluid. After the pressure peak, the LP cylinder pressure progressively decreases as the piston continues its motion and the compressed charge is transferred to the HP cylinder.

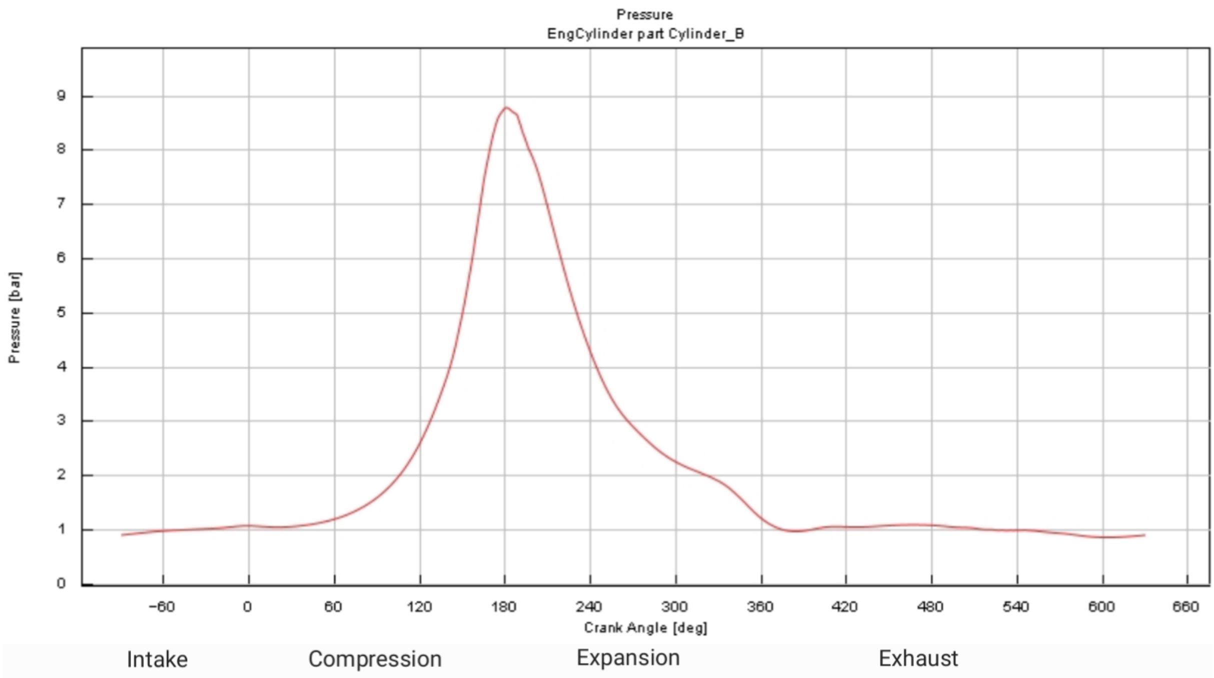

Figure 4.1: In-cylinder pressure trace of the low-pressure (LP) cylinder as a function of crank angle at the baseline operating condition.

A **consistent behaviour** is observed when analysing the pressure trace of the HP cylinder, shown in Figure 4.2. At the **beginning of its effective compression** phase, the **pressure level is already of the order of 8.5 bar**, which is comparable with the pressure reached at the end of the LP compression process. This indicates continuity in the thermodynamic state of the working fluid during the transfer from the LP cylinder to the HP cylinder.

The second compression stage takes place in the HP cylinder, where the pressure rises rapidly from approximately 8.5 bar to a peak value of about 257bar, reached shortly after 360CAD. This peak pressure corresponds to the highest pressure level in the cycle and is associated with the second compression stage followed by the combustion event.

The pressure levels reached in the two cylinders are therefore significantly different. While the LP cylinder operates within a pressure range of approximately 1 to 9 bar, the HP cylinder experiences much higher pressures, reaching peak values close to 260 bar. The maximum pressure in the HP cylinder is therefore almost thirty times higher than the maximum pressure reached in the LP cylinder.

After the peak pressure, the HP cylinder undergoes the first expansion process and the pressure decreases progressively. However, even after a substantial part of the expansion, the pressure remains well above ambient pressure, with values of the order of 10 to 15bar.

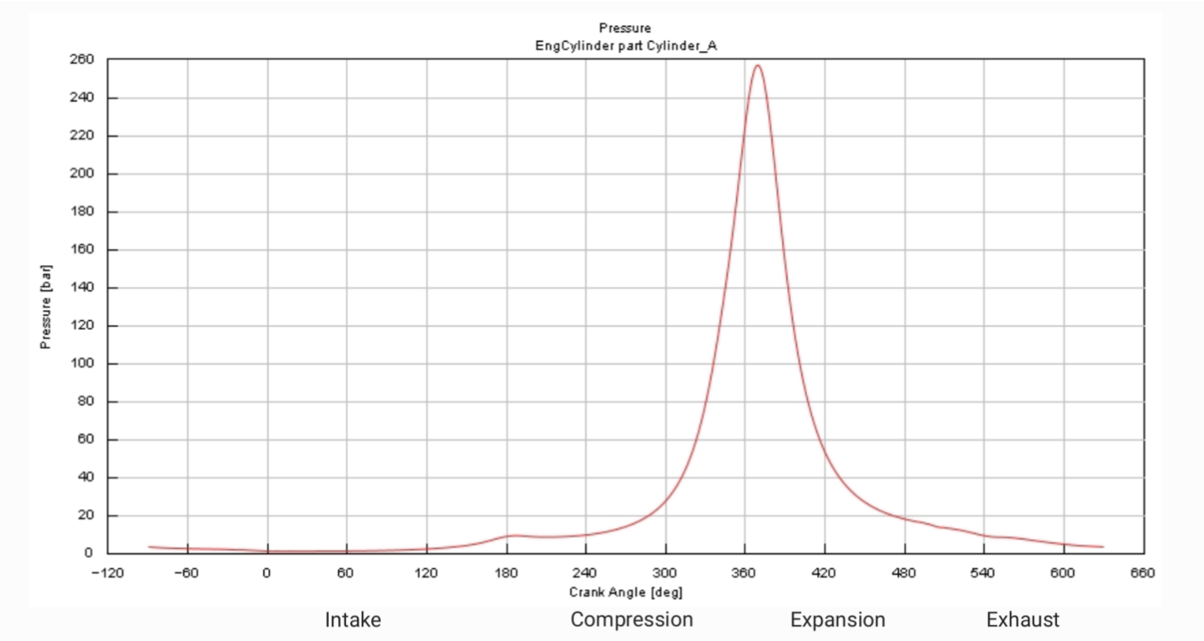

Figure 4.2: In-cylinder pressure trace of the high-pressure (HP) cylinder as a function of crank angle at the baseline operating condition.

This indicates that the working fluid still retains a significant amount of thermodynamic potential after the first expansion stage.

The two plots below highlight the pressure evolution during gas transfer between the LP and HP units, demonstrating how it aligns and subsequently increases or decreases depending on whether the region in proximity to the compression valve opening or the expansion valve opening is analyzed

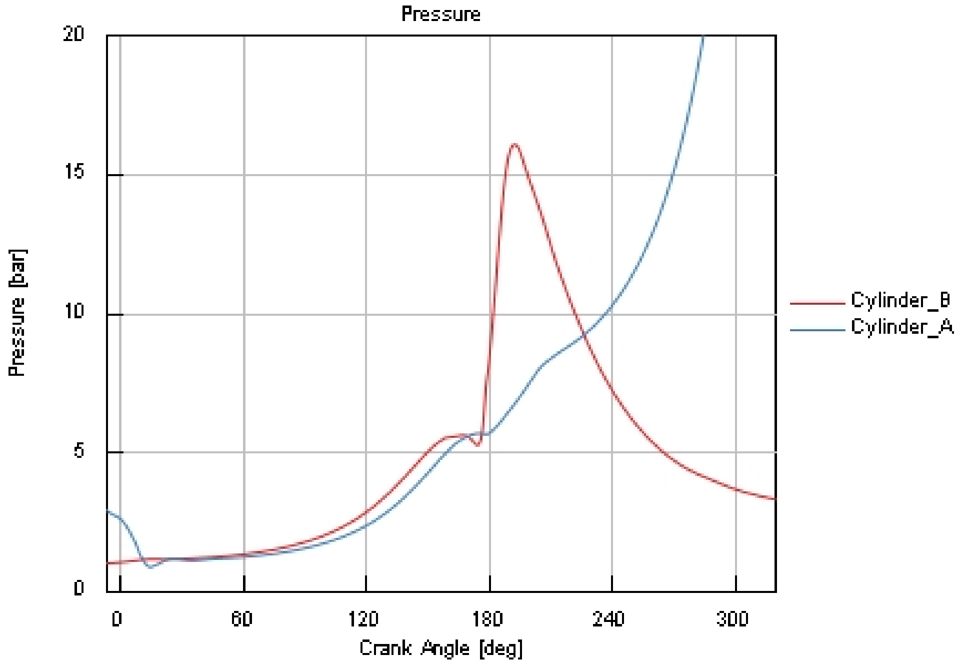

Figure 4.3: Zoom on pressure match during compression stroke

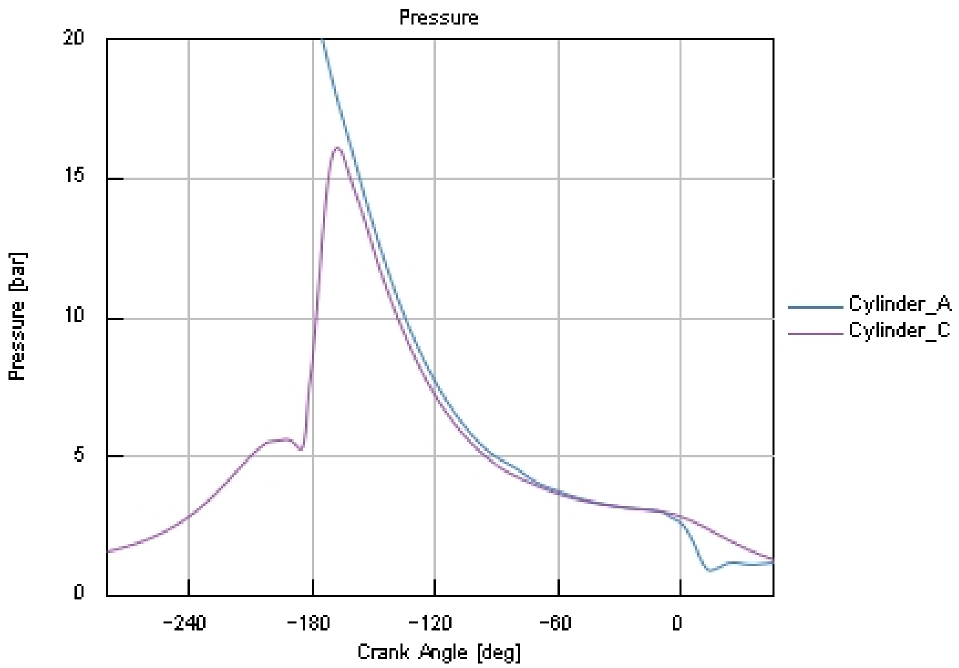

Figure 4.4: Zoom on pressure match during expansion stroke

Another important observation concerns the timing of the pressure peaks. The LP cylinder reaches its maximum pressure at approximately 180 CAD, whereas the HP cylinder reaches its peak shortly after 360 CAD. The two cylinders therefore experience their maximum pressure at different crank angle positions, reflecting the sequential nature of the thermodynamic processes occurring in the two cylinders.

In the picture below it's possible to appreciate how the Compression valve (i.e. the valve connecting LP and HP units) opens to transfer the gas causing a slight fast pressure drop.

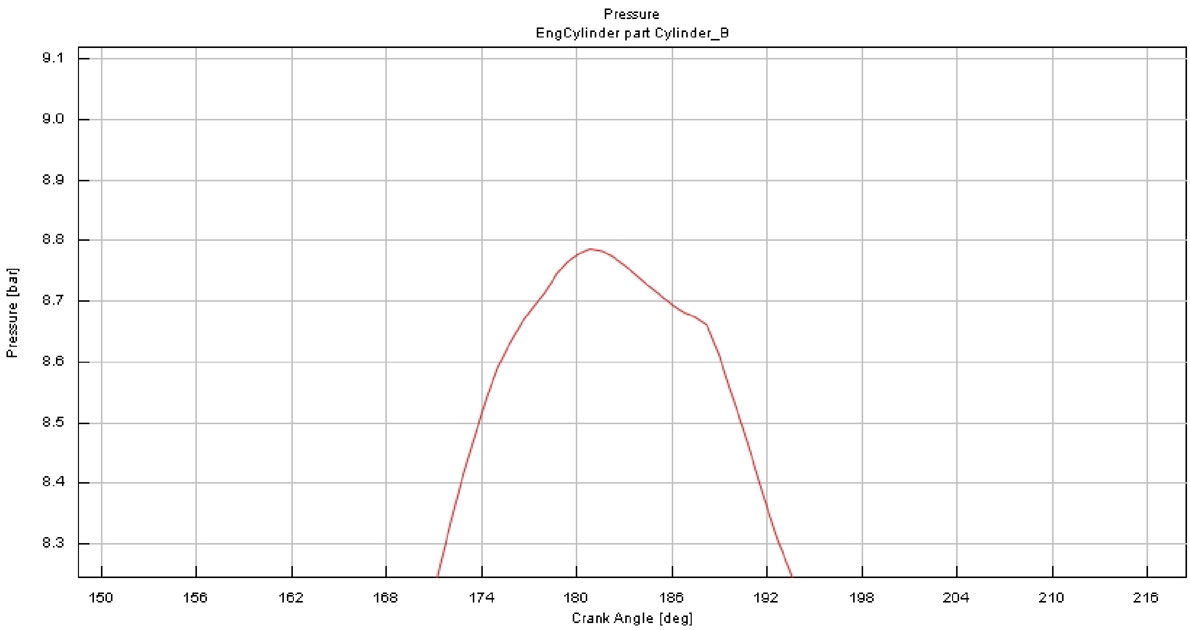

Figure 4.5: Zoom on the pressure drop

In the picture below it's possible to appreciate the valves' lift profiles with respect to CA in to understand better what's happening in the cylinder.

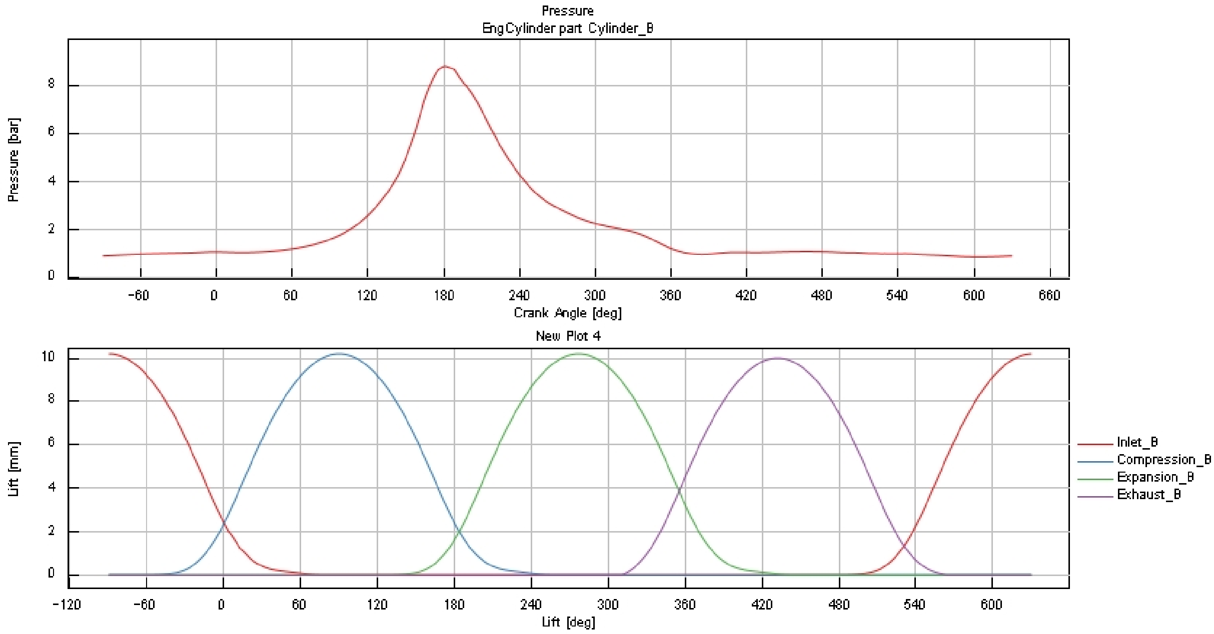

Figure 4.6: Pressure trace and valves' lift profile of low pressure unit

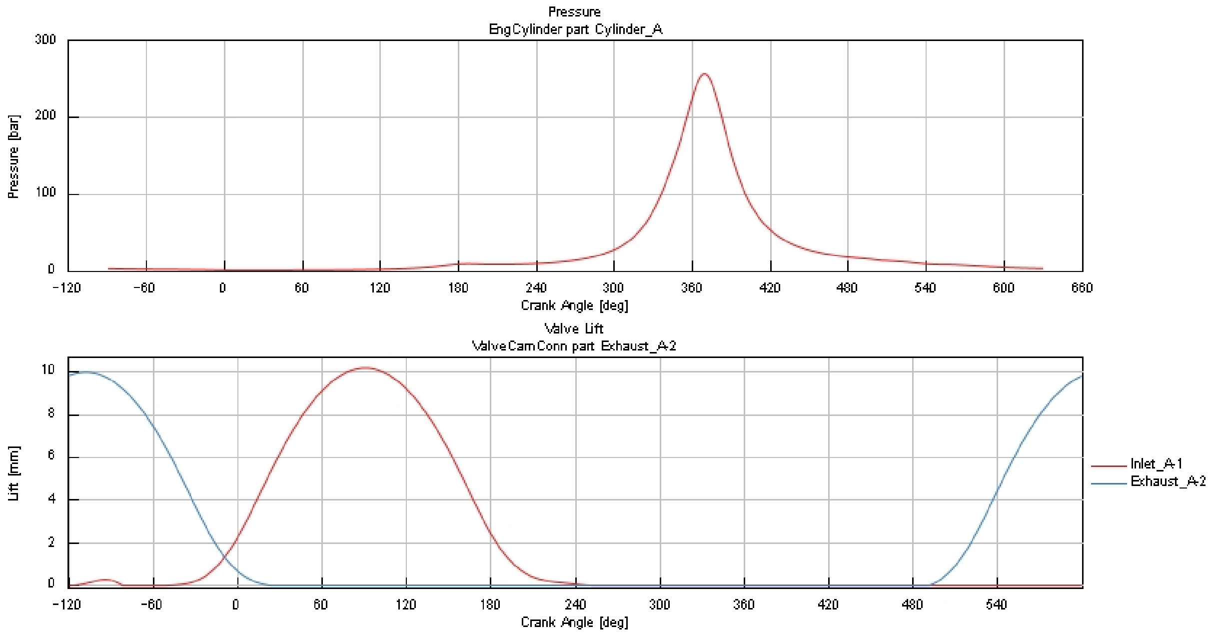

Figure 4.7: Pressure trace and valves' lift profile of high pressure unit

4.3. Pressure - Volume diagrams

The pressure–volume diagrams provide a direct representation of the work exchange occurring during the engine cycle. Starting from the pressure and volume data exported from the GT-Power simulations, the p–V diagrams of the HP and LP cylinders were reconstructed and the enclosed areas were evaluated numerically.

The indicated work was calculated from the pressure–volume loop according to

$$W = \oint p\,dV \tag{4.1}$$

For a four-stroke cycle, the gross indicated work is obtained by integrating the loop over the compression and expansion part of the cycle only, whereas the pumping work is associated with the low-pressure gas exchange loop. Accordingly, the following definitions were used:

$$W_{\text{gross}} = \int_{\text{total}} p\,dV \tag{4.2}$$

$$W_{\text{pump}} = \int_{\text{intake + exhaust}} p\,dV \tag{4.3}$$

$$W_{\text{net}} = W_{\text{gross}} + W_{\text{pump}} \tag{4.4}$$

Figure 4.8 shows the pressure–volume diagrams of the LP and HP cylinders at the baseline operating condition.

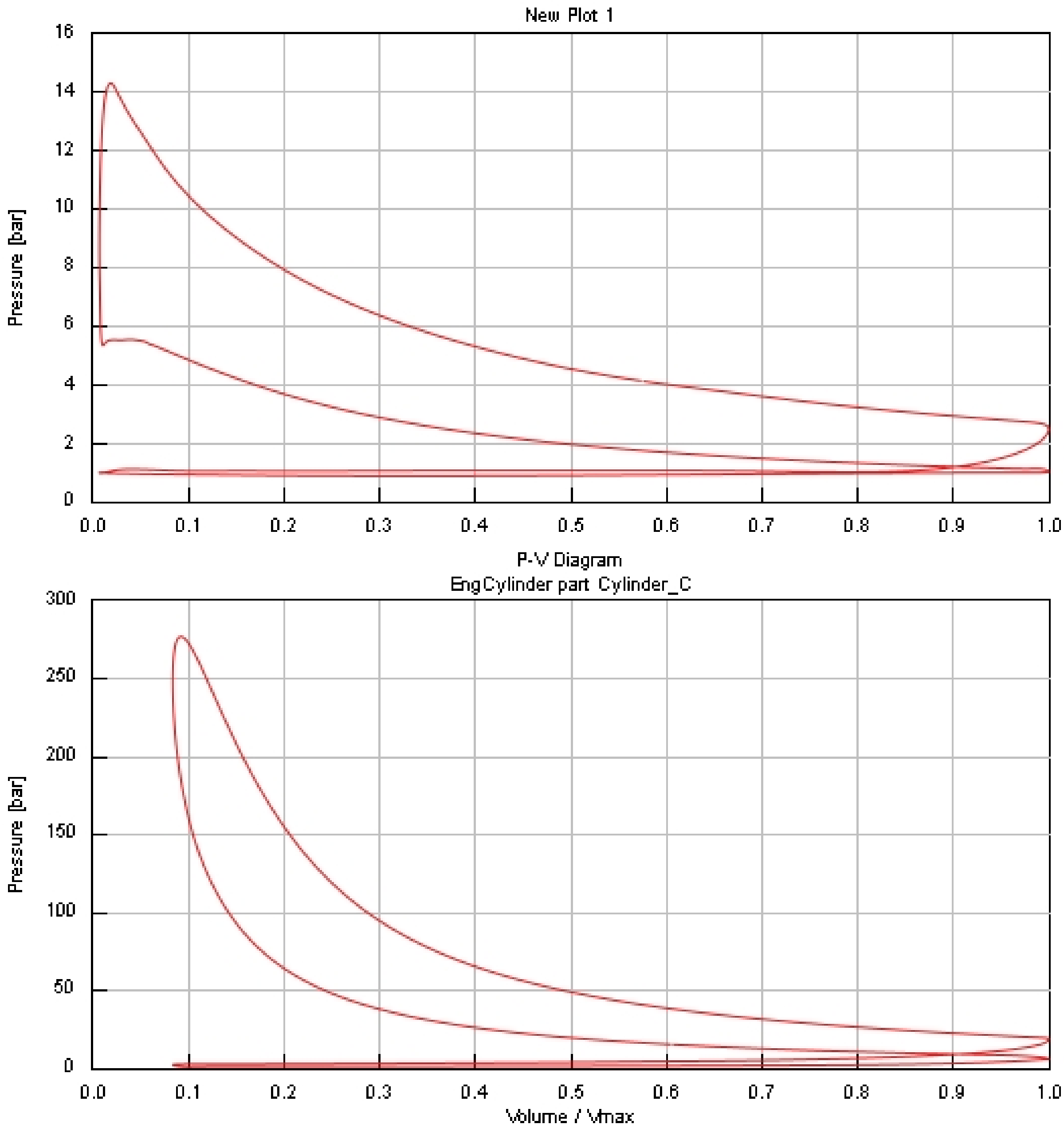

Figure 4.8: Pressure–volume diagrams of the LP cylinder (top) and HP cylinder (bottom) at the baseline operating condition.

The calculated work values are summarized in Table 4.1.

The consistency of the calculated values can be verified directly. The total net work is obtained as

$$W_{\text{net,tot}} = 2\left(W_{\text{net,HP}} + W_{\text{net,LP}}\right) \tag{4.5}$$

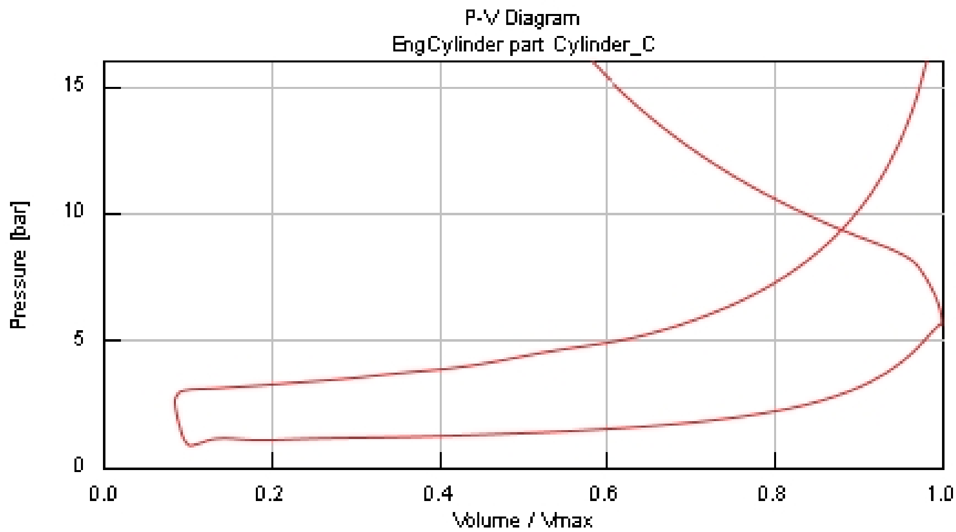

Figure 4.9: Zoom on low pressure zone of p-V diagram of HP cylinder

Table 4.1: Work values obtained from numerical integration of the p–V diagrams.

Quantity	Value [J]
Total net work, $W_{\mathrm{net,tot}}$	4235.62
Total gross work, $W_{\mathrm{gross,tot}}$	4580.15
Total pumping work, $W_{\mathrm{pump,tot}}$	-344.54
Net work, HP cylinder, $W_{\mathrm{net,HP}}$	1619.67
Net work, LP cylinder, $W_{\mathrm{net,LP}}$	498.14
Gross work, HP cylinder, $W_{\mathrm{gross,HP}}$	1759.82
Gross work, LP cylinder, $W_{\mathrm{gross,LP}}$	530.26

$$W_{\text{net,tot}} = 2\,(1619.67 + 498.14) = 4235.62\ \text{J} \tag{4.6}$$

Similarly, the total gross work is

$$W_{\text{gross,tot}} = 2\,(W_{\text{gross,HP}} + W_{\text{gross,LP}}) \tag{4.7}$$

$$W_{\text{gross,tot}} = 2\,(1759.82 + 530.26) = 4580.15\ \text{J} \tag{4.8}$$

The relation between total net, gross and pumping work is

$$W_{\text{net,tot}} = W_{\text{gross,tot}} + W_{\text{pump,tot}} \tag{4.9}$$

$$4235.62 = 4580.15 - 344.54 \tag{4.10}$$

The contribution of the HP cylinder to the net work is substantially larger than that of the LP cylinder. The ratio between the net works of the two cylinders is

$$\frac{W_{\text{net,HP}}}{W_{\text{net,LP}}} = \frac{1619.67}{498.14} = 3.25 \tag{4.11}$$

A similar trend is obtained for the gross work:

$$\frac{W_{\text{gross,HP}}}{W_{\text{gross,LP}}} = \frac{1759.82}{530.26} = 3.32 \tag{4.12}$$

Therefore, the HP cylinder provides more than three times the work contribution of the LP cylinder, both in terms of net and gross indicated work.

The relative magnitude of the pumping work with respect to the total gross work is

$$\frac{|W_{\text{pump,tot}}|}{W_{\text{gross,tot}}} = \frac{344.54}{4580.15} = 0.0752 \tag{4.13}$$

which corresponds to approximately

$$0.0752 \times 100 = 7.52\% \tag{4.14}$$

Thus, the pumping losses are limited compared to the total gross work, while the dominant contribution to the work output is associated with the HP cylinder.

4.4. Heat release rate

The combustion process inside the high-pressure cylinder can be analyzed through the apparent rate of heat release (RoHR). This parameter describes the rate at which chemical energy from the fuel is converted into thermal energy during the combustion process as a function of the crank angle.

The heat release evolution is commonly described using the **Wiebe function**, which provides a parametric representation of the cumulative heat release during combustion. The normalized mass fraction burned (MFB) can be expressed as

$$x_b(\theta) = 1 - \exp\left[-a\left(\frac{\theta - \theta_0}{\Delta\theta}\right)^{m+1}\right] \tag{4.15}$$

where x_b is the burned mass fraction, θ is the crank angle, θ_0 is the start of combustion, $\Delta\theta$ is the combustion duration, a is a shaping constant typically chosen to ensure complete combustion, and m is the **Wiebe exponent**, which determines the shape of the heat release profile.

The apparent rate of heat release is obtained by differentiating the cumulative heat release with respect to the crank angle:

$$RoHR = \frac{dQ}{d\theta} \tag{4.16}$$

Figure 4.10 shows the apparent gross heat release rate obtained from the simulation.

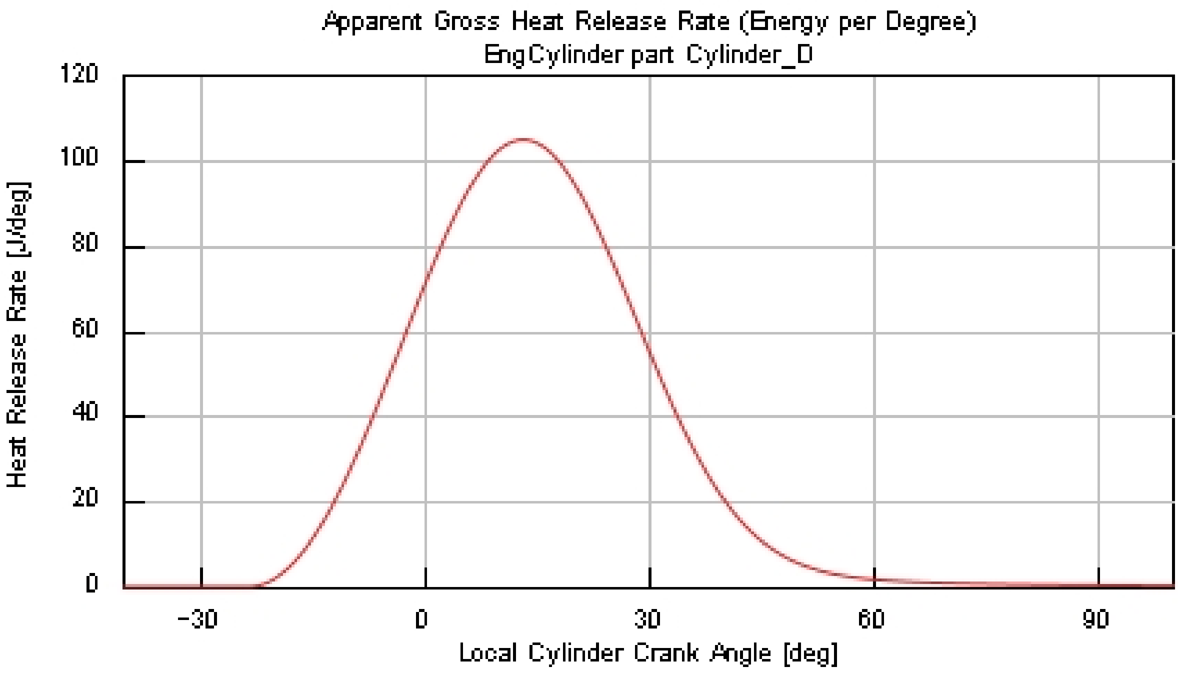

Figure 4.10: Apparent gross heat release rate as a function of crank angle for the high-pressure cylinder.

4.5. In-cylinder temperature evolution

The in-cylinder temperature evolution provides additional insight into the thermodynamic processes occurring in the low-pressure (LP) and high-pressure (HP) cylinders. Figure 4.11 and Figure 4.12 show the temperature traces as a function of crank angle for the LP and HP cylinders respectively.

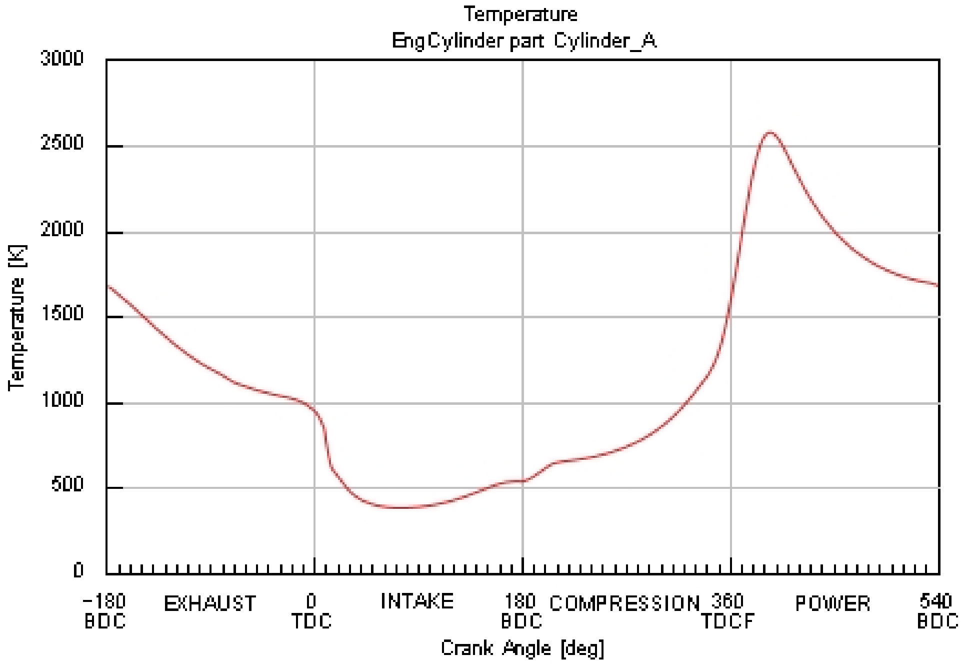

Figure 4.11: Temperature evolution in the low-pressure cylinder.

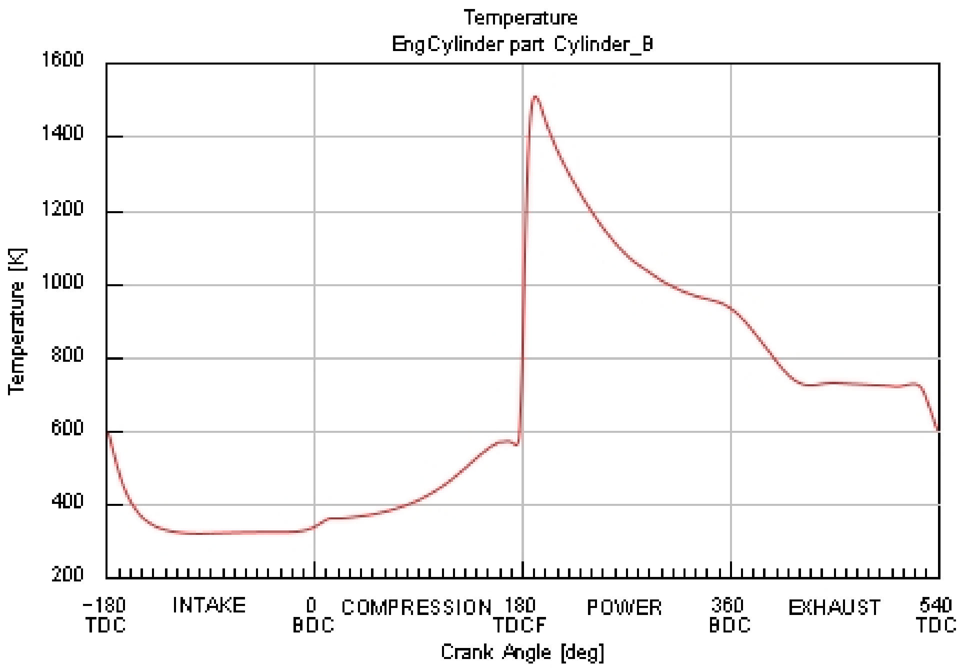

Figure 4.12: Temperature evolution in the high-pressure cylinder.

A clear difference between the two cylinders can be observed. The maximum temperature in the **high-pressure** cylinder reaches approximately **2300–2400**,K, while the peak temperature in the **low-pressure** cylinder remains around 1300–1350 K. This difference is expected since the **combustion process occurs exclusively in the HP cylinder**.

During the compression phase in the HP cylinder, the temperature increases from approximately $600\,K$ to about $900\,K$. Following the ignition and combustion process, a rapid increase in temperature occurs, leading to a peak temperature of approximately $2300\,K$ shortly after top dead center. During the subsequent expansion phase, the temperature progressively decreases as thermal energy is converted into mechanical work.

In contrast, the temperature increase observed in the low-pressure cylinder is mainly associated with the compression process and with the transfer of hot gases coming from the HP cylinder. The maximum temperature remains significantly lower than in the HP cylinder.

A significant temperature drop can be observed during the LP expansion process, with temperatures decreasing to values close to $300\,K$ before the exhaust phase. This indicates that a substantial portion of the thermal energy of the exhaust gases is further converted into mechanical work through the additional expansion stage. Such behavior is consistent with the thermodynamic principle of the double compression expansion engine, which aims at improving the overall cycle efficiency by extracting additional work from the combustion products.

During the compression phase in the HP cylinder, the temperature increases from approximately $600\,K$ to about $900\,K$ due to the compression of the working fluid transferred from the LP cylinder. Following the ignition and combustion process, a rapid increase in temperature occurs, leading to a peak temperature of approximately $2300\,K$ shortly after top dead center. During the subsequent expansion phase, the temperature progressively decreases as thermal energy is converted into mechanical work.

4.6. Engine Performance

The main performance quantities at the baseline operating condition are summarized in the table below. In order to provide a more complete interpretation of the engine output, the brake torque and brake power are also normalized with respect to three different reference displacements: the total displacement of the HP cylinders only, the total displacement of the LP cylinders only, and the overall engine displacement.

Table 4.2: Engine performance and specific metrics with different normalization volumes

Parameter	Unit	Value
Engine speed, N	rpm	3000
Brake torque, T_b	Nm	331.92
Brake power, P_b	kW	104.27
HP displacement, $V_{d,HP}$	L	2×0.398
LP displacement, $V_{d,LP}$	L	2×1.590
Total displacement, $V_{d,tot}$	L	2×1.988
Specific torque (HP), $T_b/V_{d,HP}$	Nm/L	417.0
Specific torque (LP), $T_b/V_{d,LP}$	Nm/L	104.4
Specific torque (total), $T_b/V_{d,tot}$	Nm/L	83.5
Specific power (HP), $P_b/V_{d,HP}$	kW/L	131.0
Specific power (LP), $P_b/V_{d,LP}$	kW/L	32.8
Specific power (total), $P_b/V_{d,tot}$	kW/L	26.2

At the considered operating point, the engine delivers a brake torque of 331.92 Nm and a brake power of 104.27 kW (139.83 hp) at 3000 rpm. These values describe the absolute output of the engine at the baseline condition.

This marked dependence on the selected reference displacement is a direct consequence of the split-cycle nature of the engine. Normalization with respect to the HP displacement highlights the performance intensity of the combustion-dominant cylinder subsystem, whereas normalization based on the total displacement provides a more representative metric for comparison at the complete engine level.

Brake torque behavior can be observed in the picture below over a full-crank rotation.

From this plot is possible to appreciate how the positive torque is not only given when the two HP units undergo the 1^{st}-stage expansion strokes (second and fourth quarter of the plot), but also when the LP units undergo the 2^{nd}-stage expansion stroke (earlier part of first and third quarter of the graph).

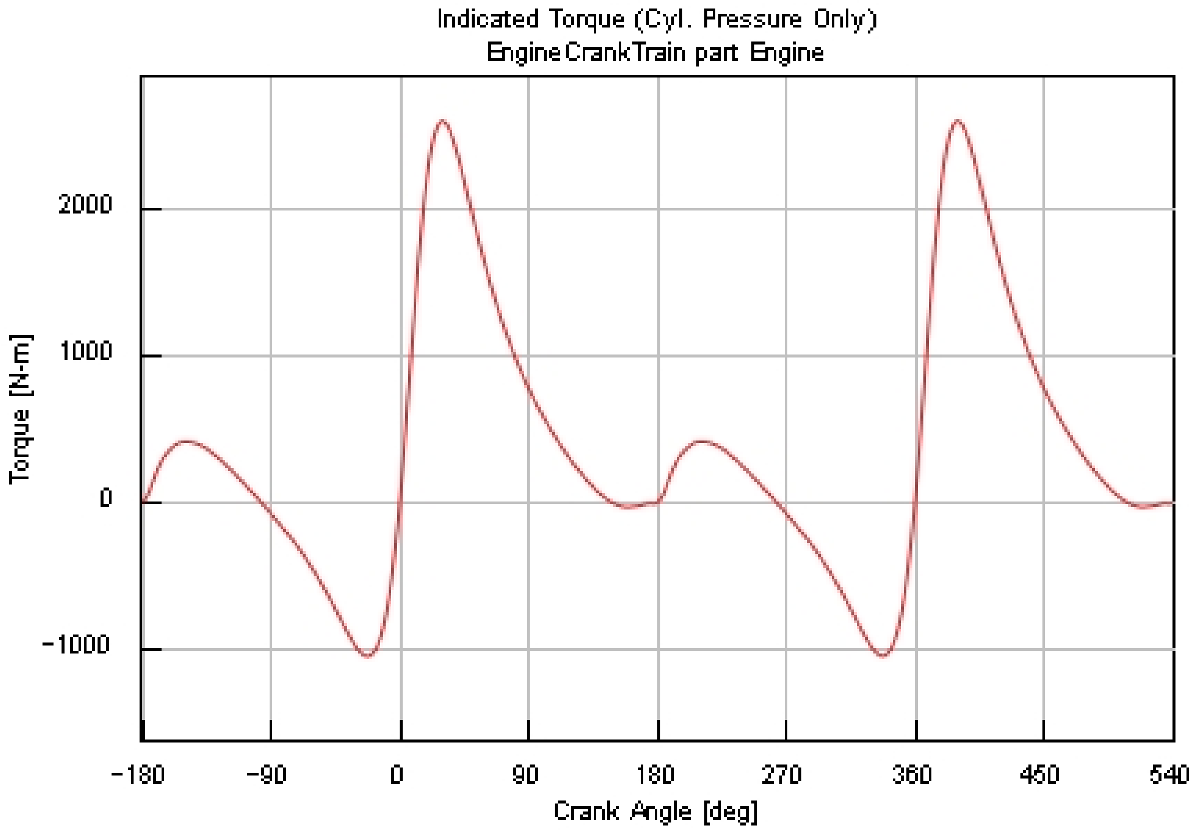

Figure 4.13: Torque vs Crank Angle

4.7. Mean Effective Pressures Analysis

In this section, the engine performance is characterized through the analysis of Mean Effective Pressure (MEP) parameters.

The analysis follows the following thermodynamic approach:

1. **FuelMEP** is calculated from the fuel injection profile which is known and imposed in GT-Power.
2. **QMEP** is calculated by exporting the combustion efficiency from GT-Power, and multiplying it for the FuelMEP.
3. **IMEP**$_{gross}$ calculated using MatLab from the p-V diagrams generated in GT-Power. The integral of such diagrams is calculated to compute the gross work and then divided by the chosen volume to compute IMEP$_{gross}$
4. **PMEP** is taken as an output from GT-Power and subtracted from IMEP$_{gross}$ to obtain **IMEP**$_{net}$

5. **FMEP** is calculated by GT-Power and taken as an output
6. **BMEP** is calculated knowing finale shaft torque and engine's RPMs.

Due to the asymmetrical displacement of the HP and LP stages, all MEP parameters have been normalized using three different reference volumes to provide a comprehensive view of the engine's energy distribution.

4.7.1. Experimental Data and Normalization Results

The following tables summarize the displacement values and the resulting MEPs for each normalization case. The engine operates at a torque of 331.92Nm with a fuel mass flow rate of 5.06g/s and a Lower Heating Value (LHV) of 43MJ/kg.

Table 4.3: MEP values normalized with respect to the High Pressure cylinders total volume ($V_{d,HP,tot} = 795.22cm^3$).

Parameter	**Value [bar]**
FuelMEP	109.37
QMEP	109.15
IMEP$_{gross}$	57.59
IMEP$_{net}$	53.26
PMEP	-4.33
BMEP	52.45
FMEP	0.8122

Table 4.4: MEP values normalized with respect to the Low Pressure cylinders total volume ($V_{d,LP,tot} = 3180.86cm^3$).

Parameter	**Value [bar]**
FuelMEP	27.34
QMEP	27.28
IMEP$_{gross}$	14.39
IMEP$_{net}$	13.31
PMEP	-1.08
BMEP	13.11
FMEP	0.2031

The high values of net indicated mean effective pressure (IMEP$_{net}$) and brake mean effective pressure (BMEP) obtained throughout the analysis confirm the capability of the DCEE architecture to maintain competitive load levels despite the strong focus on efficiency optimization. This result suggests that the split-cycle configuration is able to preserve a significant work extraction capability while simultaneously improving the ther-

Table 4.5: MEP values normalized with respect to the total engine displacement ($V_{d,tot} = 3976.08cm^3$).

Parameter	**Value [bar]**
FuelMEP	21.87
QMEP	21.83
IMEP$_{gross}$	11.52
IMEP$_{net}$	10.65
PMEP	-0.8665
BMEP	10.49
FMEP	0.1624

modynamic efficiency of the cycle. In particular, the high IMEP$_{net}$ values indicate an effective conversion of the combustion process into useful indicated work, whereas the corresponding BMEP levels demonstrate that the mechanical losses, although increased in the optimized configurations, remain sufficiently contained to preserve an overall favourable engine output.

4.7.2. Efficiency Analysis

In this section, the different efficiency components of the internal combustion engine are analyzed, starting from the Mean Effective Pressure (MEP) values calculated in the previous subchapter. These parameters allow for a breakdown of the energy conversion process, from the chemical energy of the fuel to the effective mechanical work at the crankshaft.

Commentary on Results

The obtained results show a high level of performance for the analyzed engine. Specifically:

- The **Thermal Efficiency** ($\eta_T \approx 54.3\%$) is remarkably high, suggesting low losses due to heat transfer and exhaust gases.
- The **Combustion effiecency** ($\eta_C \approx 99.8\%$) is high, meaning full-combustion occurs in the cycle.
- The **Gas Exchange Efficiency** ($\eta_{GE} \approx 91.9\%$) indicates relatively low pumping losses.
  Such pumping losses have been reduced via different iterations by modifying the valve timing and ducts dimension, leading to an acceptably low value of PMEP.
- The **Mechanical Efficiency** ($\eta_M \approx 95.5\%$) reflects very low internal friction.

Table 4.6: Summary of calculated engine efficiencies and their physical interpretations.

Efficiency Name	Symbol	Formula	Value	Physical Meaning
Combustion	η_C	$\frac{QMEP}{FuelMEP}$	99.80	Fraction of fuel which undergoes full combustion
Thermal	η_T	$\frac{IMEP_g}{QMEP}$	54.25	Conversion of fuel heat into gross indicated work; accounts for heat transfer and exhaust losses.
Gas Exchange	η_{GE}	$\frac{IMEP_n}{IMEP_g}$	91.90	Energy losses during the pumping cycle (intake and exhaust strokes).
Mechanical	η_M	$\frac{BMEP}{IMEP_n}$	95.52	Fraction of net work after overcoming friction and driving auxiliaries.
Brake	η_B	$\eta_C\eta_T\eta_{GE}\eta_M$	47.53 %	Global engine efficiency: ratio of useful brake work to total energy input.

- Consequently, the **Brake Efficiency** ($\eta_B \approx 47.5\%$) it's a good result to start improving the brake efficiency of the model, considering that conventional N/A engine reach around 30-35 % % BTE and Atkinson or Miller's cycles reaching up to 41 %.

5 | Parametric Sensitivity Analysis

5.1. Introduction

The primary objective of this chapter is to conduct a systematic **parametric sensitivity analysis** to evaluate how variations in fundamental engine operating variables influence global performance. The investigation focuses on quantifying the impact of these parameters on the **Mean Effective Pressure (MEP)** and the overall **engine efficiencies** (η), including thermal, volumetric, and fuel conversion efficiency.

By isolating individual variables, the non-linear response of the system can be characterized, identifying the critical trade-offs between power density, fuel economy, and emissions. The analysis is structured into the following sub-sections:

- **Fuel-Air Ratio (F/A):** An analysis of mixture strength and its effect on chemical energy release and adiabatic flame temperature.
- **Valve Lift Profile Overlap:** An investigation into the gas exchange process, scavenging effectiveness, and residual gas fraction.
- **Combustion Phasing and Duration:** A study on the impact of the **Start of Combustion (SOC)** and the $10\% - 90\%$ **Mass Fraction Burned (MFB)** interval.

5.2. Impact of the Fuel-Air Ratio (F/A)

This section explores the influence of the fuel-air equivalence ratio, defined as the ratio between the actual and the stoichiometric fuel-air proportions:

$$\lambda = \frac{(F/A)_{actual}}{(F/A)_{stoich}} \tag{5.1}$$

The variation of λ significantly affects the thermodynamic properties of the working fluid, particularly the specific heat ratio $\gamma = c_p/c_v$. The analysis focuses on how the transition from lean-burn conditions ($\lambda < 1$) to rich mixtures ($\lambda > 1$) alters the peak cylinder pressure (P_{max}) and the resulting thermal efficiency (η_{th}).

The baseline simulations were performed at a relative air-fuel ratio of $\lambda = 0.83$, representative of slightly rich operating conditions.

A total of 20 simulations were carried out by varying λ over a wide range, spanning from fuel-rich ($\lambda \approx 0.78$) to highly lean mixtures ($\lambda \approx 1.58$). The adopted distribution of λ values is non-uniform, with a finer resolution in the vicinity of stoichiometric conditions ($\lambda \approx 1$), where combustion sensitivity is higher, and coarser spacing at more extreme lean conditions.

The average increment between consecutive λ values is approximately $\Delta\lambda_{\text{avg}} = 0.0426$. However, it is important to note that this value is not representative of the local resolution across the entire range. In particular, near-stoichiometric conditions are characterized by much smaller increments (on the order of 10^{-3}), enabling a more detailed analysis of the transition in combustion behavior and performance.

This setup allows for a comprehensive evaluation of the impact of mixture composition on mean effective pressures and efficiency metrics across different operating regimes.

Table 5.1: Air-fuel ratio values (λ) and incremental variation

λ	$\Delta\lambda$
0.7758	–
0.8270	0.0513
0.8918	0.0648
0.9600	0.0682
0.9663	0.0063
0.9747	0.0084
0.9811	0.0064
0.9876	0.0065
0.9939	0.0063
1.0006	0.0067
1.0077	0.0071
1.0140	0.0063
1.0209	0.0069
1.0252	0.0043
1.0345	0.0093
1.0394	0.0049
1.1368	0.0974
1.2579	0.1211
1.4003	0.1424
1.5842	0.1839

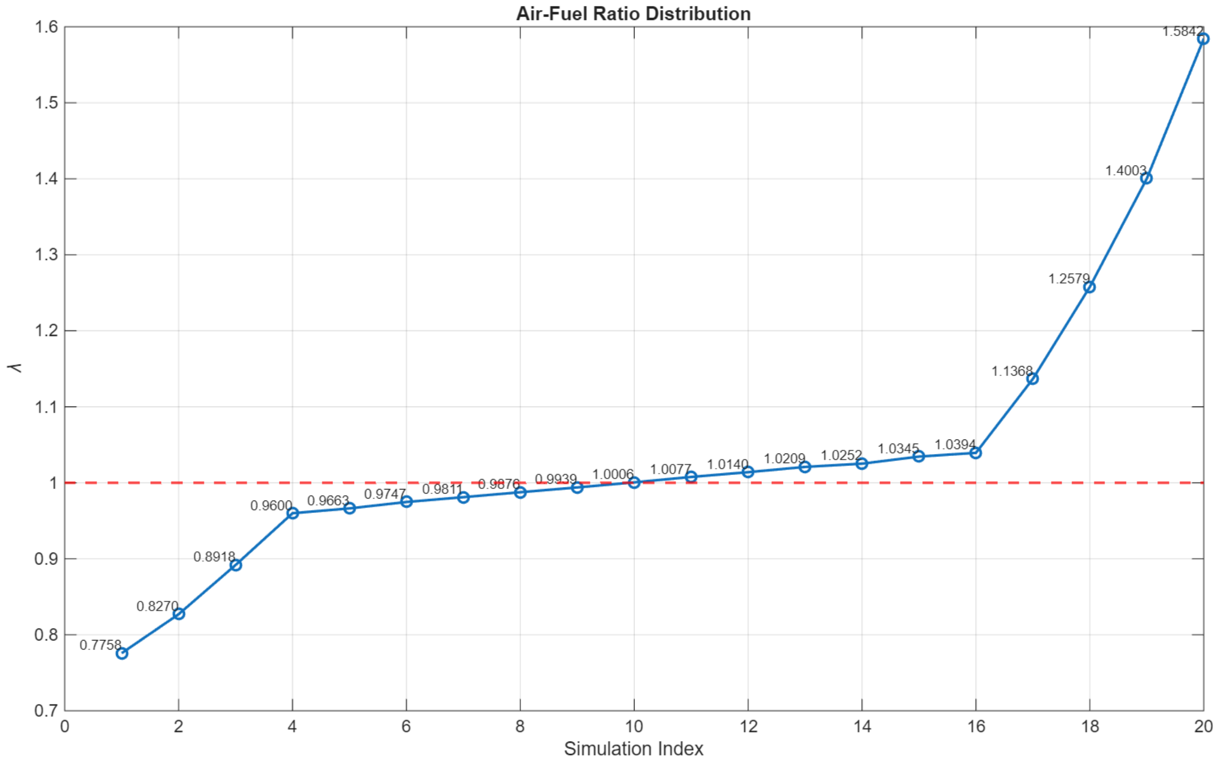

Figure 5.1: Lambda values of the chosen operating points

5.2.1. Effect on combustion efficiency

The combustion efficiency as a function of the air-fuel ratio was fitted using a logistic function:

$$\eta_C(\lambda) = \frac{L}{1 + \exp\left[-k(\lambda - \lambda_0)\right]} \tag{5.2}$$

where the fitted parameters are: $L = 1.0006$, $k = 20.07$, and $\lambda_0 = 0.699$.

The results show a rapid transition from incomplete to nearly complete combustion in the rich-to-stoichiometric region, followed by a plateau at $\eta_C \approx 1$ for lean mixtures.The combustion efficiency as a function of the air-fuel ratio was fitted using a logistic function:

$$\eta_C(\lambda) = \frac{L}{1 + \exp\left[-k(\lambda - \lambda_0)\right]} \tag{5.3}$$

where the fitted parameters are: $L = 1.0006$, $k = 20.07$, and $\lambda_0 = 0.699$.

The results show a rapid transition from incomplete to nearly complete combustion in the rich-to-stoichiometric region, followed by a plateau at $\eta_C \approx 1$ for lean mixtures.

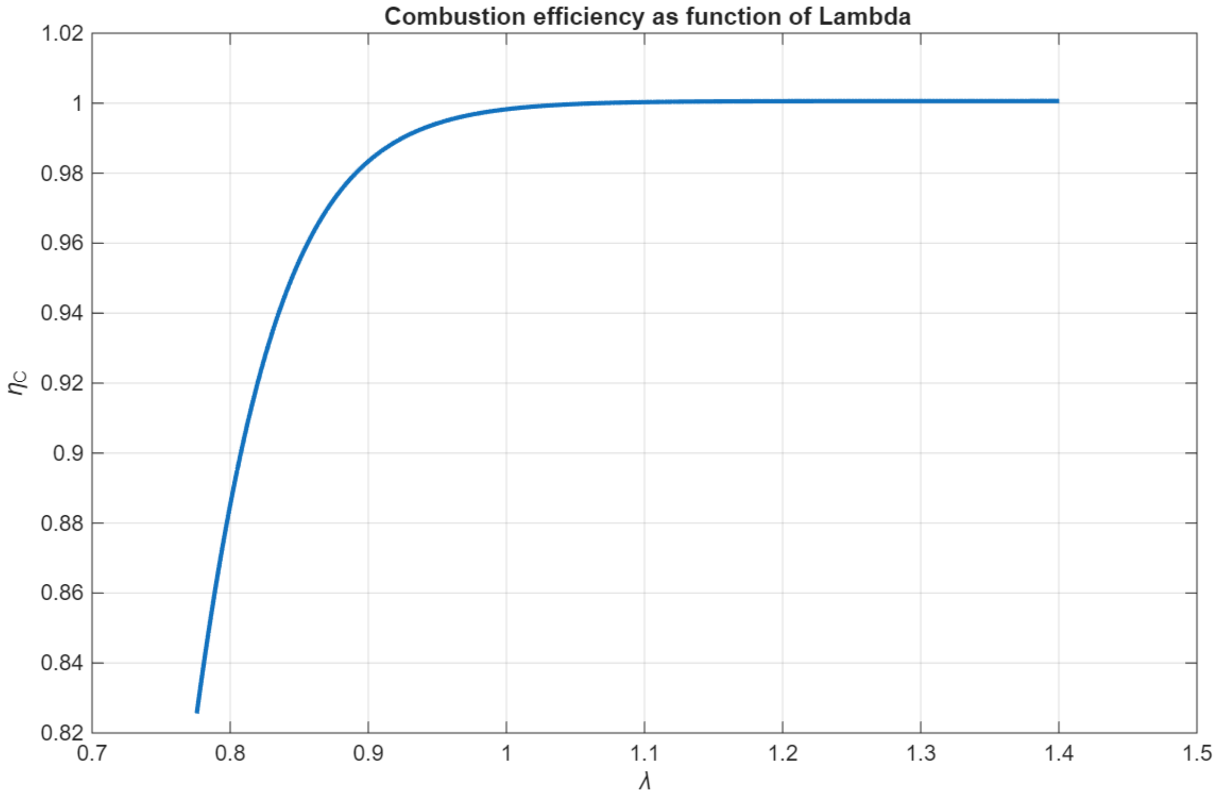

Figure 5.2: Combustion efficiency as function of λ

A logistic function was selected to fit the combustion efficiency as a function of the air-fuel ratio, as it captures the characteristic sigmoidal behavior of the process.

In fuel-rich conditions, combustion efficiency is limited by oxygen availability, leading to incomplete combustion. As the air-fuel ratio approaches stoichiometric conditions, a rapid transition occurs, resulting in near-complete combustion.

This behavior naturally leads to a bounded, non-linear response with a saturation level at $\eta_C \approx 1$, which is inherently represented by the logistic model.

5.2.2. Effect of Air-Fuel Ratio on Efficiencies

The figure below shows the variation of the main efficiency contributions as a function of the air-fuel ratio λ.

The combustion efficiency exhibits the expected behavior, with a rapid increase in the rich region followed by a plateau close to unity for $\lambda \geq 0.9$, indicating nearly complete combustion under stoichiometric and lean conditions.

The thermal efficiency shows a more complex trend. After an initial decrease in the rich region, a noticeable increase is observed for $\lambda > 1$, reaching a local maximum at $\lambda =$

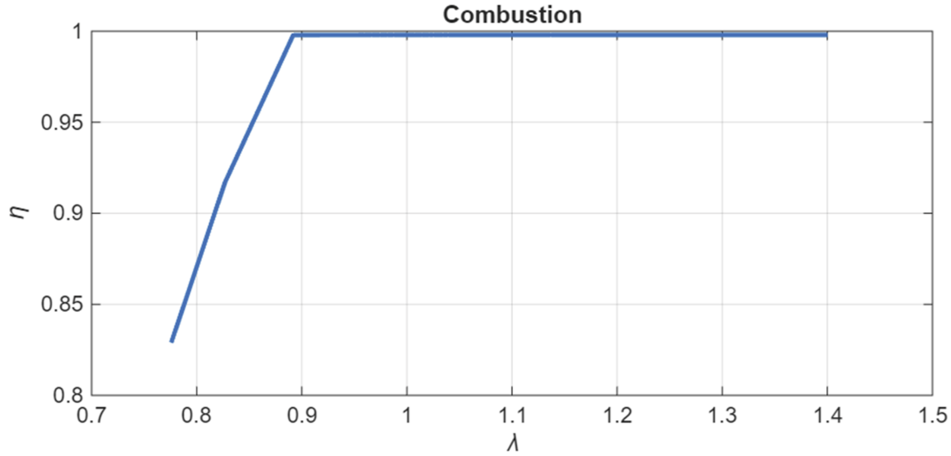

Figure 5.3: η_c vs λ

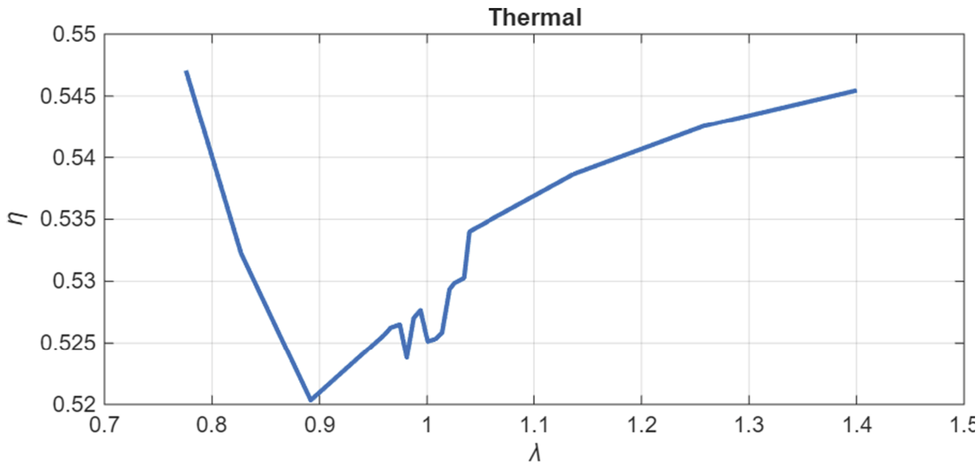

Figure 5.4: η_{th} vs λ

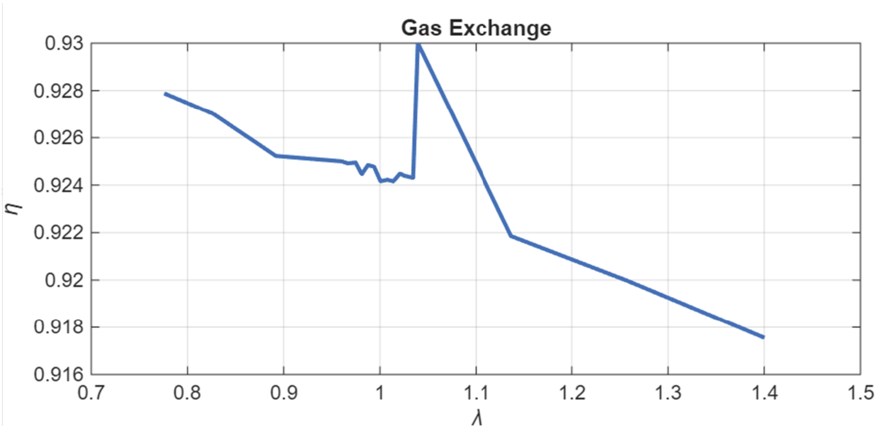

Figure 5.5: η_{ge} vs λ

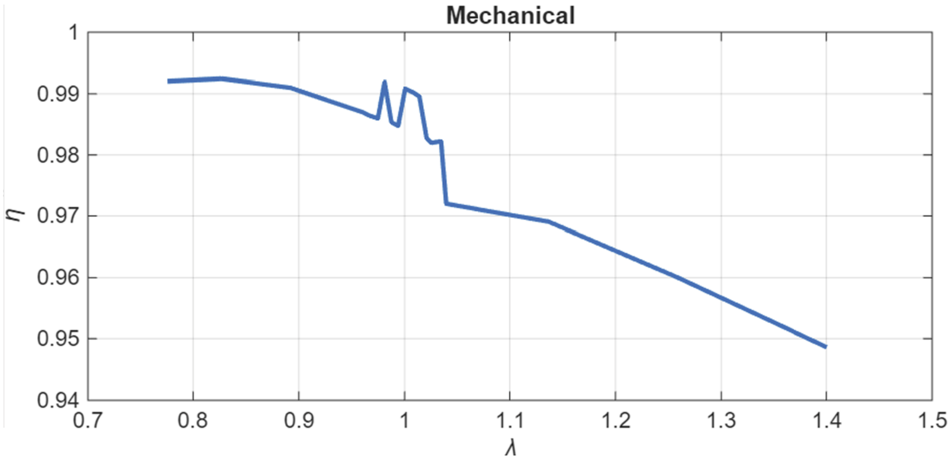

Figure 5.6: η_m vs λ

1.04. This improvement can be attributed to more favorable thermodynamic conditions associated with leaner mixtures, such as reduced heat losses and improved expansion characteristics.

On the other hand, the gas exchange efficiency gradually decreases with increasing λ, suggesting increased pumping losses or less effective cylinder filling under lean conditions. Similarly, the mechanical efficiency shows a slight but consistent reduction as λ increases, likely due to variations in in-cylinder pressure levels affecting friction-related losses.

The combined effect of these competing trends results in a maximum brake efficiency of 48.17% **at** $\lambda = 1.04$. This operating point represents the best trade-off between the different efficiency contributions. Therefore, $\lambda = 1.04$ is selected as the reference condition for further optimization of the engine configuration.

The following plot compares the brake efficiency calculated directly via GT-Power with the one calculated exporting the MEPs calculated on Matlab

5.3. Valve Lift Profile Overlap

The overlap period, defined as the crank angle interval during which both intake and exhaust valves are simultaneously open.

Building upon the results discussed in the previous sub-chapter, where the optimal air-fuel ratio was identified, this section investigates the impact of the valve overlap duration ($\Delta\theta_{overlap}$) on the overall engine performance and efficiency contributions.

In particular, three distinct configurations are considered:

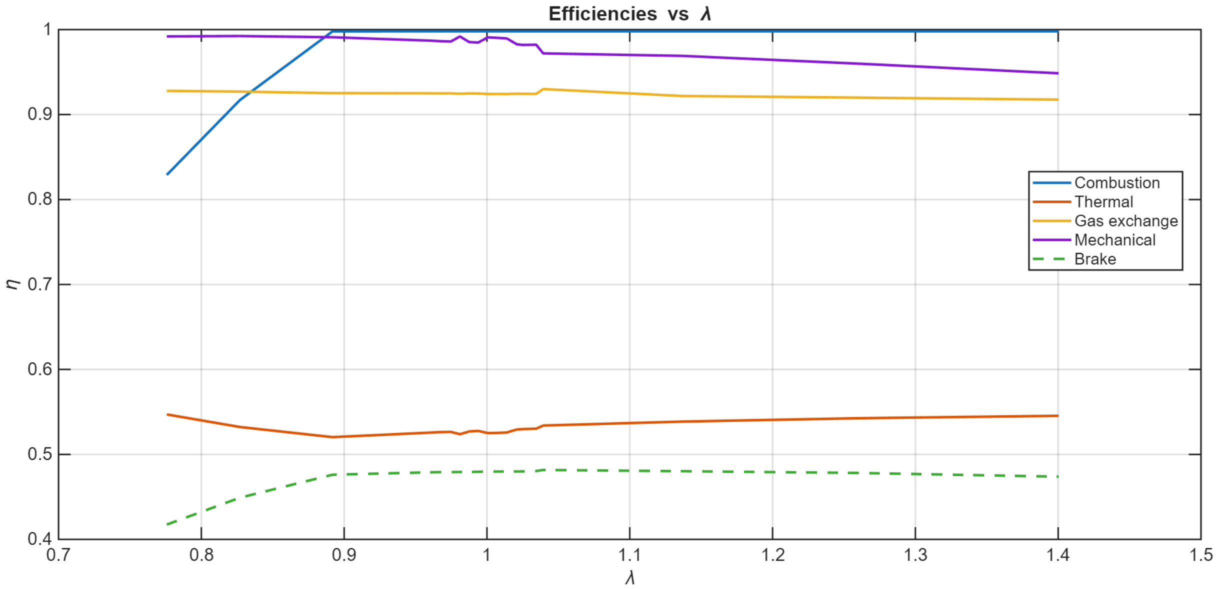

Figure 5.7: Superposition of the efficiencies vs λ

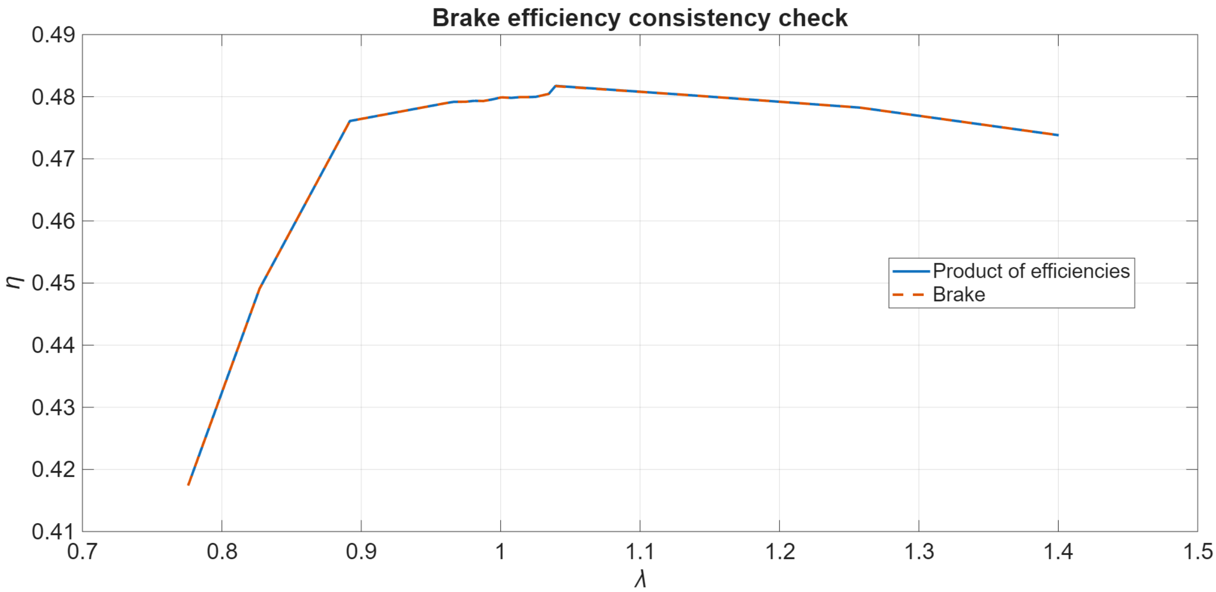

Figure 5.8: η_B vs λ

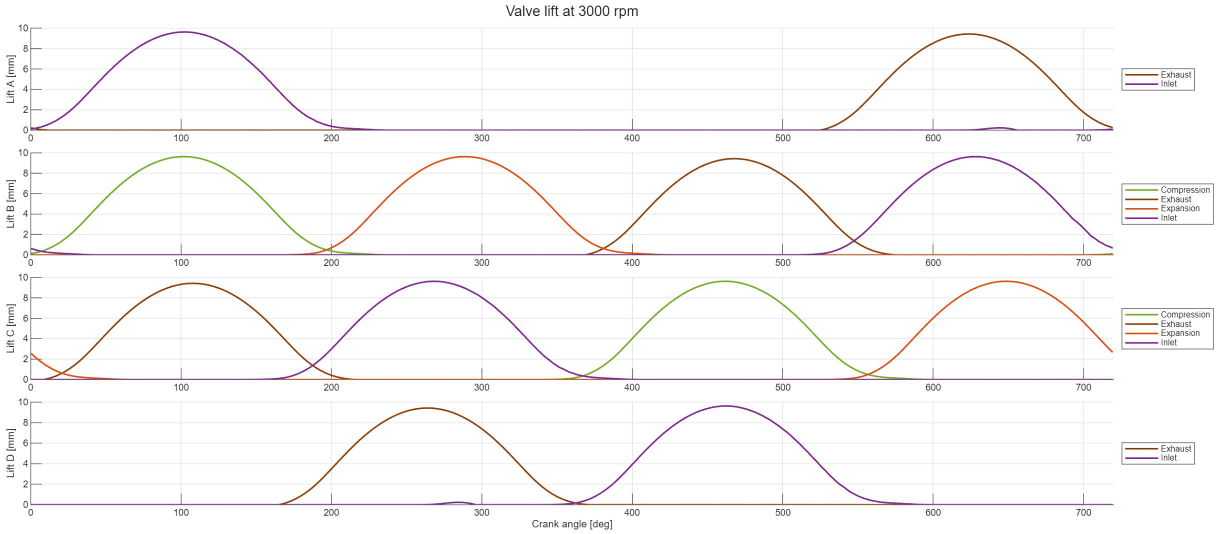

Figure 5.9: Lift Profile with moderate Overlapping

- **Zero overlap**: no simultaneous opening of intake and exhaust valves,
- **Moderate overlap**: limited overlap between valve lift profiles, the lift profiles of the valves are overlapped of about 15 degrees.
- **High overlap**: extended overlap duration, the lift profiles of the valves are overlapped of about 30 degrees

It should be noted that the **moderate overlap** configuration will not be further investigated in this section, as it corresponds to the baseline valve timing adopted in the previous simulations. Therefore, the following analysis will focus exclusively on the comparison between the **zero overlap** and **high overlap** cases.

These configurations allow for a systematic assessment of the trade-off between improved scavenging and increased short-circuiting losses, and their combined effect on combustion, thermal, mechanical, and gas exchange efficiencies, as well as on the resulting brake performance.

5.3.1. Low Overlap lift profiles

The transition from the baseline valve overlap configuration to the zero-overlap case results in a measurable impact on engine performance and efficiency. In particular, at 3000 rpm, the brake power decreases from **82.3 kW** to **80.7 kW**, corresponding to a reduction of approximately **1.9%**.

From an efficiency standpoint, the most significant variation is observed in the **thermal efficiency**, which drops sharply from **66.0%** to **50.3%**. A noticeable decrease is also found in the **gas exchange efficiency**, from **93.78%** to **89.13%**. On the other hand, both **mechanical efficiency** and **combustion efficiency** remain essentially unchanged across the two configurations.

The combined effect of these variations leads to a reduction in overall engine performance, with the **brake efficiency** decreasing from **48.09%** to **43.42%**. This highlights how the removal of valve overlap, while slightly affecting the delivered power, has a much more pronounced impact on the thermodynamic and gas exchange processes, ultimately penalizing the global efficiency of the engine.

The observed reduction in thermal and gas exchange efficiencies can be primarily attributed to the worsened scavenging process and in-cylinder flow dynamics. Without overlap, the momentum of the exhaust gases is no longer exploited to promote the inflow of fresh charge, leading to a less effective cylinder filling and an increase in residual gas fraction.

The higher presence of residual gases dilutes the fresh mixture, lowering the effective oxygen concentration and reducing the combustion temperature. This results in a less favorable thermodynamic cycle, with reduced peak pressures and a lower expansion work, thereby explaining the significant drop in thermal efficiency.

At the same time, the deterioration in gas exchange efficiency is linked to increased pumping losses and less efficient mass exchange during the intake and exhaust phases. The lack of overlap prevents beneficial pressure wave interactions between intake and exhaust systems, which would otherwise enhance volumetric efficiency. Consequently, the engine operates with a reduced fresh charge mass and less efficient gas renewal, directly impacting both gas exchange and overall thermodynamic performance.

Parameter	**Baseline (Moderate Overlap)**	**Zero Overlap**	**Variation**
Brake Power [kW]	82.3	80.7	-1.9%
Thermal Efficiency [%]	66.0	50.3	-23.8%
Gas Exchange Efficiency [%]	93.78	89.13	-5.0%
Mechanical Efficiency [%]	–	–	$\approx$ const.
Combustion Efficiency [%]	–	–	$\approx$ const.
Brake Efficiency [%]	48.09	43.42	-9.7%

Table 5.2: Effect of valve overlap removal on engine performance and efficiencies at 3000 rpm

5.3.2. High overlap lift profiles

The transition from the baseline valve overlap configuration to the high-overlap case results in a noticeable impact on engine performance and efficiency. In particular, at 3000 rpm, the brake power decreases from **82.3 kW** to **65.3 kW**, corresponding to a reduction of approximately **20.7%**.

From an efficiency standpoint, a significant decrease is observed in the **thermal efficiency**, which drops from **66.0%** to **44.16%**. The **gas exchange efficiency** shows a slight reduction, from **93.78%** to **92.95%**. Additionally, the **mechanical efficiency** decreases from **96.9%** to **95.41%**, while the **combustion efficiency** remains essentially unchanged.

The combined effect of these variations leads to a marked reduction in overall engine performance, with the **brake efficiency** decreasing to **39.11%**. This highlights how excessive valve overlap, while potentially beneficial for scavenging under certain conditions, introduces significant short-circuiting losses that penalize both the thermodynamic cycle and the effective energy conversion into useful work.

Parameter	Baseline (Moderate Overlap)	High Overlap	Variation
Brake Power [kW]	82.3	65.3	-20.7%
Thermal Efficiency [%]	66.0	44.16	-33.1%
Gas Exchange Efficiency [%]	93.78	92.95	-0.9%
Mechanical Efficiency [%]	96.9	95.41	-1.5%
Combustion Efficiency [%]	–	–	≈ const.
Brake efficiency [%]	48.09	39.11	-8.98%

Table 5.3: Effect of increased valve overlap on engine performance and efficiencies at 3000 rpm

5.4. Combustion Characteristics: SOC and Duration

The thermodynamic cycle is highly sensitive to the Heat Release Rate (HRR) phasing. In this section, the sensitivity of the $P-\theta$ diagram is examined with respect to two primary parameters:

- **Start of Combustion (SOC):** The angular position (expressed in Crank Angle Degrees, CAD) where the energy release initiated relative to Top Dead Center (TDC).

- **Combustion Duration ($\Delta\theta_{10-90}$):** The interval required for the oxidation of the bulk of the fuel mass.

The reference configuration is characterised by a **start of combustion** at 7.1° before TDC of the cycle and a **combustion duration (10% to 90%) of 24.5° crank angle**. Starting from this baseline, a parametric study has been conducted by systematically varying both parameters in order to assess their combined effects. The start of combustion has been modified to **5%, 10%**, and **13%**, while the combustion duration has been extended to **27.5%, 30%, 32.5%**, and **35%**. All possible combinations of these values have been simulated, resulting in a comprehensive matrix of operating conditions.

The objective of this analysis is to evaluate how variations in combustion phasing and heat release rate affect key performance indicators, including efficiency metrics and overall engine behaviour. By comparing the results across the different configurations, it is possible to identify trends and trade-offs associated with earlier or delayed combustion timing, as well as with shorter or longer combustion durations.

5.4.1. Mechanical efficiency

In this part of the sensitivity study, η_m was monitored to evaluate the impact of different combustion phasings and durations ($\Delta\theta_{10-90}$).

The results, summarized in the table below, demonstrate that the mechanical efficiency remains substantially stable across the investigated operating points, with values consistently centered around 0.974.

Combustion Duration	**Spark Advance [CAD]**			
(10-90) [CAD]	**5**	**7.1**	**10**	**13**
24.5	0.97456	0.97314	0.97558	**0.97764**
27.5	0.97348	0.97579	0.97414	0.97442
30	0.97224	0.97376	0.97589	0.97283
32.5	0.97476	0.97358	0.97715	0.97537
35	0.97414	0.97353	0.97427	0.97479

Table 5.4: Mechanical efficiency (η_m) as a function of combustion duration and spark advance.

This trend is physically justified by the fact that mechanical losses are primarily dominated by engine speed (RPM) and mean piston speed, which were kept constant throughout the simulations. While variations in combustion parameters induce changes in the cylinder pressure trace and peak pressure (P_{max}), these effects appear to have a negligible impact on the Friction Mean Effective Pressure (FMEP). Furthermore, since the intake and exhaust boundary conditions remained unaltered, the pumping work contribution to the mechanical offset stayed constant.

The slight fluctuations observed (in the order of 10^{-3}) can be attributed to minor numerical variances in the solver's convergence or negligible changes in the instantaneous force distribution on the crankshaft bearings, which do not significantly alter the overall energy balance of the engine.

5.4.2. Analysis of Combustion Efficiency

Throughout the sensitivity analysis, the combustion efficiency remained high and constant, with a value of approximately 99.8%. This stability is reported in the table below and reflects a near-complete oxidation of the air-fuel mixture. It's worth to remember that such simulations are ran with a mixture corresponding to $\lambda = 1.04$.

Combustion Duration	**Spark Advance [CAD]**			
(10-90) [CAD]	**5**	**7.1**	**10**	**13**
24.5	0.998	0.998	0.998	0.998
27.5	0.998	0.998	0.998	0.998
30	0.998	0.998	0.998	0.998
32.5	0.998	0.998	0.998	0.998
35	0.998	0.998	0.998	0.998

Table 5.5: Combustion efficiency (η_c) for different combustion durations and spark advances.

The invariance of η_c suggests that, within the investigated range of spark advance and combustion duration, the conditions of **Optimal Mixture Preparation, Absence of quenching effects, thermal stability** were maintained.

In conclusion, since η_c remains constant at 99.8%, any variation observed in the overall thermal efficiency or power output can be exclusively attributed to thermodynamic factors (such as the phasing of the heat release) rather than to a loss in the chemical conversion efficiency.

5.4.3. Analysis of Gas Exchange Efficiency

The gas exchange efficiency (η_{ge}) values obtained from the sensitivity analysis are presented in the table below. The data shows a high degree of consistency, with values ranging between 0.921 and 0.938.

Combustion Duration (10-90) [CAD]	**Spark Advance [CAD]**			
	5	**7.1**	**10**	**13**
24.5	0.92351	**0.9378**	0.92531	0.92531
27.5	0.92214	0.92423	0.92245	0.92123
30	0.92446	0.92431	0.92361	0.92286
32.5	0.92375	0.92341	0.92361	0.92180
35	0.92331	0.92279	0.92196	0.92086

Table 5.6: Gas exchange efficiency (η_{ge}) for different combustion durations and spark advances.

This substantial invariance is expected since the gas exchange process is primarily governed by the intake and exhaust manifold pressures, valve timing, and cylinder geometry, all of which remained constant during the simulations. The minor fluctuations observed can be analyzed as follows:

- **Exhaust Blowdown Effects:** Variations in spark advance and combustion duration slightly alter the cylinder pressure and temperature at the moment of Exhaust Valve Opening (EVO). However, these changes are not sufficient to significantly modify the pumping work or the residual gas fraction.
- **Thermal Interaction:** The different heat release rates have a secondary effect on the local gas density during the exhaust stroke, leading to the negligible variances (within 0.5%) recorded in the table.
- **Numerical Robustness:** The stability of η_{ge} confirms that the boundary conditions at the ports were well-defined and that the solver correctly decoupled the combustion thermodynamics from the fluid dynamics of the scavenging process.

In conclusion, the results demonstrate that the gas exchange efficiency is not a sensitive parameter to the phasing of the combustion process within the investigated range.

5.4.4. Analysis of Thermal Efficiency

The thermal efficiency (η_{th}) values obtained from the sensitivity analysis are presented in the table below. The data shows a maximum value of 53.92 % for, corresponding to the maximum value obtained up to the previous process of the sensitivity analysis.

Combustion Duration	Spark Advance [CAD]			
(10-90) [CAD]	5	7.1	10	13
24.5	53.05	53.27	53.45	53.52
27.5	52.41	52.63	52.81	52.90
30	51.86	52.09	**53.92**	52.35
32.5	51.24	51.49	51.66	51.72
35	50.60	50.84	51.04	51.10

Table 5.7: Thermal efficiency (η_t) [%] for different combustion durations and spark advances.

The trends observed in the data can be justified by:

- **Impact of Combustion Duration:** A clear decrease in η_t is observed as the combustion duration increases (moving from 24.5 to 35 CAD). A longer combustion deviates from the ideal constant-volume heat addition of the Otto cycle, causing a larger portion of the energy to be released during the expansion stroke at a lower effective expansion ratio.

- **Impact of Spark Advance:** Increasing the spark advance generally improves the thermal efficiency within the observed range. By advancing the ignition, the combustion process is shifted closer to the Top Dead Center (TDC), resulting in higher peak cylinder pressures and temperatures, which enhance the thermodynamic cycle's work extraction.

- **Combined Effect:** The maximum efficiency (53.92%) is reached at the medium combustion duration (24.5 CAD) and an advance of 13 CAD. Conversely, the minimum value (50.60%) occurs at the longest duration and lowest advance, where the combustion is most "diluted" during expansion.

These results confirm that optimizing the heat release phasing is critical for maximizing the work output per unit of fuel, as even minor changes in combustion timing lead to percentage-point variations in thermal efficiency.

5.4.5. Analysis of Brake Efficiency

The brake efficiency (η_{brake}), is calculated as the product of the individual efficiency components previously discussed. Table 5.8 summarizes these results.

Table 5.8: Brake efficiency (η_{brake}) [%] as a product of partial efficiencies.

Combustion Duration	**Spark Advance [CAD]**			
(10-90) [CAD]	**5**	**7.1**	**10**	**13**
24.5	47.65	48.17	48.25	48.42
27.5	46.96	47.47	47.46	47.48
30	46.52	46.89	**48.66**	47.48
32.5	46.05	46.29	46.63	46.51
35	45.42	45.67	45.85	45.87

Based on the updated data presented in Table 5.8, the following considerations describe the engine's performance as a function of combustion duration and spark advance. The current results indicate a shift in the global optimum compared to previous iterations, revealing a complex interaction between combustion phasing and thermodynamic losses.

- **Identification of the Global Optimum:** The peak brake efficiency of **48.66%** is achieved at a *Combustion Duration* of **30 CAD** and a *Spark Advance* of **10 CAD**.
- **Impact of Partial Efficiencies:** A cross-analysis of the efficiency components confirms that the brake efficiency peak is primarily driven by the indicated thermal efficiency (η_{th}), which reaches its maximum of 53.92% at the (30 CAD, 10 CAD) operating point. The combustion efficiency (η_c) remains nearly ideal at 99.8% across all tests, while the mechanical efficiency (η_m) exhibits minimal variance, thereby exerting a secondary influence on the location of the optimal point.
- **Sensitivity to Spark Timing:** For a fixed combustion duration of 30 CAD, the system demonstrates high sensitivity to ignition timing. Increasing the spark advance from 7.1 CAD to 10 CAD results in a substantial efficiency gain (from 46.89% to 48.66%). However, advancing the timing further to 13 CAD leads to a performance degradation (47.48%), indicating that 10 CAD represents the optimal phasing for centering the heat release rate around the Top Dead Center (TDC).

In conclusion, the **30 CAD duration and 10 CAD spark advance** configuration constitutes the most effective compromise between combustion speed and pressure phasing, yielding the highest overall mechanical performance for the tested engine conditions.

5.5. Conclusion of the sensitivity study

In this subsection the final engine DCEE 4+4 model will be analysed, after this first optimisation, in terms of performances, efficiencies and mean effective pressures.

5.5.1. Engine's performance

Following the comprehensive analysis of partial efficiencies, the engine performance quantities at the identified optimal operating point (Combustion Duration of 30 CAD and Spark Advance of 10 CAD) were calculated. These results describe the engine's absolute and normalized output when configured for maximum overall brake efficiency. To provide a complete interpretation consistent with the split-cycle architecture, the brake torque and brake power have been normalized with respect to three different reference displacements: the total High-Pressure (HP) cylinder displacement, the total Low-Pressure (LP) cylinder displacement, and the overall engine displacement (sum of HP and LP). These performance parameters are summarized in Table X.Y below.

Table 5.9: Engine performance and specific metrics with different normalization volumes

Parameter	Unit	Value
Engine speed, N	rpm	3000
Brake torque, T_b	Nm	288.57
Brake power, P_b	kW	90.7
HP displacement, $V_{d,HP}$	L	2×0.398
LP displacement, $V_{d,LP}$	L	2×1.590
Total displacement, $V_{d,tot}$	L	2×1.988
Specific torque (HP), $T_b/V_{d,HP}$	Nm/L	362.5
Specific torque (LP), $T_b/V_{d,LP}$	Nm/L	90.7
Specific torque (total), $T_b/V_{d,tot}$	Nm/L	72.6
Specific power (HP), $P_b/V_{d,HP}$	kW/L	114.0
Specific power (LP), $P_b/V_{d,LP}$	kW/L	28.5
Specific power (total), $P_b/V_{d,tot}$	kW/L	22.8

At this considered operating point, the engine delivers a brake torque of **288.57 Nm** and a brake power of **90.66 kW** at 3000 rpm. The dependence of the normalized values on the selected reference displacement remains a key feature, directly derived from the split-cycle nature. In this configuration, the normalization based on the total displacement (2 x 1.988 L) provides the most representative metric for comparison at the complete engine level. This analysis confirms that the selected 30 CAD/10 CAD operating point successfully synthesizes the high partial efficiencies discussed previously into a robust and balanced overall engine output.

Remarks on pre vs post optimisation

A comparison between the pre-optimization and post-optimization configurations highlights a clear trade-off between performance and efficiency-oriented tuning. In the pre-optimization case, the engine delivers a brake torque of **331.92 Nm,** corresponding to a brake power of **104.27 kW** at 3000 rpm. After optimization, the brake torque decreases significantly to **228 Nm,** with a proportional reduction in brake power to 90.7 Nm. This drop is also reflected in the specific metrics: both specific torque and specific power decrease across HP, LP, and total displacement normalizations, indicating a lower overall power density of the system. In particular, the HP cylinders—being the main contributors to performance—show a marked reduction in their specific output.

This behavior is expected, as the **optimization strategy prioritizes improved thermodynamic conditions over peak performance**. The reduced torque and power suggest a less aggressive combustion and/or gas exchange process, likely associated with lower in-cylinder pressures or more conservative timing. However, this apparent performance penalty sets the stage for the subsequent analysis of efficiencies, where improvements in combustion, indicated efficiency, and possibly mechanical losses are anticipated.

5.5.2. Mean Effective Pressures

The following tables summarize the displacement values and the resulting MEPs for each normalization case.

Table 5.10: MEP values normalized with respect to the High Pressure cylinders total volume ($V_{d,HP,tot} = 795.22cm^3$).

Parameter	Value [bar]
FuelMEP	93.87
QMEP	93.69
IMEP$_{gross}$	50.26
IMEP$_{net}$	46.66
PMEP	-3.86
BMEP	45.6
FMEP	0.85

Table 5.11: MEP values normalized with respect to the Low Pressure cylinders total volume ($V_{d,LP,tot} = 3180.86 cm^3$).

Parameter	Value [bar]
FuelMEP	23.47
QMEP	23.42
IMEP$_{gross}$	12.63
IMEP$_{net}$	11.66
PMEP	-0.97
BMEP	11.40
FMEP	0.26

Table 5.12: MEP values normalized with respect to the total engine displacement ($V_{d,tot} = 3976.08 cm^3$).

Parameter	Value [bar]
FuelMEP	18.78
QMEP	18.74
IMEP$_{gross}$	10.11
IMEP$_{net}$	9.33
PMEP	-0.77
BMEP	9.12
FMEP	0.21

Remarks on Mean Effective Pressures

The post-sensitivity MEP results exhibit a systematic reduction across all key performance indicators when compared to the baseline configuration, reflecting a shift toward a less energy-intensive operating condition. Considering the High Pressure (HP) normalization as the most representative case, FuelMEP decreases from 109.37 bar to 93.87 bar, corresponding to a reduction of approximately 14.2%. This directly indicates a lower chemical energy input per unit displaced volume, which inherently limits the achievable thermodynamic work.

This reduction is consistently mirrored in QMEP (from 109.15 to 93.69 bar, -14.2%) and IMEP$_{gross}$ (from 57.59 to 50.26 bar, -12.7%), confirming that the entire combustion process scales down proportionally with the reduced fuel input. Notably, the slightly smaller reduction in IMEP$_{gross}$ compared to FuelMEP suggests a marginal improvement in combustion effectiveness, linked to **more favorable combustion phasing or reduced heat losses.**

The IMEP$_{net}$ follows the same trend, decreasing from 53.26 bar to 46.66 bar (-12.4%). The difference between IMEP$_{gross}$ and IMEP$_{net}$ remains nearly constant in absolute terms, indicating that internal irreversibilities (e.g., heat transfer and incomplete combustion effects) scale proportionally with the load reduction. This implies that the overall indicated efficiency is only marginally affected by the sensitivity study.

From the gas exchange perspective, PMEP improves from -4.33 bar to -3.86 bar, corresponding to a reduction in pumping losses of about 10.9%. This suggests that the modified operating conditions (likely related to valve timing or reduced mass flow) lead to a more efficient intake and exhaust process. However, despite this improvement, the absolute gain remains limited in comparison to the loss in indicated work.

The combined effect is reflected in the BMEP, which drops from 52.45 bar to 45.6 bar (-13.1%), closely tracking the reduction observed in IMEP_{net}. This indicates that the mechanical output penalty is primarily driven by the reduced in-cylinder work rather than by additional external losses.

FMEP remains substantially the same as before as it doesn't depend on parameters analysed during the sensitivity study, but on the internal friction of the engine components. Such friction is modeled directly by GT-Power taking as input parameters that have been discussed before which remain unchanged during the sensitivity study.

In summary, the post-sensitivity configuration leads to a globally upscaled engine operation characterized by reduced fuel energy input, lower indicated and brake performance, and slightly improved pumping behavior.

6 | Conclusion

6.1. Overview

The numerical model developed in this work was conceived to investigate how a DCEE in a 4+4 configuration, can improve the performance of a conventional four-stroke engine, with particular emphasis on efficiency.

To this end, the split-cycle architecture was analysed in detail, with the primary objective of providing a preliminary assessment of its potential benefits and limitations. The study focused on gaining a deeper understanding of the thermodynamic and gas-exchange mechanisms governing the DCEE concept, as well as identifying the key parameters influencing its behaviour.

A dedicated sensitivity analysis and optimization study were carried out in order to evaluate how far the efficiency of such an architecture could be improved. In particular, this work represents a first attempt to systematically investigate the synchronized version of the DCEE 4+4 configuration through one-dimensional simulations performed in GT-Power.

The adopted methodology combines numerical simulations with insights derived from previous literature, allowing the identification and analysis of the most influential parameters affecting engine performance. It is important to underline that the primary goal of the study was not to maximize engine performance in terms of torque or power output, but rather to optimize the system setup with a strong focus on improving overall efficiency.

6.1.1. Key Findings

The analysis conducted in this work provides a detailed assessment of the behaviour of the DCEE 4+4 split-cycle architecture, highlighting both its potential advantages and its intrinsic limitations. The results, obtained through a systematic numerical investigation and supported by a sensitivity-based optimization approach, reveal a complex interplay between thermodynamic efficiency, gas exchange processes, and mechanical losses.

Engine Performance The transition from the baseline to the optimized configuration led to a substantial reduction in brake torque and, consequently, in power output. This result is a direct consequence of the adopted optimization strategy, which prioritizes thermodynamic efficiency over performance metrics. The reduction in torque can be primarily attributed to a combination of factors, including modified combustion phasing, changes in trapped mass, and variations in in-cylinder pressure evolution. In particular, operating conditions that favour higher efficiency tend to reduce the effective pressure during the early expansion phase or limit the overall mass flow processed by the engine, ultimately leading to a lower indicated work per cycle. This behaviour clearly highlights the inherent trade-off between maximizing energy conversion efficiency and maintaining high power density, a well-known constraint in advanced engine concepts.

Thermodynamic and Mechanical Efficiencies One of the most significant outcomes of the study is the improvement in thermal efficiency achieved through the optimization process. This enhancement is strongly linked to a more favourable heat release phasing, allowing a larger fraction of the combustion process to occur closer to top dead centre, thereby increasing the effective expansion work. Additionally, a more controlled combustion duration contributes to reducing irreversibilities associated with non-ideal heat transfer and late combustion.

However, these thermodynamic gains are partially offset by a deterioration in mechanical efficiency. The observed increase in friction mean effective pressure (FMEP) suggests higher mechanical losses, which can be attributed to increased peak pressures, higher loads on moving components, and potentially more severe lubrication conditions. As a result, while the indicated efficiency improves, the corresponding brake efficiency gain is mitigated by these additional losses. This highlights a critical aspect of split-cycle architectures: improvements at the thermodynamic level do not automatically translate into proportional gains at the shaft output, due to the non-negligible impact of mechanical dissipation.

Gas exchange efficiency also plays a crucial role in defining the overall system performance. Its variation across the investigated configurations confirms the strong dependence on valve timing and pressure differentials between the different stages of the split cycle. In particular, the interaction between intake and exhaust processes becomes more complex in the DCEE architecture, where multiple cylinders and pressure levels are involved.

Sensitivity to Combustion Parameters The sensitivity analysis identified the start of combustion (SOC) and the combustion duration as two of the most influential parameters governing engine behaviour. Advancing the SOC generally leads to an increase in thermal efficiency, as it allows the pressure rise to occur earlier in the cycle, thus improving the expansion work extraction. However, excessive advancement can result in diminishing returns due to increased compression work and potential deviations from optimal pressure phasing.

Similarly, reducing the combustion duration tends to improve efficiency by approximating an ideal, more constant-volume heat release process. This reduces entropy generation and enhances the thermodynamic cycle efficiency. Nevertheless, overly short combustion durations may introduce steep pressure gradients, increasing mechanical stresses and potentially contributing to higher friction losses, thereby reinforcing the coupling between thermodynamic and mechanical aspects.

Influence of Valve Overlap The investigation of valve overlap revealed its dual and highly nonlinear impact on engine performance. On one hand, increased overlap can enhance scavenging efficiency, promoting the removal of residual gases and improving the quality of the fresh charge. This effect can be beneficial for combustion stability and efficiency, particularly in configurations where residual dilution is a limiting factor.

On the other hand, excessive overlap leads to increased short-circuiting of the fresh charge, resulting in direct losses of unburned mixture and a deterioration of gas exchange efficiency. Furthermore, higher overlap can increase pumping work due to less favourable pressure gradients during the valve transition phases. In the context of the DCEE architecture, these effects are further amplified by the interaction between the different cylinders and pressure levels, making the identification of an optimal overlap window particularly critical.

Global System Behaviour and Trade-offs The combined analysis of performance, efficiencies, and sensitivity results clearly demonstrates that the DCEE 4+4 architecture is characterized by strong interdependencies between its governing parameters. Improvements in one domain, such as thermodynamic efficiency, often induce penalties in others, including mechanical losses and power output.

Overall, the results confirm that the DCEE concept has a significant potential for achieving high thermal efficiencies, especially when the system is operated under carefully optimized conditions. However, the associated reduction in performance and the increase in system complexity suggest that its practical implementation would require a multi-objective design approach, capable of balancing efficiency gains with acceptable levels of power density and mechanical reliability.

6.1.2. Key Findings - Quantitative

Building upon the qualitative observations, the following quantitative results highlight the fundamental behaviour and the optimal operating conditions of the synchronized 4+4 DCEE architecture:

- **Engine Performance:** The optimization process prioritized efficiency over raw performance, resulting in a deliberate power reduction. The baseline configuration delivered a brake power of 104.27 kW and a brake torque of 331.92 Nm at 3000 rpm. In the optimized setup, the brake power decreased by approximately 13% to 90.7 kW, with a corresponding torque reduction to 288.57 Nm. Consequently, the total specific power density dropped from 26.2 kW/L to 22.8 kW/L.
- **Thermodynamic and Mechanical Efficiencies:** The engine demonstrated exceptional indicated performance, with the thermal efficiency peaking at 53.92% under optimal combustion phasing. Mechanical efficiency remained extremely stable, fluctuating only slightly around 95.5% to 97.4% across different operating points due to constant engine speed. The gas exchange efficiency also proved robust, maintaining high values between 92.0% and 93.8%.
- **Sensitivity to Combustion Parameters:** A comprehensive parametric sweep identified the global optimum at a combustion duration of 30 CAD and a spark advance of 10 CAD. This specific configuration yielded the peak brake efficiency of 48.66%. Deviating from these values caused noticeable efficiency penalties; for instance, a longer combustion duration (35 CAD) paired with a late spark advance (5 CAD) reduced the brake efficiency to its minimum recorded value of 45.42%.
- **Influence of Valve Overlap:** The system proved highly sensitive to valve overlap duration. Compared to the baseline moderate overlap (yielding 48.09% brake efficiency and 82.3 kW power), removing the overlap entirely caused a severe 23.8% drop in thermal efficiency and reduced brake efficiency to 43.42%. Conversely, a high overlap of approximately 30 degrees introduced massive short-circuiting losses , slashing brake power by 20.7% (to 65.3 kW) and plummeting thermal efficiency by 33.1% (to 44.16%).
- **Global System Behaviour and Trade-offs (MEP Analysis):** The transition to the efficiency-optimized configuration was reflected in a systematic reduction of Mean Effective Pressures. The FuelMEP was reduced by 14.2% (from 109.37 bar to 93.87 bar), indicating a leaner energy input per unit volume. While BMEP dropped by 13.1% (from 52.45 bar to 45.6 bar) tracking the reduced work output, the system

saw a 10.9% improvement in pumping losses, with PMEP improving from -4.33 bar to -3.86 bar.

6.1.3. Limitations of the Study

Despite the comprehensive analysis carried out in this work, several limitations must be acknowledged, as they influence both the quantitative accuracy of the results and their direct applicability to a real engine implementation.

Absence of Knock Modelling No knock model was included in the simulations. While this choice allowed for a more tractable and computationally efficient model, it prevents the assessment of one of the most critical constraints in highly efficient engine operation. In particular, the optimization of combustion phasing towards advanced conditions may lead to operating points that would be limited by knock in a real engine. As a consequence, the achievable efficiency improvements reported in this study should be interpreted as theoretical upper bounds rather than directly attainable values.

Simplified Inter-Cylinder Duct Geometry In order to avoid the introduction of significant dead volumes, which would make the architecture closer to a non-synchronized configuration with buffer tanks, the ducts connecting the cylinders were modelled with extremely reduced lengths. While this assumption enables the representation of an idealized synchronized architecture, it neglects important fluid-dynamic effects such as wave propagation, pressure losses, and flow inertia. In a real implementation, the physical dimensions of these ducts would inevitably introduce additional losses and dynamic effects, potentially altering the overall system behaviour.

Thermal Interaction in Ducts Differently from previous studies on non-synchronized architectures, the inter-cylinder ducts were not thermally insulated. As a result, heat transfer between the working fluid and the surroundings was allowed, introducing additional thermal losses during the transfer process. While this choice increases the physical realism of the model, it also introduces uncertainty, as the actual thermal boundary conditions in a real engine would strongly depend on design-specific solutions, such as insulation strategies or material selection.

Valve Sizing and Actuation Strategy No dedicated optimization of valve sizing or lift profiles was performed. The adopted valve characteristics were derived from literature data related to conventional four-stroke engines, which may not be fully representative of the requirements of a split-cycle architecture. Given the fundamentally different gas exchange process in the DCEE concept, a non-optimized valve system may significantly affect volumetric efficiency, pumping losses, and overall performance.

Limitations of the 1D Modelling Approach The use of a one-dimensional simulation environment inherently limits the ability to capture complex three-dimensional phenomena, such as turbulence generation, in-cylinder flow structures, and local mixture inhomogeneities. These effects can play a crucial role in combustion development, heat transfer, and ultimately engine efficiency. Therefore, the results obtained should be considered as a first-order approximation of the real system behaviour.

Combustion Model Simplifications The combustion process was modelled using a simplified approach, which does not fully account for detailed chemical kinetics or spatial variations within the combustion chamber. As a consequence, the influence of factors such as fuel-air mixing quality, local temperature gradients, and detailed ignition phenomena is not explicitly resolved.

Lack of Experimental Validation The model was not validated against experimental data for the specific DCEE 4+4 synchronized architecture. While the simulation setup is based on established modelling practices and literature references, the absence of experimental validation limits the confidence in the absolute values of the predicted performance and efficiencies.

Restricted Operating Range The analysis was conducted over a limited set of operating conditions, focusing on a specific engine speed and load. This choice is consistent with the objective of performing a detailed parametric study, but it does not allow for a full assessment of the engine behaviour over a complete operating map. Indeed, Studying how the model would behave at higher loads would significantly increase its power density.

Scope of the Study Finally, it is important to underline that this work was conceived as a preliminary investigation of the DCEE 4+4 synchronized architecture. The objective was not to deliver a fully optimized or directly implementable engine design, but rather to assess whether this concept presents sufficient potential to justify further, more detailed studies.

6.1.4. Implications for the DCEE Concept

The results obtained in this work provide a comprehensive perspective on the potential and limitations of the DCEE 4+4 split-cycle architecture, allowing a more informed assessment of its practical viability. From a thermodynamic standpoint, the analysis confirms that the separation of compression and expansion processes can offer a significant advantage over conventional four-stroke engines. This architectural feature enables a more flexible control of the combustion phasing and of the pressure evolution within the cycle, ultimately leading to improved conditions for energy conversion and higher thermal efficiencies.

However, the extent to which these theoretical advantages can be effectively exploited is strongly dependent on the behaviour of the gas exchange process. Unlike conventional engines, where intake and exhaust are confined within a single cylinder, the DCEE concept relies on the transfer of the working fluid between different cylinders operating at distinct pressure levels. As a consequence, any inefficiency in this transfer process, whether due to pressure mismatches, flow losses, or non-optimal valve timing, directly impacts the overall system performance. The sensitivity of the results to valve overlap and to the characteristics of the inter-cylinder connections highlights how critical this aspect is, effectively representing one of the main limiting factors of the architecture.

In addition to gas exchange constraints, the analysis also reveals that the thermodynamic benefits are partially counterbalanced by mechanical and system-level penalties. The increased complexity of the architecture, combined with the need to manage multiple interacting units, introduces additional sources of friction and imposes stricter requirements on synchronization and control. This is particularly evident in the synchronized configuration investigated in this work, where the absence of intermediate storage volumes makes the system inherently more sensitive to timing inaccuracies and transient effects.

Another important implication emerging from the study is the clear trade-off between efficiency and performance. The configurations that maximize thermal efficiency tend to operate with reduced power output, as a consequence of both the modified combustion phasing and the constraints imposed by the gas exchange process. This suggests that the DCEE concept may not be ideally suited for applications where high power density is the primary objective, but could instead be more effectively exploited in scenarios where efficiency is prioritized, such as steady-state operation or in combination with hybrid powertrains.

Overall, the findings indicate that the DCEE 4+4 architecture represents a promising but inherently complex solution. Its potential to achieve high efficiencies is evident, yet its practical implementation would require a careful and integrated design approach, capable of simultaneously addressing thermodynamic optimization, gas exchange effectiveness, mechanical losses, and control strategy development. In this sense, the concept cannot be considered as a straightforward evolution of the conventional engine, but rather as a system whose benefits can only be realized through a high level of design and operational refinement.

6.1.5. Future Work

The results obtained in this study open several directions for future developments, which would allow a more complete and realistic assessment of the DCEE 4+4 architecture.

A first and fundamental step would consist in refining the modelling of the inter-cylinder transfer process. In the present work, the connecting ducts were intentionally defined with extremely reduced dimensions in order to minimize dead volumes and isolate the behaviour of the synchronized architecture. While this approach was effective for a preliminary investigation, a more realistic representation would require the introduction of ducts with physically consistent geometries, including appropriate lengths, diameters, and material properties. This would enable a more accurate evaluation of pressure losses, wave dynamics, and thermal interactions, which are expected to play a crucial role in the overall system performance.

Another key aspect to be addressed is the inclusion of a knock model. As highlighted in the limitations of this work, the absence of knock prediction prevents the identification of the true operational limits of the engine, particularly when operating with advanced combustion phasing aimed at maximizing efficiency. The integration of a knock model would therefore allow the definition of knock-constrained optimization strategies, providing more realistic and practically achievable results.Further developments should also investigate the behaviour of the engine over a wider operating range. In particular, exploring higher load conditions would be of great interest, especially considering the potential application of this architecture in motorcycle engines, where high specific power and dynamic response are relevant requirements. Extending the analysis beyond the single operating point considered in this study would enable a more comprehensive understanding of the trade-offs between efficiency, performance, and operability.

In addition, a more detailed optimization of the gas exchange system should be considered. This includes not only valve timing parameters, such as overlap, but also valve sizing and lift profiles, which were not specifically optimized in this work. Given the strong sensitivity of the DCEE architecture to gas exchange processes, a dedicated optimization in this area could significantly influence the achievable performance and efficiency.

Finally, the adoption of higher-fidelity modelling approaches represents a natural extension of the present study. The use of three-dimensional CFD simulations would allow the investigation of in-cylinder flow structures, turbulence effects, and detailed combustion phenomena, providing a deeper understanding of the physical mechanisms governing the system. In the longer term, experimental validation would be essential to confirm the trends observed in the numerical results and to assess the practical feasibility of the concept.

An additional relevant aspect for future investigation concerns the geometric layout and overall architecture of the engine. In the present study, an in-line cylinder configuration was adopted, primarily due to its simplicity and ease of implementation within the GT-Power environment. However, this choice does not necessarily represent the optimal solution from a fluid-dynamic, mechanical, or packaging standpoint. Alternative configurations, such as square-four or V-type layouts, could offer advantages in terms of compactness, reduced flow path lengths, and improved integration of the inter-cylinder transfer system. A dedicated study on the optimal spatial arrangement of the cylinders could therefore provide further insights into how to minimize losses associated with fluid transfer and improve the overall efficiency of the concept.

Furthermore, it would be of particular interest to extend the analysis to alternative operating strategies, such as the 2+4+2 configuration. Despite its intrinsic asymmetry, where one low-pressure cylinder is dedicated to compression and another to expansion, this architecture may offer additional degrees of freedom in the design process. In particular, it would allow the compressor and expander units to be specifically optimized for their respective roles, potentially leading to improved overall system performance. Investigating whether such specialization can outweigh the penalties associated with increased system complexity and asymmetry represents a promising direction for future research.

In line with this, a systematic investigation into the engine's performance at higher rotational speeds represents a critical next step. In the present study, the engine speed was kept constant to establish a controlled baseline and isolate the fundamental thermodynamic interactions of the synchronized architecture. However, exploring higher RPM ranges is essential to characterize the sensitivity of the inter-cylinder transfer process to reduced residence times and increased gas velocities. Such an analysis would clarify how pressure wave dynamics and flow-induced losses scale with speed, ultimately defining the effective power bandwidth of the system.

Overall, these developments would contribute to bridging the gap between the present preliminary investigation and a more mature evaluation of the DCEE architecture, enabling a more reliable assessment of its real-world potential.

Bibliography

[1] H. Finneran, Basset. A review of split-cycle engines. *International Journal of Engine Research*, pages 1–44, 2018.

[2] B. Johansson. *Internal Combustion Engines*. -, 2024.

[3] B. Johansson. Dcee short. PPTX file, 9 2025.

[4] A. C. D. C. Morgan, Robert (PI)Salter. Hydrogen recuperated advanced thermal engine. *Department for Energy Security Net Zero*, 2022.

[5] L. Nut. Double compression-expansion engine concepts experimental and simulation study of a split-cycle concept for improved brake efficiency. Master's thesis, Lund University, POBox117 22100 Lund +4646-2220000, 2019.

[6] A. A. B. J. Rafig Babayev a, Hong G. Im. Hydrogen double compression-expansion engine (h2dcee): A sustainable internal combustion engine with 60 *Elsevier*, (2):1–18, 2022.

List of Figures

List of Tables

List of Symbols and Abbreviations

Variable	**Description**	**SI unit**
HP	high pressure	-
LP	low pressure	-
FuelMEP	Fuel Mean Effective Pressure	bar
BMEP	Brake Mean Effective Pressure	bar
FMEP	Friction Mean Effective Pressure	bar
PMEP	Pumping Mean Effective Pressure	bar
IMEP	Indicated Mean Effective Pressure	bar
HTMEP	Heat Transfer Mean Effective Pressure	bar
QMEP	Heat-Release Mean Effective Pressure	bar
EXEP	Exhaust Mean Effective Pressure	bar
DCEE	Double Compression Expansion Engine	bar
η_{ge}	Gas-Exchange efficiency	-
η_{th}	Thermal efficiency	-
η_m	Mechanical efficiency	-
η_b	Brake efficiency	-
SOC	Start of Combustion	-
CAD	Crank-angle degrees	$^\circ$